Ultrasonic Inspection on Joined Aerospace Materials

Vemuganti Venkata Haridutt Aditya

A thesis submitted in partial fulfillment of the

requirements for the degree of

Master of Science in Mechanical Engineering

University of Washington

March 2015

Committee:

M Ramulu

Mark Tuttle

Dan Sanders

Program Authorized to Offer Degree:

Mechanical Engineering

University of Washington

ABSTRACT

Ultrasonic Inspection of Joined Aerospace Materials

Vemuganti Venkata Haridutt Aditya

Chair of the Supervisory Committee:

Professor M Ramulu

Department of Mechanical Engineering

Titanium (Ti) and its alloys are extensively used in the Aerospace industry due to its compatibility with composite materials, high tensile strength, lighter weight and corrosion resistance. But it is very hard to machine using conventional machining. Therefore solid state joining processes such as Friction Stir Welding (FSW) and Diffusion Bonding (DB) which produce near net shapes, significantly reducing the processing time with minimal wastage of material, have been developed. However there is a lot of possibility that these processes induce various defects, in the weld/bond zone, if they are properly not operated. Destructive testing proves to be very expensive to evaluate the quality of the bond. This motivates us to investigate the bond quality using Non Destructive Testing (NDT) techniques using Ultrasonic Testing.

Contents

List of Tables

List of Figures

NOMENCLATURE

ULTRASONIC AND MATERIAL PROPERTIES	
Symbol	**Description**
V_L	Longitudinal Velocity of Wave
V_T	Transverse Velocity of Wave
A_i	Amplitude of the wave reflected at the Interface
A_T	Amplitude of the wave incident on the surface
R_{AB}	Reflection Coefficient of Material A to B
K	Interficial Stiffness
ω	Angular Frequency
Ω	Characteristic Frequency
E	Young's Modulus
ρ	Density of the Material
ν	Poisson's Ratio
TITANIUM ALLOYS	
64	Ti-6Al-4V (Ti-64)
6242	Ti-6Al-2Sn-4Zr-2Mo (Ti-6242)
$54M$	Ti-5Al-4V-0.6Mo-0.4Fe (Ti-54M)
$21S$	Ti-15Mo-3Nb-3Al-0.2Si (Ti Beta 21S)
FG	Fine Grain
SG	Soft Grain
FRICTION STIR WELDING	
Represented as $(U-V\ at\ PPP/Q)$	
U	Titanium Alloy
V	Titanium Alloy
PPP	RPM
Q	Feed Rate
DIFFUSION BONDING	
Represented as $(U-V\ at\ T)$	
U	Titanium Alloy
V	Titanium Alloy
T	Temperature

ACKNOWLEDGMENTS

I would like to acknowledge the immense contribution of the following people during the course of my research.

- Prof. M Ramulu for his patience, guidance and unending support.
- And most importantly, my Family for their unending love and support.

1 INTRODUCTION & OBJECTIVES

The use of Titanium (Ti) and its alloys is increasing exponentially in the aerospace industry due to its compatibility with composite materials. Aluminum (Al) alloys are not compatible with composites with respect to the thermal expansion and corrosion resistance. Thus titanium, with advantages such as high tensile strength, lighter weight and thermal and corrosion resistance are being used for parts in place of aluminum. Additionally, there is also a potential use of titanium alloys in areas exposed to elevated temperatures by the aircraft engines.

The cost of titanium will no more be a barrier with the introduction of solid state joining processes which are used to fabricate complex geometries and structures which are not possible with traditional manufacturing techniques such as machining and forming. Components with near net shape or structures with minimal material utilization can be fabricated through the solid state joining processes such as Friction Stir Welding (FSW) and Diffusion Bonding (DB) significantly reducing the buy-to-fly ratio. Also, the strength and toughness of titanium are significantly improved when the dissimilar alloys are treated with these processes. The advancements in new materials and modern manufacturing processes are replacing the use of aluminum and traditional manufacturing in the industry.

As with the introduction of any new material or manufacturing method, appropriate quality control and inspection techniques must be developed before they can be used with confidence on safety-critical components. The inspection requirements are based on the applications and the quality control but in general it is necessary to detect defects of known types above a threshold of size or distribution. The types of probable defects should be characterized and the threshold size should be determined from mechanical testing. Currently the favored method of inspection is the Non Destructive Techniques (NDT).

Nondestructive testing (NDT) is the process of inspecting, testing, or evaluating materials, components or assemblies for discontinuities, or differences in characteristics without destroying the serviceability of the part or structure. Destructive testing on the other hand is done on a limited number of samples ("lot sampling") than on the actual materials, components or assemblies in service. These destructive tests

are often used to determine the physical properties of materials such as impact resistance, ductility, yield and ultimate tensile strength, fracture toughness and fatigue strength, but discontinuities and differences in material characteristics are more effectively found by NDT.

NDT is based on techniques that take advantage of the applications of physical principles to determine the characteristics of materials and to detect and assess flaws or defects without hampering the serviceability of the materials. The significance of NDT is apparent because of its cost effective performance, safety and versatility to a broad range of manufacturing processes to estimate the defects in the material. NDT is widely used and accepted in the aerospace, power generation, automotive, railway and petrochemical industries.

There is a broad range of NDT techniques based on physical principles of electromagnetic radiation, sound and other inherent properties of materials. This includes Ultrasonic testing, Eddy current analysis, X-ray radiography, Magnetic particle inspection, Dye penetrant application which are most widely used for industrial applications. The techniques should be chosen based on economic, safety, efficiency and time considerations. The Relative cost and characteristics of most widely used NDT techniques are outlined in Table 1 [1] and the NDT techniques are compared and analyzed in Table 2 [1].

Ultrasonic testing (UT), outlined in Table 2, is one of the widely used NDT techniques to detect sub-surface defects or characterize materials. This detection method uses high frequency sound waves, typically above 2MHz to pass through a material. It is widely used in many industries including aerospace, automotive and other transportation sectors. In ultrasonic testing, an ultrasound transducer connected to a diagnostic machine passes over the object being inspected. A probe is used which contains a piezoelectric crystal to transmit and receive ultrasonic pulses and display the signals on a cathode ray tube or digital display. The actual display relates to the time taken for the ultrasonic pulses to travel the distance to the interface and back. An interface could be at the back of a plate material or a defect. The transducer is typically separated from the test object by a couplant.

Table 1: Relative Cost and Characteristics of NDT Methods [1]

Important considerations	Test method				
	Ultrasonics	X-ray	Eddy current	Magnetic particle	Liquid penetrant
Capital cost	*Medium to high*	High	Low to medium	Medium	Low
Consumable cost	*Very low*	High	Low	Medium	Medium
Time of results	*Immediate*	Delayed	Immediate	Short delay	Short delay
Effect of geometry	*Important*	Important	Important	Not too important	Not too important
Access problems	*Important*	Important	Important	Important	Important
Type of defect	*Internal*	Most	External	External	External Surface breaking
Relative sensitivity	*High*	Medium	High	Low	Low
Formal record	*Expensive*	Standard	Expensive	Unusual	Unusual
Operator skill	*High*	High	Medium	Low	Low
Operator training	*Important*	Important	Important	Important	Important
Training needs	*High*	High	Medium	Low	Low
Portability of equipment	*High*	Low	High to medium	High to medium	High
Dependent on material composition	*Very*	Quite	Very	Magnetic only	Little
Ability to automate	*Good*	Fair	Good	Fair	Fair
Capabilities	*Thickness gaging: some composition testing*	Thickness gaging	Thickness gaging; grade sorting	Defects only	Defects only

Table 2: Comparison of NDT Methods [1]

Method	Characteristics detected	Advantages	Limitations	Example of use
Ultrasonics	Changes in acoustic impedance caused by cracks, non-bonds, inclusions, or interfaces	**Can penetrate thick materials; excellent for crack detection; can be automated**	**Normally requires coupling to material either by contact to surface or immersion in a fluid such as water. Surface needs to be smooth.**	Adhesive assemblies for bond integrity; welds; laminations; hydrogen cracking
Radiography	Changes in density from voids, inclusions, material variation; placement of internal parts	Can be used to inspect wide range of materials and thicknesses; versatile; Film provides record of inspection	Radiation safety requires precautions; expensive; detection of cracks can be difficult unless perpendicular to x-ray film	Pipeline welds for penetration, inclusions and voids; Internal defects in casting
Visual optical	Surface characteristics such as finish, scratches, cracks, or color; strain in transparent materials; corrosion	Often convenient; can be automated	Can be applied only to surfaces, through surface openings, or to transparent material	Paper, wood, or metal for surface finish and uniformity
Eddy current	Changes in electrical conductivity caused by material variations, cracks, voids, or inclusions	Readily automated; moderate cost	Limited to electrically conducting materials; limited penetration depth	Heat exchanger tubes for wall thinning and cracks
Liquid penetrant	Surface openings due to cracks, porosity, seams, or folds	Inexpensive, easy to use, readily portable, sensitive to small surface flaws	Flaw must be open to surface Not useful on porous materials or rough surfaces	Turbine blades for surface cracks or porosity; grinding cracks
Magnetic particles	Leakage magnetic flux caused by surface or near-surface cracks, voids, inclusions, or material or geometry changes	Inexpensive or moderate cost, sensitive both to surface and near- surface flaws	Limited to ferromagnetic material; surface preparation and post-inspection demagnetization may be required	Railroad wheels for cracks; large castings

Ultrasonic testing stands out of the other NDT methods, particularly in the application to DB and FSW, in practice today as it is sensitive to both surface and subsurface discontinuities. The depth of penetration for flaw detection is superior to other NDT methods. It is also used to estimate the size and shape of defects. With these benefits and being an affordable yet effective method to detect discontinuities, Ultrasonic Testing is chosen to be the NDT method to investigate the defects pertaining to solid state joining processes (FSW and DB). Additionally, Ultrasonic testing is capable of estimating the Young's Modulus (E) of the materials through the characteristic velocity.

The objective of our research is to use the UT capabilities to the FSW and DB joints to detect defects of various kinds. Relatively little data is available on UT testing on FSW involving similar and dissimilar alloys of titanium. Most of literature is based on its counterpart, aluminum, which we will be analyzing to lay a foundation for this research. The focus is on establishing a methodology for inspection of these new materials through NDT, comparing the accuracy of inspection with the mechanical testing data. The samples consisting of similar and dissimilar joints of Ti alloys by diffusion bonding and friction stir welding (FSW) processes. By justification of this methodology it can save time and production costs spent in destructive testing. The benefits and limitations of this process can also be clearly identified with experimentation.

The thesis is divided into four sections which deal with Literature review and background, experimental methodology explaining the sample specification and inspection procedure, results and discussions and finally conclusions.

2 BACKGROUND & LITERATURE REVIEW

2.1 Principles of Ultrasonic Testing

Ultrasonic testing uses the same principle as is used in naval SONAR and fish finders. Ultra-high frequency sound is introduced into the part being inspected and if the sound hits a material with a different acoustic impedance (density and acoustic velocity), some of the sound will reflect back to the sending unit and can be presented on a visual display. By knowing the speed of the sound through the part (the acoustic velocity) and the time required for the sound to return to the sending unit, the distance to the reflector (the indication with the different acoustic impedance) can be determined. The most common sound frequencies used in UT are between 1.0 and 10.0 MHz, which are too high to be heard and do not travel through air. The lower frequencies have greater penetrating power but less sensitivity (the ability to "see" small indications), while the higher frequencies don't penetrate as deeply but can detect smaller indications. [2]

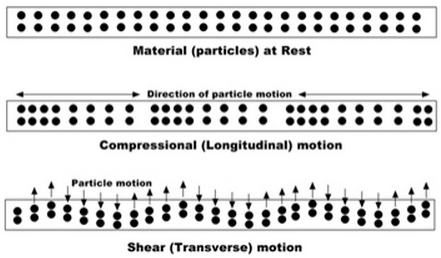

Figure 1: Wave Types and their motion [2]

The two most commonly used types of sound waves used in industrial inspections are the compression (longitudinal) wave or L-Wave and the shear (transverse) wave or S-Wave, as shown in Figure 1 [2]. A L-Wave is generated by applying a normal stress to the material surface as shown in Figure 1. In this mode, particle vibrations occur in the direction of wave propagation and cause compression and rarefaction regions along the propagation path. S-wave is excited by applying a shear force at the surface of a medium; this causes wave propagation through the medium by shear stresses. This mode results in atomic oscillations perpendicular to the direction of wave propagation. In general L-waves cause the atoms in a part to vibrate back and forth parallel to

the sound direction and S-Waves cause the atoms to vibrate perpendicularly (from side to side) to the direction of the sound and travel approximately half the speed of longitudinal waves.

Sound is introduced into the part using an ultrasonic transducer ("probe") that converts electrical impulses from the UT machine into sound waves, then converts returning sound back into electric impulses that can be displayed as a visual representation on a digital or LCD screen (on older machines, a CRT screen) as shown in Figure 2 [3]. If the machine is properly calibrated, the operator can determine the distance from the transducer to the reflector, and in many cases, an experienced operator can determine the type of discontinuity (like slag, porosity or cracks in a weld) that caused the reflector. Because ultrasound will not travel through air (the atoms in air molecules are too far apart to transmit ultrasound), a liquid or gel called "couplant" is used between the face of the transducer and the surface of the part to allow the sound to be transmitted into the part.

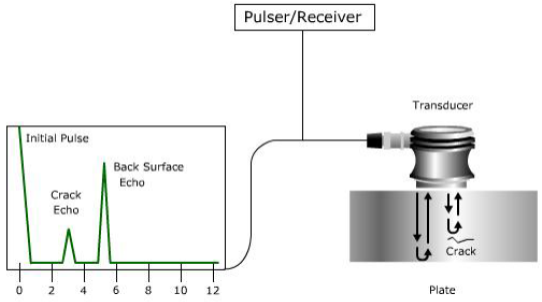

Figure 2: Ultrasonic Inspection Technique [3]

In ultrasonic testing, the inspector must make a decision about the frequency of the transducer that will be used. Changing the frequency when the sound velocity is fixed will result in a change in the wavelength of the sound. The wavelength of the ultrasound used has a significant effect on the probability of detecting a discontinuity. A general rule of thumb is that a discontinuity must be larger than one-half the wavelength to stand a reasonable chance of being detected. Ultrasonic Testing Equipment has developed in leaps and bounds in the previous few decades making it a competitive and safe practice for the quality evaluation of high-risk components in various industries. Table 3 [4] gives us a glimpse of the evolution of the UT equipment. Phased Array Technique is described in the next section of this chapter while

Table 3: Evolution of Ultrasonic Testing [4]

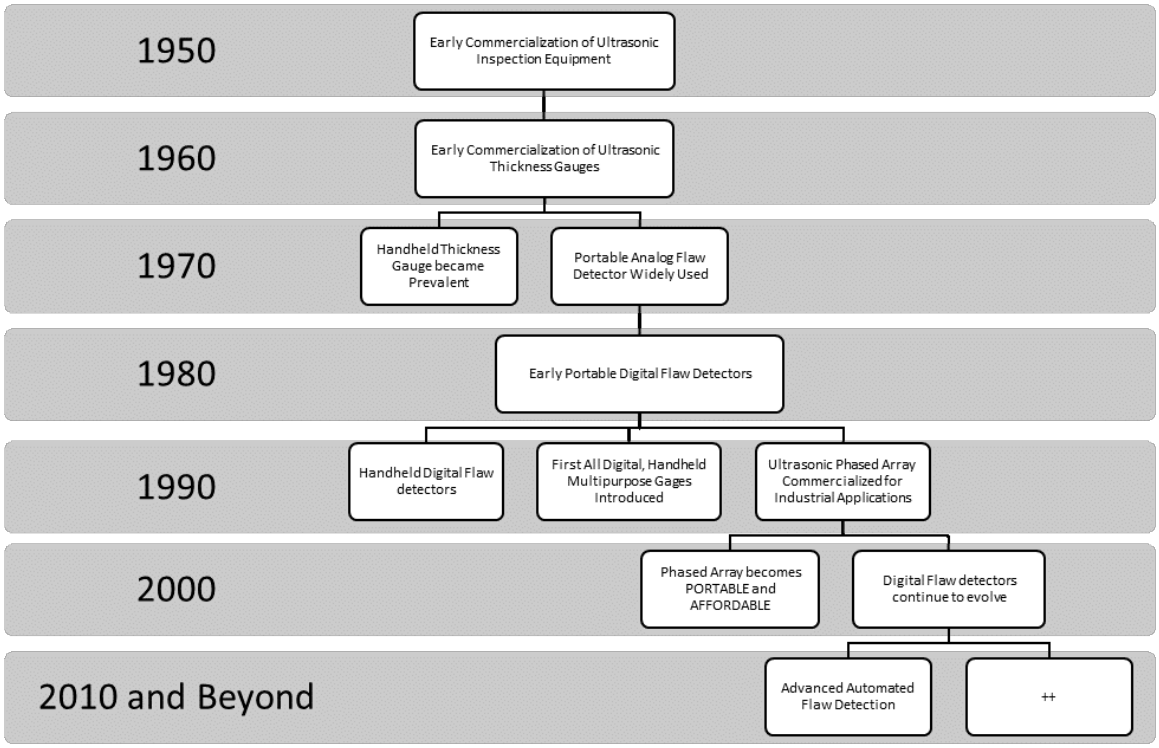

the Ultrasonic Techniques are briefly described in the Appendix A.

2.1.1 Interpretation of Conventional Ultrasonic Data

Ultrasonic data can be collected and displayed in a number of different formats known in the NDT terminology as A-scan, B-scan and C-scan presentations. Each presentation mode provides a different way of looking at and evaluating the region of material being inspected. Modern computerized ultrasonic scanning systems can display data in all three presentation forms simultaneously. [5]

A-Scan Presentation: The A-scan presentation displays the amount of received ultrasonic energy as a function of time. The relative amount of received energy is

plotted along the vertical axis and the elapsed time (which may be related to the sound energy travel time within the material) is displayed along the horizontal axis. Most instruments with an A-scan display allow the signal to be displayed in its natural radio frequency form (RF), as a fully rectified RF signal, or as either the positive or negative half of the RF signal. In the A-scan presentation, relative discontinuity size can be estimated by comparing the signal amplitude obtained from an unknown reflector to that from a known reflector. Reflector depth can be determined by the position of the signal on the horizontal sweep.

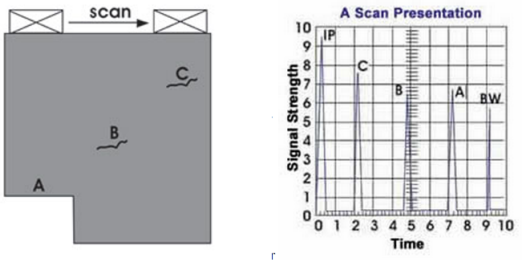

Figure 3: Representation of an A-scan in UT [5]

In Figure 3 [5], the initial pulse generated by the transducer is represented by the signal IP, which is near time zero. As the transducer is scanned along the surface of the part, four other signals are likely to appear at different times on the screen. When the transducer is in its far left position, only the IP signal and signal A, the sound energy reflecting from surface A, will be seen on the trace. As the transducer is scanned to the right, a signal from the backwall BW will appear later in time, showing that the sound has traveled farther to reach this surface. When the transducer is over flaw B, signal B will appear at a point on the time scale that is approximately halfway between the IP signal and the BW signal. Since the IP signal corresponds to the front surface of the material, this indicates that flaw B is about halfway between the front and back surfaces of the sample. When the transducer is moved over flaw C, signal C will appear earlier in time since the sound travel path is shorter and signal B will disappear since sound will no longer be reflecting from it.

The B-scan presentations is a profile (cross-sectional) view of the test specimen is represented in Figure 4 [5]. In the B-scan, the time-of-flight (travel time) of the sound energy is displayed along the vertical axis and the linear position of the transducer is displayed along the horizontal axis. From the B-scan, the depth of the reflector

and its approximate linear dimensions in the scan direction can be determined. The B-scan is typically produced by establishing a trigger gate on the A-scan. Whenever the signal intensity is great enough to trigger the gate, a point is produced on the B-scan. The gate is triggered by the sound reflecting from the backwall of the specimen and by smaller reflectors within the material. In the B-scan image above, line A is produced as the transducer is scanned over the reduced thickness portion of the specimen. When the transducer moves to the right of this section, the backwall line BW is produced. When the transducer is over flaws B and C, lines that are similar to the length of the flaws and at similar depths within the material are drawn on the B-scan. It should be noted that a limitation to this display technique is that reflectors may be masked by larger reflectors near the surface.

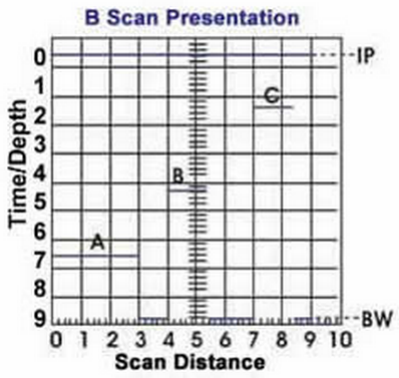

Figure 4: Representation of a B-Scan in UT [5]

The C-scan presentation provides a plan-type view of the location and size of test specimen features is represented in Figure 5 [5]. The plane of the image is parallel to the scan pattern of the transducer. C-scan presentations are produced with an automated data acquisition system, such as a computer controlled immersion scanning system. Typically, a data collection gate is established on the A-scan and the amplitude or the time-of-flight of the signal is recorded at regular intervals as the transducer is scanned over the test piece. The relative signal amplitude or the time-of-flight is displayed as a shade of gray or a color for each of the positions where data was recorded. The C-scan presentation provides an image of the features that reflect and scatter the sound within and on the surfaces of the test piece.

When an ultrasonic wave hits an interface between two media with different mechanical properties, a part of sound is reflected back into the first medium and the

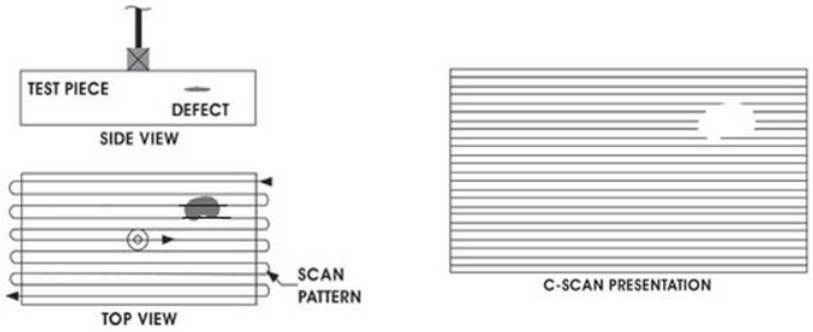

Figure 5: Representation of a C-Scan in UT [5]

rest is refracted and transmitted into the second medium according to Snell's Law. The ratio of the amplitude (energy) of the reflected pulse and the incident is called the reflection coefficient. The ratio of the amplitude of the incident pulse and the transmitted pulse is called the transmission coefficient. Both are dependent on the differences in acoustic impedance of the two materials. The acoustic impedance of a medium is the speed of sound in the material $\times$ the density:

$$Z = \rho\, V \tag{1}$$

Where Z is the Acoustic Impedance Where ρ is the Density of the Material Where V is the Velocity of the Wave

Thus, if the velocities of sound in two materials are very different, the reflection will be close to total, and no energy will pass into the deeper material. This means that the deepest material can be considered to be in a shadow. Also it is important to realize that the actual amount of energy that is reflected back to the probe; i.e. the amplitude of the reflected signal, is not only dependent on the reflection coefficient. The direction of the reflected signal is also important. Thus an irregular scatter will reflect only a portion back to the probe and a more regular scatter will reflect more if the reflecting surfaces are perpendicular to the ultrasound beam.

In Figure 6 [6], the two images on the left shows a perfect reflecting surface. Most of the energy (but not all, as the wavefront is not flat), will reflect back to the transducer resulting in a high amplitude echo, when the surface is perpendicular to the ultrasound beam. On the other hand, if this surface is tilted 45^O, almost all

energy will be reflected away from the surface, resulting in a very low amplitude return echo to the probe. The next two images shows a scatter with a more curved surface, resulting in more energy being spread out in different directions, this will give a lower amplitude signal back to the probe, but may reflect more energy back towards the probe if it is tilted, as for instance when the heart contracts, walls changing direction. Finally, to the left, a totally irregular surface will reflect the sound in all directions, but very little net reflections toward the probe. The term: Reflection is used about the return signal, while scattering is used about dispersion of the reflected signal[1].

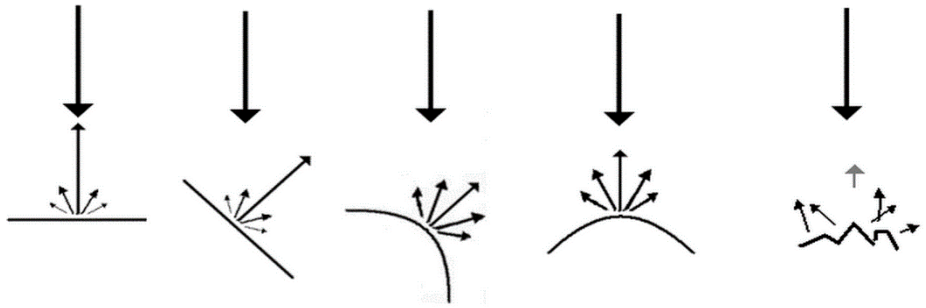

Figure 6: Effect of size and direction of the reflecting surface [6]

Attenuation of the signal can be dealt with by gain, increasing gain amplifies the reflected signal in post processing. However, increased gain increases signal and noise in the same manner. Gain can be done at acquisition, or in post processing [6]. The methods and representation of scans above can be best described by the term "Conventional Ultrasonics" or "Conventional Ultrasonic Methods". We call them conventional because of the advancements made to this field are significant and technologically ahead. The next section describes the advanced ultrasonic method we would be using in our research namely "Phased Array Ultrasonic Technique". The other advancements in this field are briefly described in the Appendix-A.

2.1.2 Phased Array Ultrasonic Technique (PAUT)

Phased Array Ultrasonic Technique (PAUT) is an advanced ultrasonic method gaining prominence in the engineering field, especially in the area of welding. It uses the

[1]Source :https://www.nde"dash"ed"dot"org

principle of constructive and destructive interference of waves, first demonstrated by English scientist Thomas Young in 1801 in a notable experiment that utilized two point sources of light to create interference patterns. Waves that combine in phase reinforce each other, while waves that combine out-of-phase will cancel each other. Phase shifting, or phasing, is in turn a way of controlling these interactions by time-shifting wave fronts that originate from two or more sources. It can be used to bend, steer, or focus the energy of a wave front.[4]

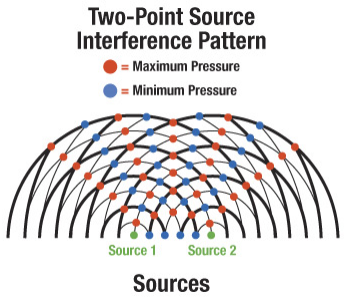

Figure 7: Two point source interference pattern [4]

Inspection using phased arrays has much in common with conventional UT, since the physics of wave propagation, reflection, refraction, mode conversion and diffraction remain the same. It is the method of generating and receiving the ultrasonic waves that is different. The beam from a phased array probe can be moved electronically without the movement of the probe and can be swept through a wide volume of material at elements each of which can be pulsed individually at a computer calculated timing. The term phased refers to the timing and array refers to the multiple elements. The representation of phased array scan is known as the S-Scan or sectorial scan described in the Figure 8(a).[7]

An ultrasonic phased-array probe is comprised of multiple elements or many small ultrasonic transducers, usually between 16 and 128, each of which can be pulsed independently. The elements may be arranged in a variety of patterns as shown in the Figure 8(b) [8], the simplest of which is a linear array. Each element in the array can be pulsed individually or as part of a group to produce a wavefront. The multiple wavefronts produced from the elements then interfere to generate an overall wavefront or beam profile through constructive interference, which may be modified by varying the amplitude and timing of the excitation of each element. This beam can be steered electronically and is swept like a searchlight through the object being examined as

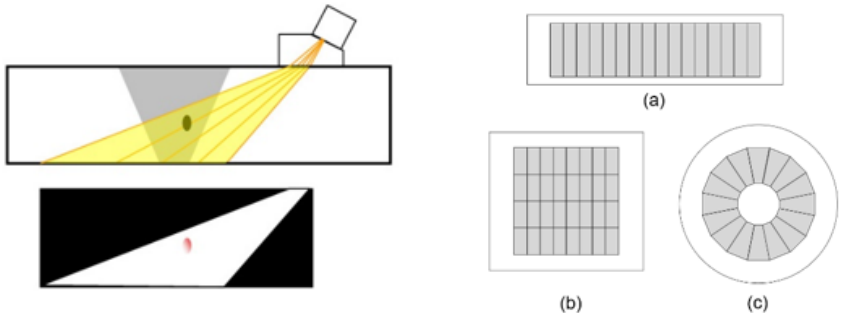

(a) (b)

Figure 8: PAUT Elements and Pulse Represenation: a)The depiction of a phased array ultrasonic pulse b)Examples of simple phased array element patterns.[30] (a) A 16-element linear array, (b) a 32-element matrix, and (c) a 16 element annular array [7]

shown in Figure 8(a). The data collected from multiple beams are put together to make a visual image showing a slice through the object through what is referred to as 'Focal law'. [8][10]

Conventional ultrasonic transducers commonly consist of a single piezoelectric element which can function as transmitter, receiver or both. A phased array transducer, however, contains 16 to 128 multiple individual piezoelectric elements. The elements are connected to separate electric channels and can be pulsed individually. Figure 9 illustrates a linear array phased array probe. [9][10][11][12]

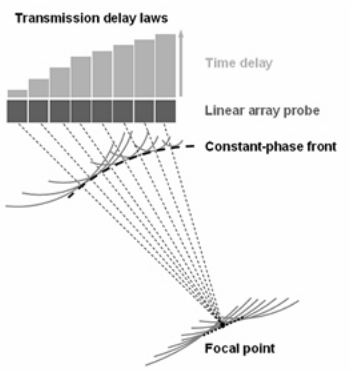

Figure 9: Linear Phased Array Transducer

The piezoelectric elements in a phased array transducer can be fired at different

times. After being pulsed, the waves generated by different elements undergo constructive and destructive interference with each other to create a new composite wave. The element firing times can be adjusted to steer the composite beam at different angles, or to create a focused beam at a point located at a depth specified by the user. [9][10][11][12]

To generate a wave to propagate through the material the piezoelectric elements should be pulsed with relative time delays for constructive interference between the individually pulsed waves to produce uniform acoustic pressure. The delay pattern for a desired beam depends on the velocity of the wave, spacing between the array and propagation angle. These factors and their synchronization to form a composite wave is termed as "Focal Law". By changing the focal law applied to array elements, the angle of the generated beam can be controlled electronically. [12]

A sequence of incremental changes in the focal law results in steering the composite beam generated by the array, i.e., sweeping out a fan-shaped sector [45]. The array can also be used to generate a composite beam focused at a specified point in the medium. To achieve this, an appropriate focal law must be applied to the elements such that waves generated by individual elements all interfere constructively at the desired location. Travel times of the waves from each element to the focal point are evaluated to obtain the appropriate focal law. Figure 10 illustrates beam steering and focusing with phased arrays. [9][10][11][12]

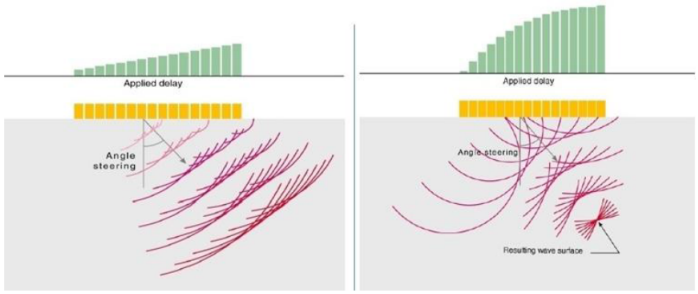

Figure 10: Beam steering with phased arrays, (a) unfocused beam (plane wave) and (b) focused beam [9]

In the sectorial scanning configuration ultrasonic pulses are launched sequentially at a sequence of angles into the test specimen by automated application of multiple focal laws. Focal laws are produced to generate beams which sweep through an

angular range with a specific increment. Figure 11 illustrates the principle of sectorial scan.[12]

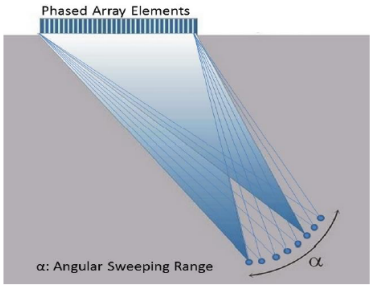

Figure 11: Principle of Sectorial Scan [14]

Ultrasonic phased array systems can potentially be employed in almost any test where conventional ultrasonic flaw detectors have traditionally been used. Weld inspection and crack detection are the most important applications, and these tests are done across a wide range of industries including aerospace, power generation, petrochemical, metal billet and tubular goods suppliers, pipeline construction and maintenance, structural metals, and general manufacturing. Phased arrays can also be effectively used to profile remaining wall thickness in corrosion survey applications.

There are specific benefits in using ultrasonic phased arrays for pulse-echo shear-wave inspection of thick-section welds including FSW joints. [8]

- The geometry of a weld determines the ultrasonic inspection angles that are required. A sectorial scan enables the inspection angle to be varied and tailored to the weld geometry and is particularly useful for inspections with restricted access. A typical sectorial scan involves a stationary probe, where the beam is made to sweep through a range of angles.

- The scan image produced allows instant visualization of any discontinuities detected. In some inspection situations, particular discontinuity orientations are expected (e.g., transverse cracks). Phased-array systems allow the inspection angle to be set accurately and modified to easily optimize the response from a detected discontinuity.

- Depending on weld and transducer dimensions, a phased-array transducer will likely need to be mechanically moved along a weld length for complete coverage

– this can be done manually or automatically. By attaching an encoder to the probe head, its position can be recorded and the ultrasonic data for each position displayed.

- A two-dimensional array could be used to reduce or eliminate the requirement for probe movement along the weld length, however this approach must be weighed against the significantly increased cost of large two dimensional probes, and the added difficulty of achieving good ultrasonic coupling with a large probe footprint.

- When a weld discontinuity has been detected and located, inspection angles and focal spot sizes can be easily optimized for accurate sizing and improved characterization of that particular discontinuity – resulting in improved inspection reliability.

- Furthermore, like a number of conventional ultrasonic systems, some phased-array systems are capable of performing time-of-flight diffraction (TOFD) inspections, which is a defect-sizing technique that is often more accurate than standard amplitude sizing methods. [8]

Despite the advantages of ultrasonic phased arrays, there are limitations that need attention prior to employing this technology for non-destructive inspections. The risk for not reliably detecting discontinuities is much greater especially for FSW welds. Phased-array equipment is more complex and hence more difficult to operate than conventional instruments and assimilating the wide range of data presentation modes offered by the equipment.

The selection if the angle of incidence is very important in the inspection of welds, hence it is wrong perception that one wide angled sectorial scan will detect all the discontinuities in the weld. As ultrasonic response is dependent on:

- Angle of incidence on discontinuity

- Location of the array

- Thickness of plate

Many discontinuities will not be oriented at favorable angles to be detected. Consequently fixed angle scans should be used to inspect the fusion faces of the weld to ensure that the beam is maintained normal to the weld preparation angle. In effect, this approach is similar to the conventional UT but with the benefit of being able to configure other beam profiles to achieve greater coverage within the weld volume. [8]

2.2 Review of UT on Friction Stir Welding

FSW is a solid-state welding process experimentally proven at The Welding Institute (TWI), UK in the year 1991. Since its inception it has been successfully applied to the joining of metals such as aluminum, magnesium, copper and steel. Recent advancements in FSW technology, especially in University of Washington's Solheim Manufacturing Science and Technology Laboratory has made it possible to extend its reach to titanium and its alloys, high strength materials, very efficiently including joining of dissimilar alloys.

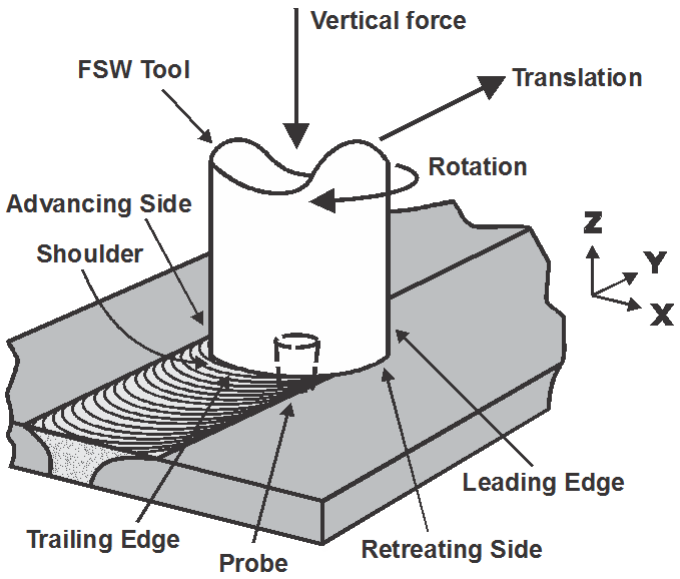

Figure 12: Schematic of FSW[2]

FSW is performed without any filler material or flux and at lower temperatures than the fusion temperatures of the joining materials, leading to low level of joint distortion and residual tension. In this process the metal is not melted but it is

Table 4: Advantages of FSW [15]

Metallurgical Benefits	Environmental Benefits	Energy benefits
Solid phase process	No shielding gas required	Improved materials use (e.g., joining different thickness) allows reduction in weight
Low distortion of work piece	No surface cleaning required	Only 2.5% of the energy needed for a laser weld
Good dimensional stability and repeatability	Eliminate grinding wastes	Decreased fuel consumption in light weight aircraft, automotive and ship applications
Excellent metallurgical properties in the joint area	Eliminate solvents required for degreasing	
No loss of alloying elements	Consumable material savings	
Fine microstructure		
Replace multiple parts joined by fasteners		
Absence of cracking		

mechanically plasticized at the place of joining by a specifically designed tool. Welds are made by plunging a rotating cylindrical tool into the joint to be welded. The heat the friction generates is sufficient to locally soften the work pieces, and the rotating motion of the tool stirs the work pieces together as the tool is advanced along the joint line. The schematic for this process is shown in the Figure-12[2]. Table-4 summarizes the advantages of FSW process which gives us a glimpse of how efficient the process is to the aerospace industry, both commercially and environmentally.

There are several welding parameters taking influence over the final welding quality, namely: vertical force, rotation speed, travel speed, tool geometry and tilt angle between the tool and welding materials. These parameters should be carefully selected as they directly affect the quality of the weld. Since this process retains the relatively

[2]http://robotics.engr.wisc.edu

fine grained microstructure of the parent material it lends itself to the superplastic forming process (SPF). This demands the need for better NDT techniques for better interpretation of material properties and manufacturing processes from conventional weld inspections. [16, 17]

A brief overview of these flaws is presented, followed by a review of the pertinent literature. The literature in regard the defects in FSW is well established and gives information about the types, causes and effects of faults in friction stir welding. The defects and flaws are considered as separate entities in the paper. The **Imperfection** is defined as a departure from quality characteristic from its intended condition. Flaws and Defects are two different entities which are the subset of imperfections. A **Defect** is considered to be an imperfection which compromises teh quality and integrity of the structure. It is an imperfection of size, location, shape, orientation and properties which have to be reject-able which is deemed in-tolerable. While a **Flaw** is defined as an imperfection detectable by NDT but whose significance is not been established and probably be tolerated in the structure. This implies that not all "Flaws" are "Defects" and their classification depends on the requirements of the process and design considerations. [17]

The Flaws are classified into four types:

Volumetric Flaws or Voids: Are voids or gaps in the weld, possibly breaking through the surface. An example is shown in Figure-13(a).

Weld Line Flaws or Lack of Penetration (LOP): These flaws pertain to flaws associated with the original weld line. A typical case is lack of bond along the weld-line, or a portion of the weld-line left unwelded. This is shown in Figure-13(b).

Joint Line Remnants: This is the “distribution of oxide particles through the thickness of the aluminum" and shown in Figure-13(c). It often resorts in a weaker bond.

Excessive Flash: Flash is the metal ejected from the weld. It is often attributed to excessive heat input.

These flaws have no resemblance to those of the conventional welding methods and need to be addressed distinctly. Lack of penetration occurs due to improper pin tool

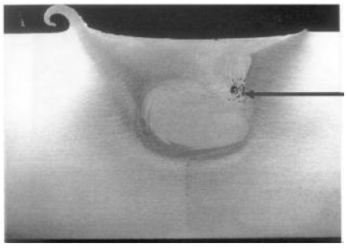

(a) Volumetric Flaw [17]

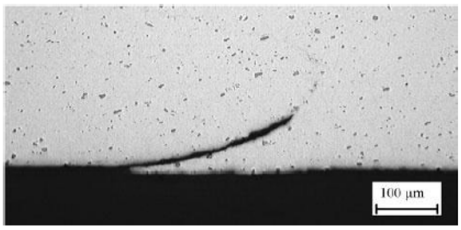

(b) LOP [17]

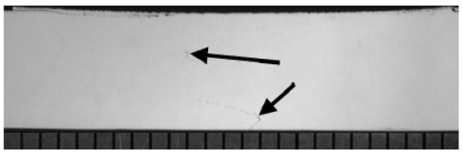

(c) Joint Line Remnant [18]

Figure 13: Classification of Flaws in FSW

penetration depth. Flow related defects can occur due to processing parameters that are considered too hot or too cold. Hot processing conditions with sticking contact conditions cause excessive material flow, flash formation, surface galling and nugget collapse. Cold conditions with slip conditions, insufficient flowing material results in surface lack of fill, wormhole, or lack of consolidation defects on the advancing side. It is assumed that optimum parameters cause a stick-slip wiping flow and the material flowing from the region ahead of the pin tool is exactly balanced with the material flowing into the vacated region behind the translating tool. The Flaws and their causes is summarized in Table-5. [18]

Ultrasonic waves propagating in a specimen under test provide great information about its invisible structure based on the transmitted and/or reflected signals. The most serious defect associated with the joint line remnant is located at the weld root. The extreme condition is a lack of bond caused by incomplete penetration, which could be caused by a shortened pin or by poor control of tool position or force. The most difficult flaw to quantify is a region of weakly bonded material in the root of the weld. Such regions can exist at the end of root flaws, but will always follow the path of the joint line remnant. They are very difficult to detect non-destructively since a bond exists. Conventional flaws, for example voids and incomplete bonds, could be detected by the conventional ultrasonic method [19]. While the vast majority of FSW joints are expected to be free of defects, it is not always possible to assume that they are completely flaw free. To improve confidence in the design, manufacture, and

Table 5: Defects, location and causes in Al FSW [18]

Flaw type	Location	Causes
Void	Advancing side at edge of weld nugget	*Reduced forging pressure *Welding speed too high *Plates not clamped close enough together. Joint gap too wide.
Void	Beneath top surface of weld	*Welding speed too high
Joint line Remnant	Weld nugget, extending from the root of the weld at the point where the original plates butted together.	*Inadequate removal of oxide by tool *Inadequate disruption and dispersal of oxide by tool *Increase in welding speed *Increase in tool shoulder diameter
Root Flaw	Weld nugget, extending from the root of the weld at the point where the original plates butted together.	*Tool pin too short *Incorrect tool plunge depth *Poor joint to tool alignment

application of FSW joints, manufacturers are seeking data on the properties of welds containing flaws and requiring validated inspection techniques. Due to the additional complexities to be addressed, as discussed above, associated with FSW, conventional UT techniques will have difficulties in focusing the ultrasonic beam on the area of interest. [20]

Phased Array Ultrasonic Testing method (PAUT), which uses use of multiple wave generating elements and the ability to focus and stir the ultrasonic beam without movement of the probe, while the images are formed by constructive interference, can be a good indicator of defects in FSW. PAUT has gained NDT acceptance in the last few years, and it is now customarily employed in weld inspection applications. The paper titled " Non-destructive detection of lack of penetration defects in friction stir welds" (C Mandache et al, 2012) has identified the LOP defect with respect to Aluminum alloys using PAUT. [21]. It compares various NDT methods and PAUT, though able to identify defects, was conservatively judged. In the paper "Correlation of Phased Array..." [20], the authors compare PAUT with the fatigue data. The results phased array testing, according to the paper, demonstrated a strong relationship

between the NDE results and the fatigue performance for the Al 2024 FSW joints.

PAUT allows a quantitative assessment of the stirring quality of the bond and indicating the presence of joint line remnant flaw. It is able to discriminate the weld nugget from the base materials and fully able to detect joint line remnant down to 0.2mm deep. The NDE method can demonstrate variances in weld quality. This technique can record the variances in the weld and has been established to measure the quality of the weld even if there is no direct signal from a flaw [20].

Ultrasonic phased array technique gives an "outstanding performance" in inspecting tiny, tight void defects by a single-pass scan according to [22]. Phased arrays also permit lateral scanning to detect transverse defects generated by FSW. NDT methods of X-ray detection, ultrasonic C-scan testing, ultrasonic phased array inspection and fluorescent penetrating fluid inspection can successfully apply in quality control of FSW joints without destroying welding material. [22]

Several investigations of NDT methods on FSW welds have been carried out by researchers since the inception of this novel manufacturing process. Most of the literature on the NDT methods is focused on Aluminum and its alloys. This is expected as the demand for Titanium in the industry has increased recently. The research of NDT methods has not yet entered the study of dissimilar alloys of Titanium and its alloys. Our research focuses to bridge the gap using phased array ultrasonics to detect the defects in similar and dissimilar Titanium alloys.

2.3 Review of UT on Diffusion Bonding

Diffusion bonding (DB) is a solid state welding process. In this process two clean metallic surfaces brought in contact in an inert atmosphere under a low pressure for a period of time at elevated temperatures usually 50 to 70% of their melting point to allow some creep deformation, interface diffusion, recrystallization and grain growth to take place. Diffusion involves transfer of atoms across the boundaries due to concentration gradients. It is a clean welding process without incurring any material loss. It can be used commercially to join similar and dissimilar metals. [23]

DB has been considered as a potential welding method and increasingly used in the field of aerospace and industry, which has many advantages such as high performance, significant cost and weight savings, and low requirement for the weldability of materials. Thin sheet diffusion bonding is normally achieved at high temperatures, mostly at 950 ^oC for Ti alloys (higher than half of the melting point, and at fairly low pressure. The DB process can be described in two stages. In the first stage, the contacting surface undergoes plastic and creep deformations so that the contact area increases. The interface consists of regions of intimate contact separated by voids and is sensitive to stress. In the second stage, volume diffusion and grain boundary migration mechanisms take place such that there is ideally no evidence of the interface. the grain boundaries are no longer planar and the small voids have been eliminated. The superplastic forming (SPF)to form a highly structured material is a great advantage of this process. [24]

The successful production of bonds depends on number of parameters including pressure, temperature, time , quality of the material, surface preparation and cleanliness. Gross deviations may lead to total failure of the bond or localized "unbonded" regions. Lack of supervision during preparatory steps may induce unwanted impurities such as oxides, grease and other organic substances on the mating surfaces. Their presence interferes with establishing a complete bond between the materials. As a result various defects are induced in the bond in the form of voids and kissing bonds at the interface to name a few. A dangerous possibility is however the formation of brittle layer of alpha case. This can happen if significant quantities of air are present during the bonding process. These defects can degrade bonding strength, especially fracture toughness and fatigue strength. Thus, it is necessary to develop non-destructive evaluation of DB.

The conventional ultrasonic technique for the detection of defects in DB bonds is to send an ultrasonic pulse into the material and look for changes in the amplitudes of the reflected wave and the distance from the surface. The transducers or probes are capable of both transmission and reception of the wave. Broadband piezo-electric transducer with a focused beam and a short duration pulse is used for this type of inspection. Pulse-Echo inspection is usually preferred to detect the planar defects and planar array of defects from which the direction of reflected energy is predominantly towards the single receiver. The detection of embedded layer of alpha case falls into

this category. Also, only single-sided access is requires eliminating the need to reach both the sides. [25]

Ultrasonic NDT on DB of Titanium was performed by [26] , dating back to 1969, and this stating that the UT C-scan was representative of actual joint quality. Though it was indicated that the artificial contaminants were not detected by the ultrasonic method. Although ultrasonic methods were constantly improved over the years, the problem of small defects is still being the issue for this method of inspection[24]. The limitation to this method is that only defects of size $250\mu m$ can be detected. Defects smaller than this method [27]. In Titanium, the sensitivity of a pulse-echo inspection is limited, since noise back-scattered by anisotropic microstructure can mask the reflections from the defects. Furthermore, diffusion bond between Ti alloys create a planar interface between 'macrozones'- the regions where grains have a preferred crystallographic orientation. While typical grain diameter is $50\mu m$ for forged titanium, a macrozone may be sevaral millimeters in diameter. The interface acts as weak but spatially coherent reflector, analogous to that between two dissimilar materials, which may mask reflections from defects.[28]

A simple interfacial spring model predicts that, for partial bonds (sub-wavelength voids distributed on the bondline) and at certain frequencies the phase of the signal can be used to separate the component of the signal due to the flaw [28]. This method will be used to analyse the diffusion bonds in our research. We will be using this method for the similar as well as the dissimilar bonds of titanium alloys. [28]

2.4 Review of UT on Composite Drilling

Composites, as we know, can be defined as a combination of two or more materials with very different mechanical, thermal and electrical properties. Due to the low weight and high strength of composites, they are widely used in aircraft and wind turbine blades. Delamination is one of the most common defects for the composite materials. It degrades the mechanical properties and also causes the failure of overall composite component. to detect the defects and ensure safe operation of composite components, NDT Techniques are used during both manufacturing and operation of the materials [29]. Although Phased Array is not rated as the best method to deal

with these kind of defects, we wanted to test the capability of PAUT on detecting the delamination of surface of drilled holes on composites. [29]

3 EXPERIMENTAL SETUP & INTERPRETATION AND ANALYSIS

3.1 Interpretation and Analysis of Diffusion Bonds

3.1.1 Interpretation of Ultrasonic Testing on DB

The pulse-echo inspection of DB is best illustrated in Figure-14. Figure-14(a) shows the defective joint and identifies schematically the reflections from each interface of the joints. In the case of low frequency transducer the transmitted wave is reflected back to the surface and the total penetration into the volume is not possible. Figure-14(b) suggest the transmission of a wave generated by a high frequency transducer. The schematic diagram identifies reflections from each of the interfaces from the joint namely R1, R2 and R3. Each time the pulse is incident on the the interface which there is change in acoustic impedance, a partial reflection takes place and returns to the transducer. The presence or absence of defect can be determined simply by using an electronic gate to limit the monitoring of reflections to the time period when the first reflection would return from the bondline. If any reflection can be detected within the gate then some change of acoustic impedance is inferred at the bondline.

According to the literature, the reflection coefficient R_{12} should be determined to assess the quality of the weld using conventional ultrasonic testing methods. The magnitude of reflection coefficient is commonly used to evaluate the interfaces. The reflection coefficient is calculated as follows.

$$R_{12} = \frac{A_i}{A_f} \tag{2}$$

Where R_{12} is the reflection coefficient, A_i is the Amplitude of the wave at the interface and A_f is the amplitude of the incident wave calculated from UT.

The reflection coefficient is also related to the Acoustic Impedance (Z) of the material as [28]:

$$R_{12_{Th}} = -\frac{Z_1 - Z_2 + i\omega(Z_1 Z_2/K)}{Z_1 + Z_2 + i\omega(Z_1 Z_2/K)} \tag{3}$$

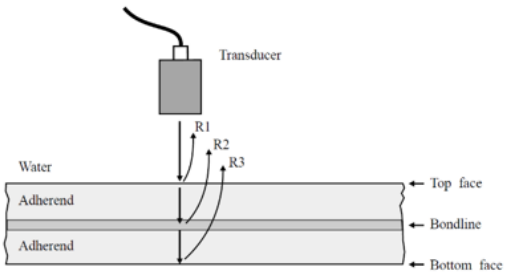

(a) A-Scan Inspection of DB

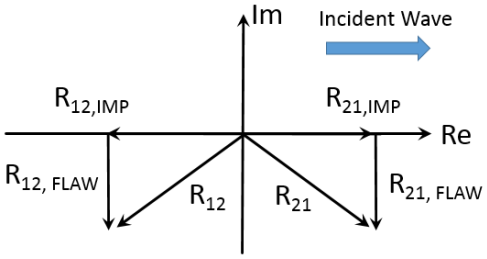

(b) Components of Signal Reflection Coefficient

Figure 14: Signal path in Diffusion Bonding Specimen [24, 30]

Where $R_{12_{Th}}$ is the reflection coefficient calculated theoretically, K is Interficial Stiffness, Z_1 and Z_2 are the acoustic impedance of dissimilar materials and ω is the angular frequency.

For an imperfect interface between the two media with different acoustic impedance, if the component of reflection coefficient, due to the flaw, is small because of the difference in acoustic impedance of the two materials. It may therefore be possible to separate well bonded and partially bonded samples through plotting the contour plot of the calculated reflection coefficient R_{BOND} by the equation given below.

$$R_{BOND} = R_{IMP} + R_{FLAW} \tag{4}$$

For similar materials, the acoustic impedance is Z, this equation boils down to

[28]:

$$R_{12} = \frac{-\frac{i\omega}{\Omega}}{1 + \frac{i\omega}{\Omega}} \tag{5}$$

where Ω is the characteristic frequency:

$$\Omega = \frac{2K}{Z} \tag{6}$$

The difference in amplitudes is a measure of the acoustic impedance of the materials, leading to the reflection and refraction of the sound waves. Electronic Gates are computer programmed to display these values on the LCD screen of the equipment. These equations form the basis of a contour plot generated with the reflection coefficients.

3.1.2 Sample Specification

The samples shown in Table-6 have been diffusion bonded together at the temperatures T1 to T8 in the increasing order of temperatures.

The pictures of samples used are displayed in Figure-15.

(a) (b)

Figure 15: DB Samples

Table 6: DB Ti Alloys with their Temperature

SL No.	**Titanium Alloys**	**Temperature**
1	21S-21S	
2	21S-6242	
3	21S-64	
4	21S-64FG	T1
5	54M-21S	T2
6	54M-54M	T3
7	54M-64	T4
8	6242-54M	T5
9	6242-6242	T6
10	6242-64	T7
11	6242-64FG	T8
12	64-64	
13	64-64FG	
14	64FG-54M	
15	64FG-64FG	

3.1.3 Inspection Methodology and Analysis

A $1.5in\ X\ 1in$ $(38mm\ X\ 25mm$J) area is identified on the specimen which is ultrasonically scanned as shown in Figure-16(b). The area is then divided into a grid of 8 X 9 squares with an average length and breadth of the square being equal to $0.1in$ ($2.5mm$) as shown in Figure-16(c). The samples are scanned from both sides to check the variance of reflection coefficients. For this a straight beam probe with frequency of $10MHz$ and diameter of $0.3in$ is used on the samples. The K value at this frequency of probe is assumed to 10^{16}N/m [28]. The probe is moved through the entire grid to cover the whole volume of the inspected area. High frequency probes have the ability to detect smaller defects in the samples compromising the penetration capability. The smallest defect we can detect through this method is $\approx$ 250 μm as given by the wavelength $\lambda = \frac{V}{f}$. For this case sound wave velocity (V) of Ti alloys is in the range of 6030 m/s and the frequency of the probe is $10MHz$.

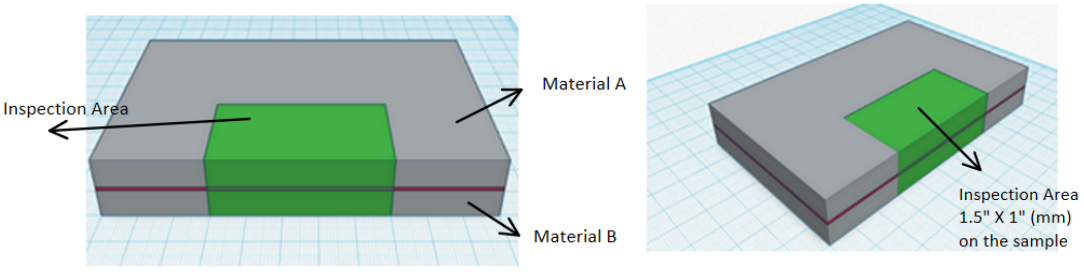

(a) Rep. of Diffusion Bond (b) Inspection Zone

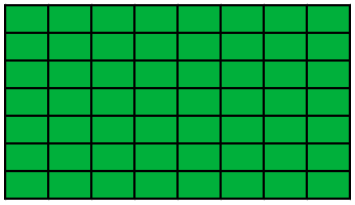

(c) Grid of 8 X 9

Figure 16: DB Samples

The data is collected from each of the 8 X 9 data points we obtained on the grid which is analyzed using EXCEL and MATLAB program which interpolates the data we collected from 72 points on the grid to 100 X 100 data points. This is plotted as a $2-D$ contour plot which gives us the magnitude of defects and their locations.

3.2 Interpretation and Analysis of Friction Stir Welds

3.2.1 Interpretation of Phased Array Ultrasonic Testing on Friction Stir Welding

The principles of PAUT is already explained in the Section 2.1.2. This section will take us through the interpretation of phased array Scan. The phased array sectorial scan or S-scan is the amalgamation of A-scans taken by each of the piezo-electric elements in the probe. The Figure-17(a) explains the sectorial scan. A probe is programmed such that it illuminates the weld as shown in Figure 17(b). In the first leg, only the bottom half of the weld is illuminated. However, with reflection from the ID surface the entire weld is illuminated and the complete weld volume can be inspected.

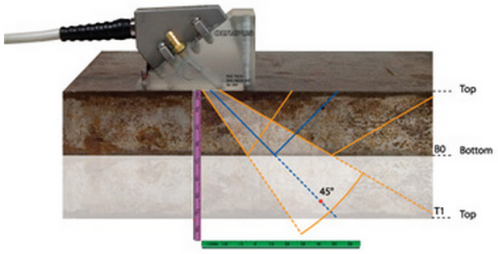

(a) Sectorial Scan Representation [12]

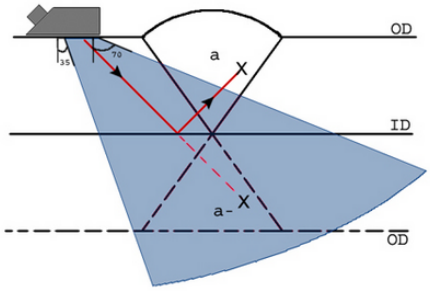

(b) Concept of Legs

Figure 17: Sectorial Scanning of FSW

Ultrasonic testing could also be utilized to estimate the Mechanical properties such as elasticity moduli (E), shear moduli (G) and Poisson ratio (ν). By determining the longitudinal velocity (V_L) and the transverse velocity (V_T) of ultrasonic waves, elastic

properties can be estimated by the following relations:

$$E = \rho\ C \tag{7}$$

$$C = V_T^2\ \frac{3V_L^2 - 4V_T^2}{V_L^2 - V_T^2} \tag{8}$$

$$G = \rho V_T^2 \tag{9}$$

$$\nu = \frac{\left(\frac{V_L}{V_T}\right)^2 - 2}{2\left[\left(\frac{V_L}{V_T}\right)^2 - 1\right]} \tag{10}$$

Where C is the characteristic velocity and ρ is the density of the material (For Ti $\rho = 4.43gm/cc$)

The process to estimate the Young's Modulus (E) is to perform a simple A-scan on the weld zone. As the sample is of known thickness, the longitudinal velocity has to be calibrated until the A-scan shows the sample thickness on the UT device. Also, the shear velocity or the transverse velocity (V_T) of sound is nearly half of that of the longitudinal velocity (V_L). By using the relations above we can estimate the Young's modulus of the region dominated by the dissimilar alloy combination of materials during the joining process. This data will be compared to the bend testing data available by mechanical testing of the same samples. The procedure employed by us to estimate the Young's Modulus will inevitably have a parallax error as the specimen are not completely smooth and hence the thickness not being constant. However this will provide an idea of the elastic modulus of the sample with combination of materials. [31, 32, 33]

3.2.2 Sample Specification

The process variables in welding the samples using FSW process are the weld speed (feed) and the tool rotation speed (RPM). The specimen are manufactured under

closely monitored FSW process performed by experts. The Table-7 represents the similar and dissimilar alloys being welded by FSW at various conditions. There are totally 57 combinations of samples in FSW with 4 Similar alloys and 8 dissimilar joined under 5 different process conditions. Figure-18 represents the schematic of the FSW sample identifying the inspection zone.

Table 7: FSW samples and their Process Conditions

Ti Alloys used	**RPM/ Feed Rate**	**RPM/ Feed Rate**
	in/min	**mm/min**
54MFG-54MFG		
54MFG-6242SG		
64SG-64SG		
54MFG-64FG	225/5	225/127
54MFG-64SG	275/4	275/101.6
64SG-6242SG	275/5	275/127
6242FG-6242FG	275/6	275/152.4
6242SG-6242SG	325/5	325/127
54MFG-6242FG		
64SG-6242FG		
64FG-64FG		
64FG-6242FG		

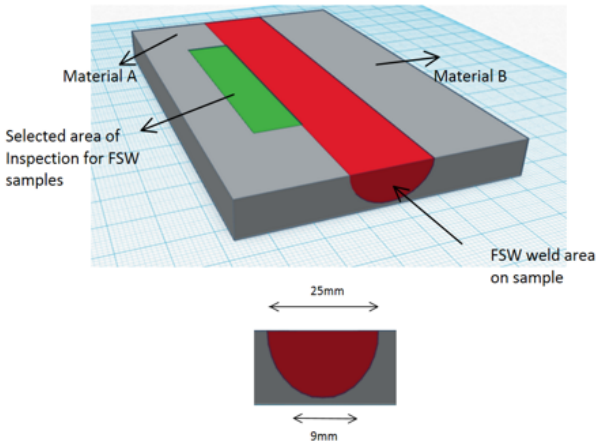

Figure 18: FSW sample representation and its inspection zone

3.2.3 Inspection Methodology and Analysis

On the samples under study, the phased array ultrasonic testing is performed at discrete locations, at intervals of approximately 12 mm along the weld on the inspection zone of 50 $mmX10\ mm$ as shown in Figure-19(a), in order to capture information on various defects. The inspections were performed from the tool side using a linear array of 10 elements, creating waves of 5 MHz frequency, adapted with a shear wave wedge able to generate waves at 39^O incidence in the Ti alloy. The wedge and array assembly were able to generate a beam spread between 45^O and 70^O in the samples under test. The gain is set based on the attenuation of the signal without interference of the external noise so that we see visible amplitudes of the echoes.

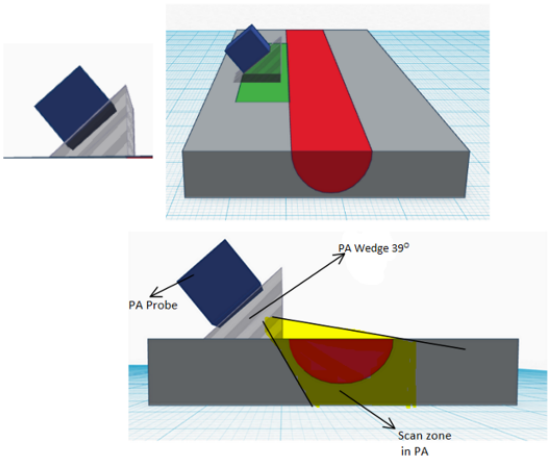

(a) PA probe and Inspection Zone representation

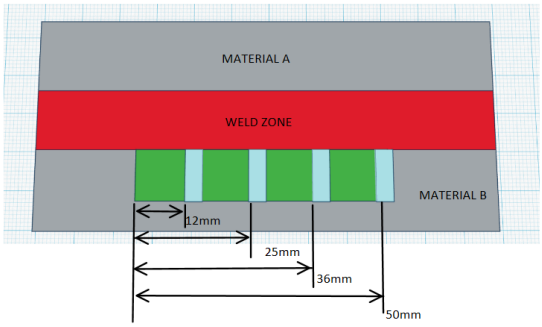

(b) Positions of Inspection on Inspection Zone

Figure 19: Schematics of Inspection methodology used in FSW

For investigating the Young's Modulus the measurements of velocity V_L are taken at four discrete points, as shown in Figure-19(b). The velocities are then averaged for estimation of the Young's Modulus (E) of the weld zone.

The probe placement and the scanning zone is shown in the Figure 20 which is called the "Scan Plan" using the principles of "Focal Law". The Focal law is nothing but "Ray Tracing" of the sound waves to cover the entire weld volume. The wedge inclined at 39^O is used to introduce refracted shear waves into the sample. The sound waves are set at the angles 45^O and 70^O to scan the complete weld zone. This sound wave scatter enables us to detect the defects oriented perpendicularly to the direction of probe.

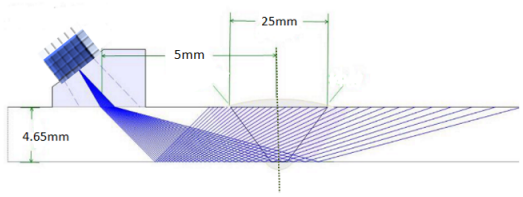

Figure 20: Scan plan of a phased array ultrasonic inspection. The blue lines represent the direction normal to the plane wave fronts generated by the active phased array elements

3.3 Equipment Used

Olympus OMNISCAN SX is a portable UT device capable of A-B-C scans and phased array technology. The major components of a typical industrial phased ultrasonic inspection system are the probe which is connected to pulser and receiver instrument and a wedge which will be in contact with the test specimen. The sound beam needs a couplant for propagation to the material. For this purpose an ultrasonic gel " The PAUT wave propagates through the wedge and refracts into the test piece where it interacts with the flaws. The echoes at the interfaces are returned to the same wedge and the transducer identifying the intensity and location of flaws. The Equipment setup is shown in the Figure-21.

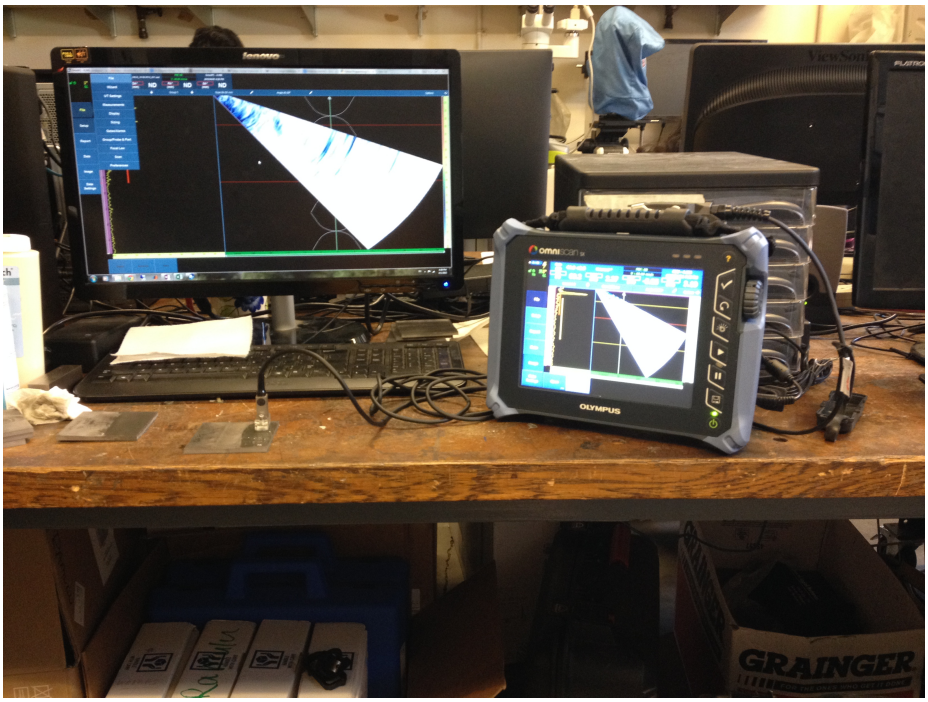

(a) Equipment

(b) Ultrasonic Couplant

Figure 21: Ultrasonic Equipment Setup

4 RESULTS AND DISCUSSION

4.1 Diffusion Bonding

The thickness after diffusion bonding are presented in the Table-8. This data will be helpful for us to identify the interface on the sample post bonding.

The samples are ultrasonically inspected following the methodology outlined in Section-3.1.3. The A-Scans of a diffusion bonding sample of Ti54M-Ti54M at T2 and T5 are shown in Figure-22.

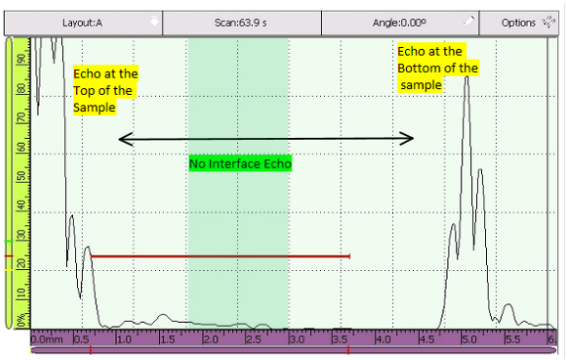

(a) Ti54M-Ti54M at T5

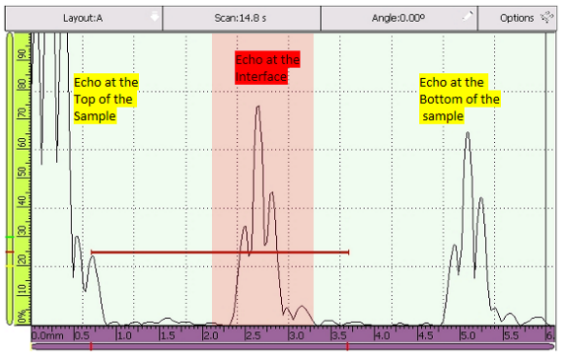

(b) Ti54M-Ti54M at T2

Figure 22: Representation an A-Scan for Ti54M-Ti54M

The location of the interface is manually displayed on the A-scan with a transparent window.For the Figure-22(a) we find the interface window in green, which signifies that there is no reflection of sound wave from the interface. This represents good bonding. However, in Figure-22 (b), the window is displayed in red which implies

Table 8: Sample Thickness Post Bonding

Ti-Alloy Combination			TEMPERATURE								
			Units	T1	T2	T3	T4	T5	T6	T7	T8
THICKNESS	64FG-64FG	64FG	in	0.99	1.00	1.00	0.99	-	-	-	-
			mm	2.52	2.55	2.55	2.51	-	-	-	-
		64FG	in	0.99	1.00	0.99	1.00	-	-	-	-
			mm	2.52	2.54	2.52	2.53	-	-	-	-
	64-64FG	64	in	0.41	0.41	0.42	0.42	0.40	-	-	-
			mm	1.05	1.05	1.07	1.06	1.03	-	-	-
		64FG	in	1.02	1.01	1.00	1.00	1.00	-	-	-
			mm	2.60	2.55	2.54	2.54	2.54	-	-	-
	64FG-21S	64FG	in	1.01	1.02	1.02	1.02	1.02	-	-	-
			mm	2.56	2.60	2.60	2.58	2.58	-	-	-
		21S	in	0.27	0.28	0.28	0.27	0.28	-	-	-
			mm	0.69	0.72	0.70	0.68	0.71	-	-	-
	64FG-6242	64FG	in	1.00	1.00	0.99	1.00	1.00	-	-	-
			mm	2.54	2.54	2.50	2.53	2.55	-	-	-
		6242	in	0.42	0.42	0.40	0.41	0.38	-	-	-
			mm	1.07	1.07	1.01	1.04	0.98	-	-	-
	54M-54M	54M	in	0.97	0.96	0.97	0.96	0.97	-	-	-
			mm	2.47	2.44	2.46	2.44	2.47	-	-	-
		54M	in	0.97	0.96	0.98	0.97	0.97	-	-	-
			mm	2.46	2.44	2.48	2.48	2.46	-	-	-
	54M-6242	54M	in	0.97	0.96	0.96	0.97	0.97	0.98	0.98	-
			mm	2.46	2.43	2.44	2.47	2.46	2.50	2.48	-
		6242	in	0.42	0.42	0.42	0.39	0.40	0.41	0.39	-
			mm	1.08	1.06	1.06	0.99	1.01	1.04	0.99	-
	54M-21S	54M	in	0.97	0.99	1.00	0.98	0.98	0.97	0.96	-
			mm	2.47	2.52	2.54	2.49	2.49	2.47	2.44	-
		21S	in	0.27	0.28	0.28	0.26	0.27	0.26	0.26	-
			mm	0.69	0.71	0.71	0.67	0.69	0.67	0.67	-
	64-54M	64	in	0.41	0.41	0.41	0.40	0.40	0.42	0.40	-
			mm	1.04	1.04	1.04	1.02	1.02	1.07	1.02	-
		54M	in	0.96	0.96	0.97	0.95	0.97	0.98	0.97	-
			mm	2.44	2.43	2.46	2.42	2.46	2.50	2.47	-
	64FG-54M	64FG	in	0.98	0.98	1.00	0.98	0.97	-	-	-
			mm	2.50	2.48	2.53	2.48	2.46	-	-	-
		54M	in	1.02	1.03	1.03	1.02	1.01	-	-	-
			mm	2.59	2.60	2.61	2.59	2.58	-	-	-

that there is a reflection from the interface of the bond. Ideally the reflection from the interface is not desired, but this signifies a defect in the material. The ultrasonic thickness of the of the samples can be correlated to the thickness of the same sample mentioned in Table-8 with an error in magnitude of $\approx 0.01\%$. The A-Scans are taken directly from the ultrasonic equipment.

The data is collected from all points of the 8 X 9 grid, as described in the section 3.1.3, for computing the reflection coefficient. The data is then processed using MATLAB, refering to the equations mentioned in Section 3.1.1, to analyze the data as a contour plot. The data is interpolated using Gaussian Distribution over the entire area. The significance of the contour plot is that it tells us the extent of defects, the net area defected and the location of it. This is similar to what a C-Scan does in certain respects. An example contour plot is shown in the Figure-23.

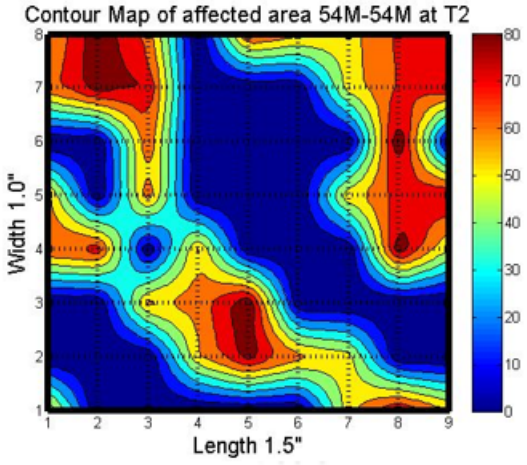

Figure 23: Contour Plot of Ti54M-Ti54M at T2

The regions of the contour plot represent the reflection coefficients we observed ultrasonically while inspection. The colorbar towards the right of the plot indicates the range of reflection coefficients calculated in the range of 0 to 100 as a percentage. The dark red region severe defects mostly implying that there is no bond between the base materials. The blue regions indicate the areas where there is no reflection from the interface. It can be considered as good bonding between the alloys, but further investigation should be carried out for determining its quality. The same methodology is carried out on all the samples of similar and dissimilar alloys and the results of few samples are displayed in the Figures-24 to 36.

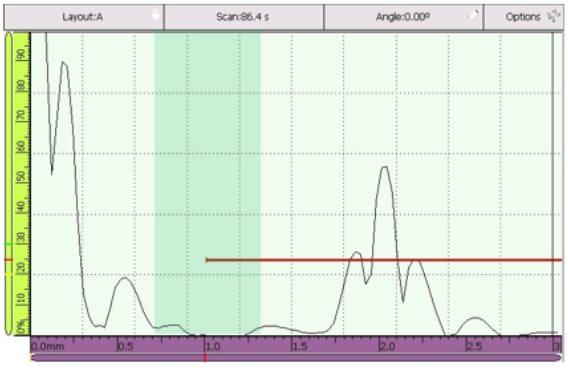

(a) A-Scan

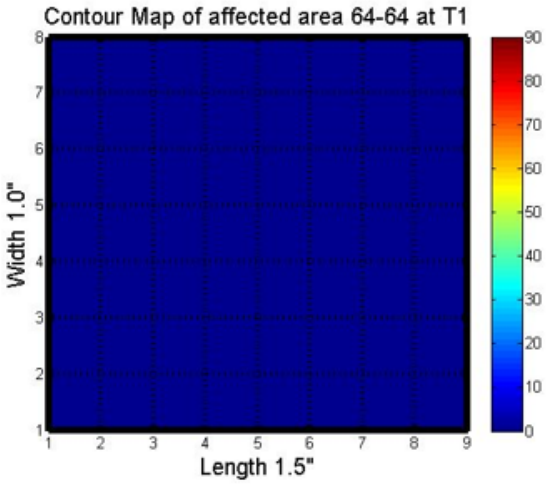

(b) Contour Plot

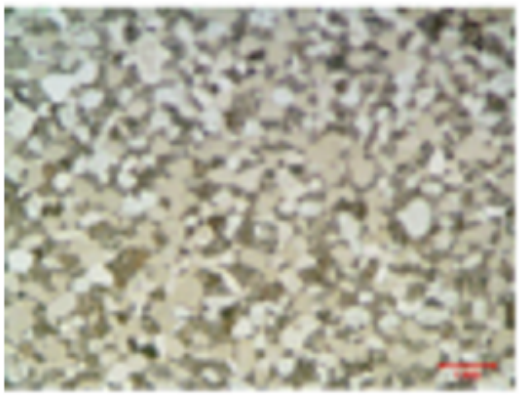

(c) Micrograph

Figure 24: Good Sample of Ti64-Ti64 at T1

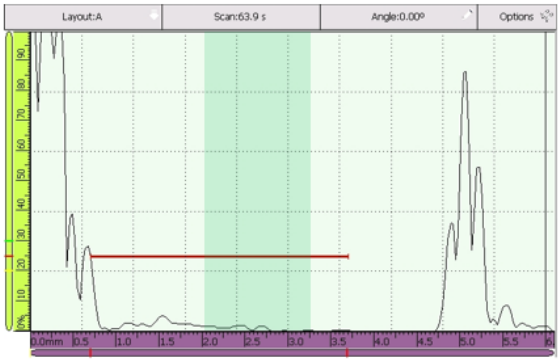

(a) A-Scan

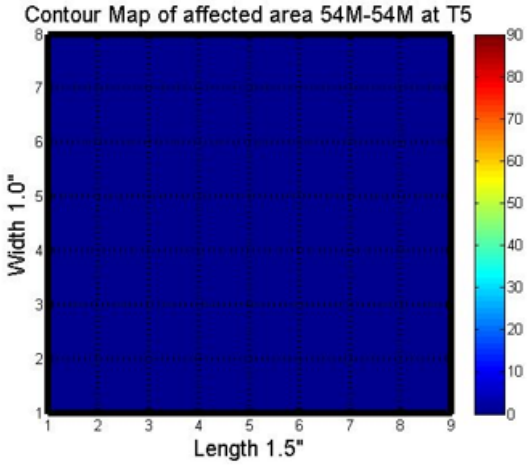

(b) Contour Plot

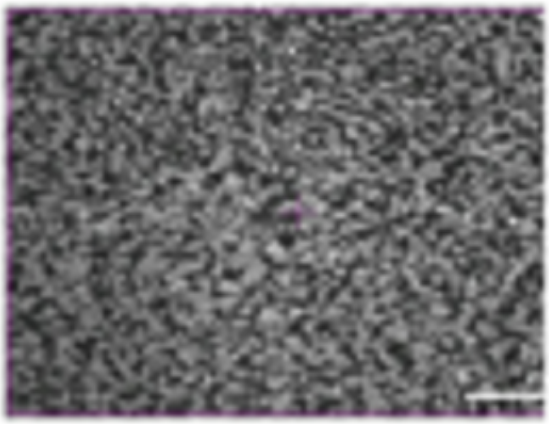

(c) Micrograph

Figure 25: Good Sample of Ti54M-Ti54M at T5

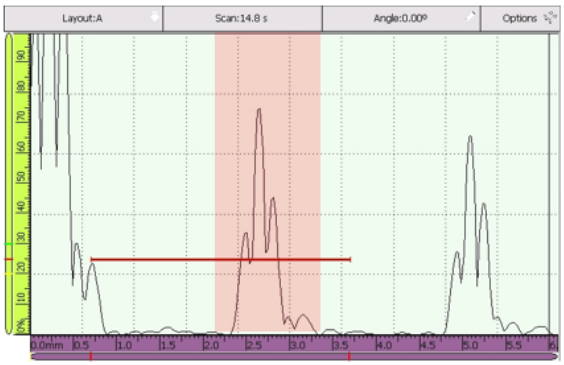

(a) A-Scan

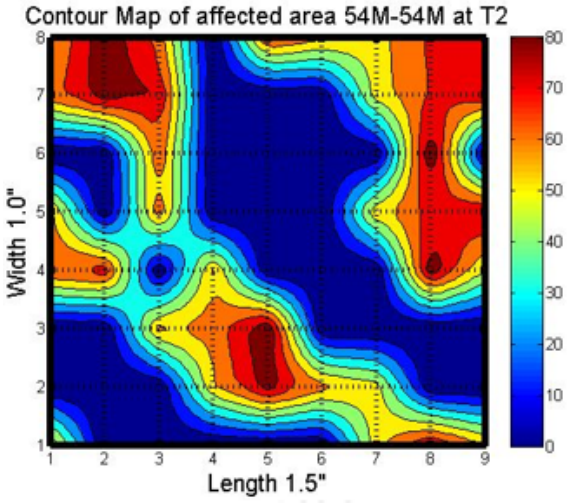

(b) Contour Plot

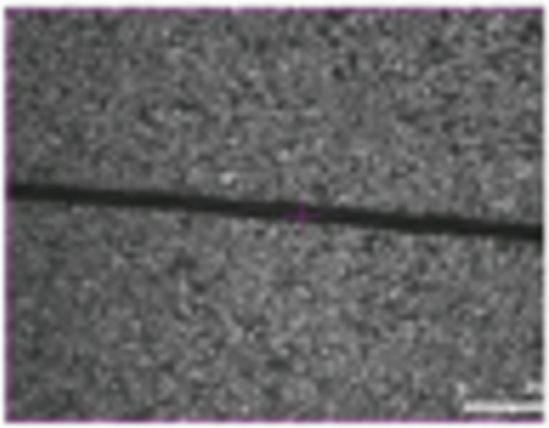

(c) Micrograph

Figure 26: Defective Sample of Ti54M-Ti54M at T2

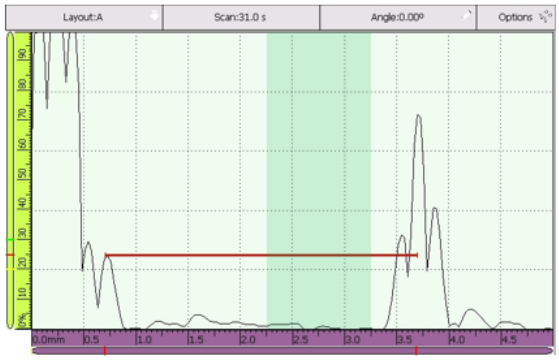

(a) A-Scan

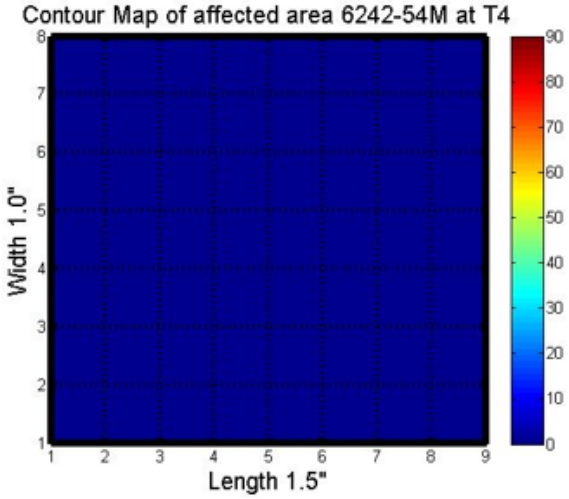

(b) Contour Plot

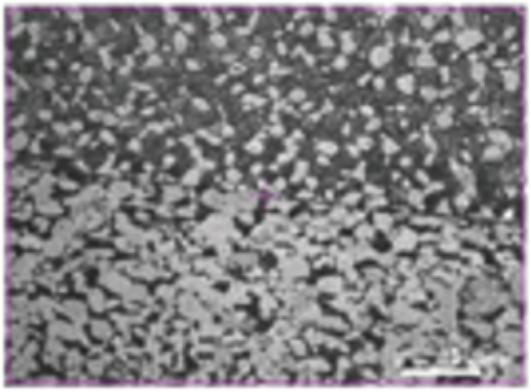

(c) Micrograph

Figure 27: Good Sample of Ti6242-Ti54M at T4

(a) A-Scan

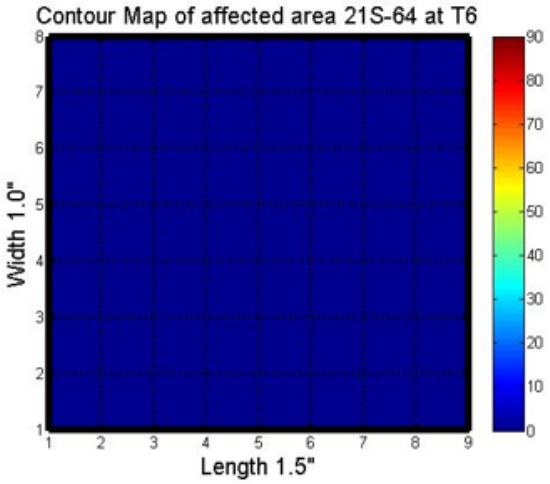

(b) Contour Plot

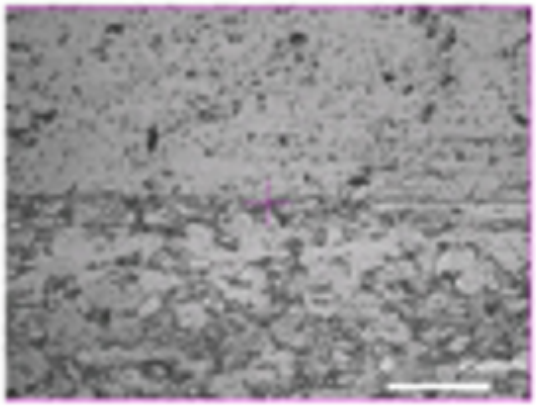

(c) Micrograph

Figure 28: Good Sample of Ti21S-Ti64 at T6

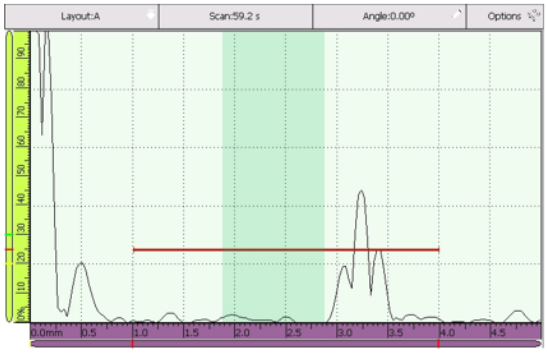

(a) A-Scan

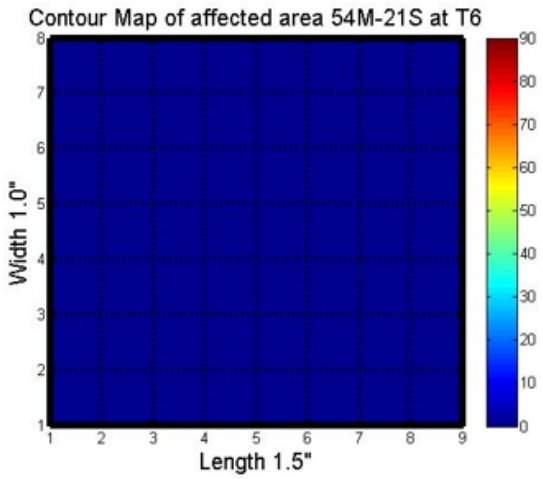

(b) Contour Plot

(c) Micrograph

Figure 29: Good Sample of Ti54M-Ti21S at T6

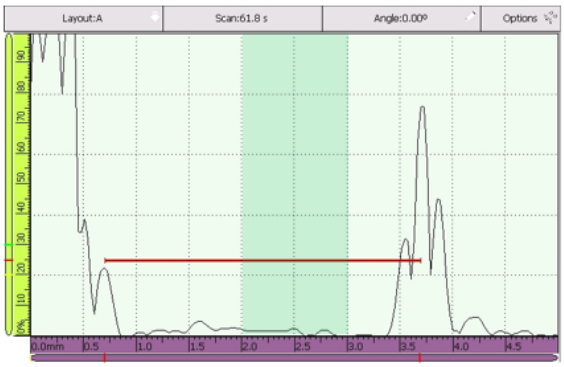

(a) A-Scan

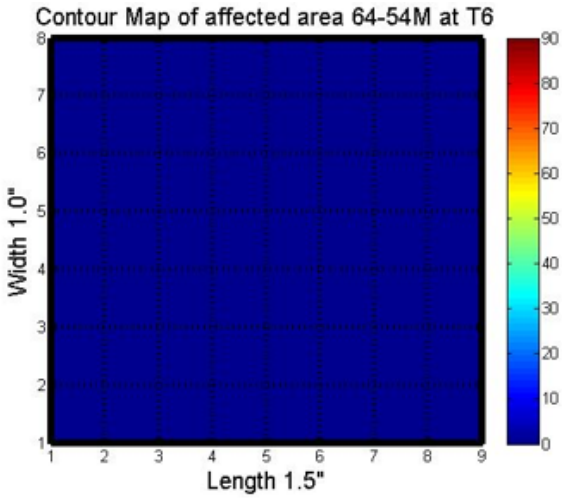

(b) Contour Plot

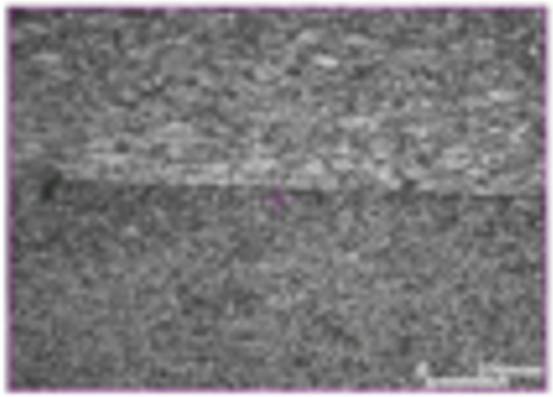

(c) Micrograph

Figure 30: Good Sample of Ti64-Ti54M at T6

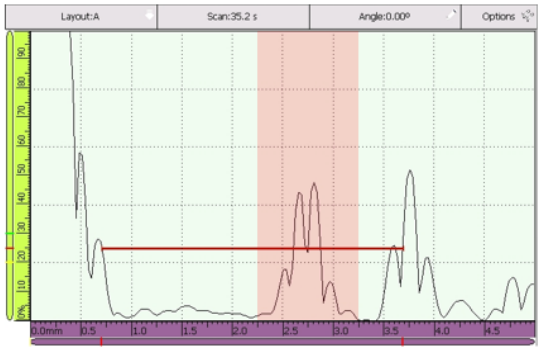

(a) A-Scan

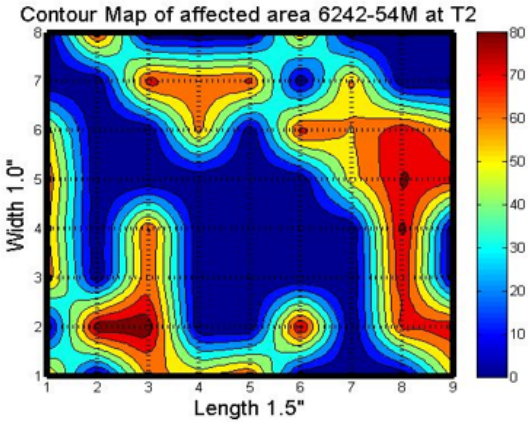

(b) Contour Plot

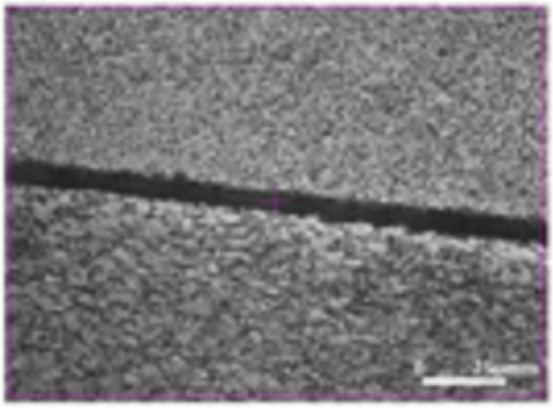

(c) Micrograph

Figure 31: Defective Sample of Ti6242-Ti54M at T2

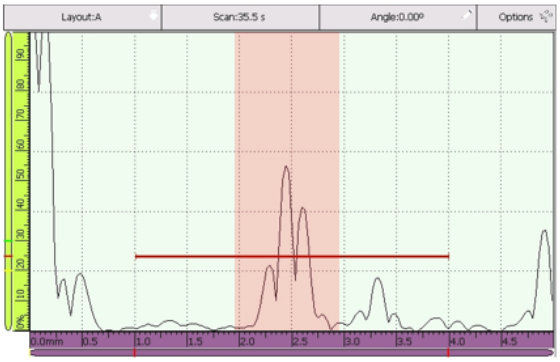

(a) A-Scan

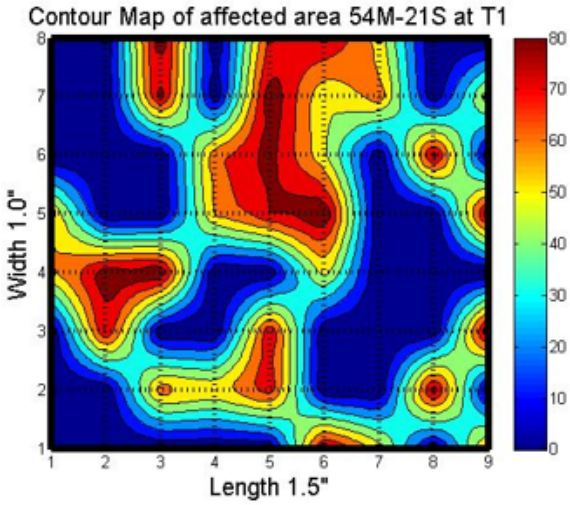

(b) Contour Plot

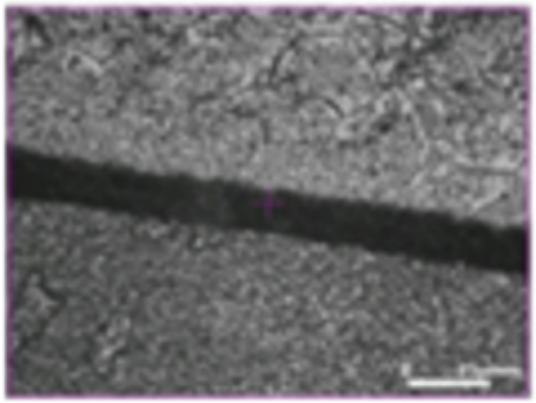

(c) Micrograph

Figure 32: Defective Sample of Ti54M-Ti21S at T1

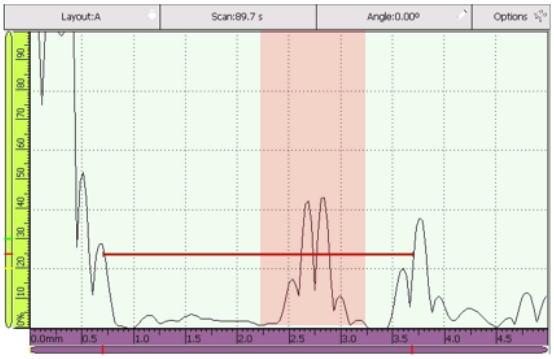

(a) A-Scan

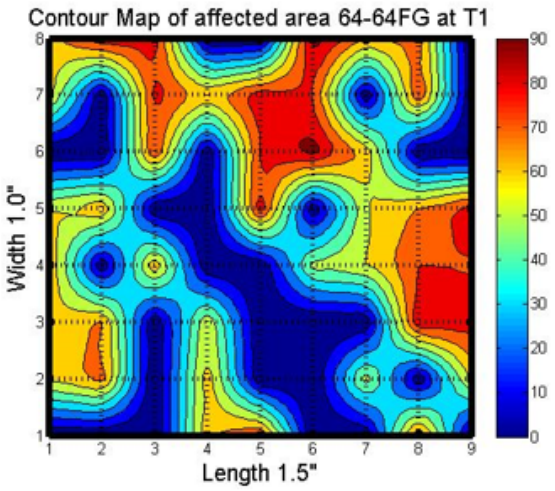

(b) Contour Plot

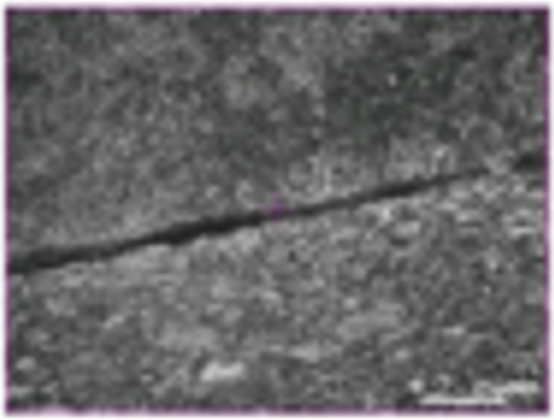

(c) Micrograph

Figure 33: Defective Sample of Ti64-Ti64FG at T1

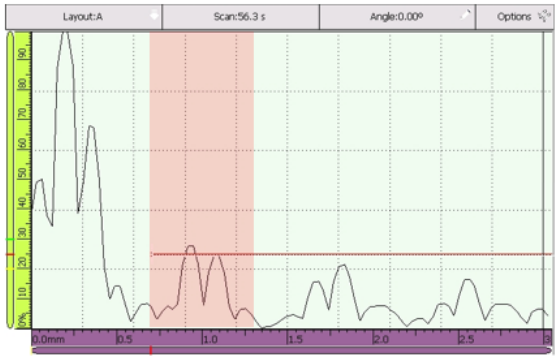

(a) A-Scan

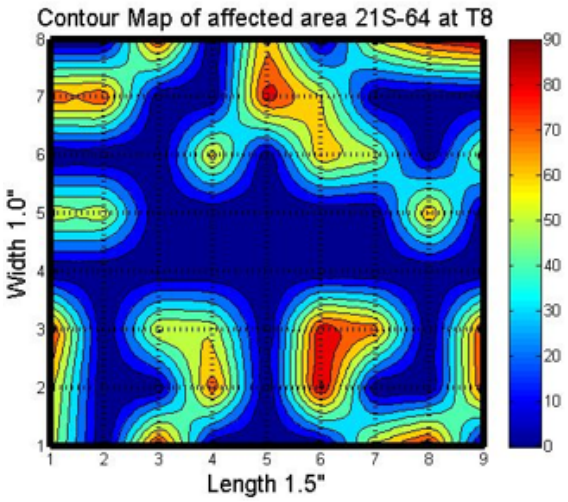

(b) Contour Plot

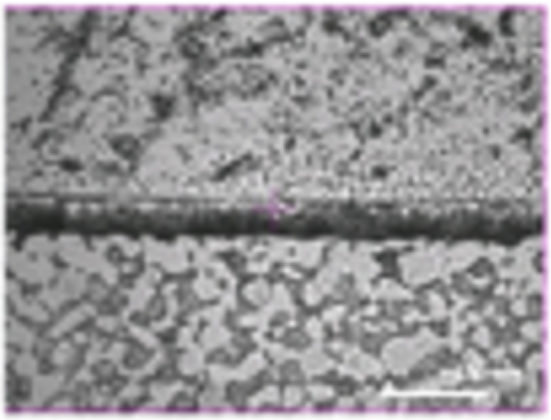

(c) Micrograph

Figure 34: Defective Sample of Ti21S-Ti64 at T8

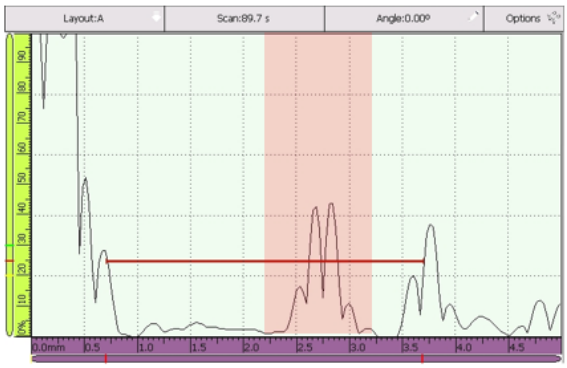

(a) A-Scan

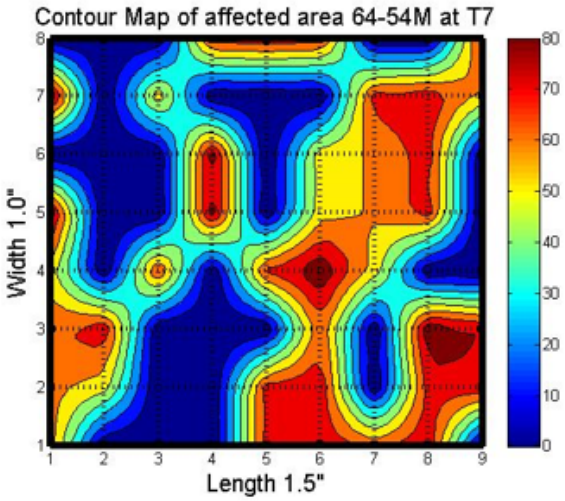

(b) Contour Plot

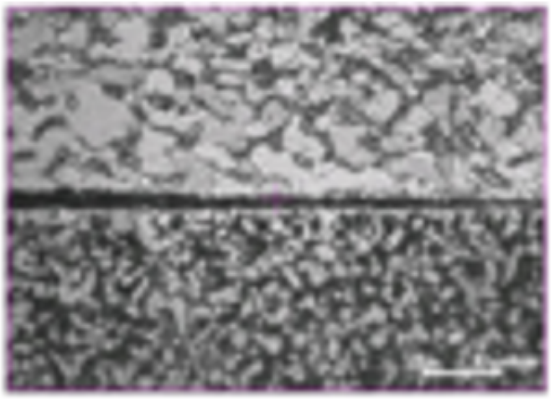

(c) Micrograph

Figure 35: Defective Sample of Ti64-Ti54M at T7

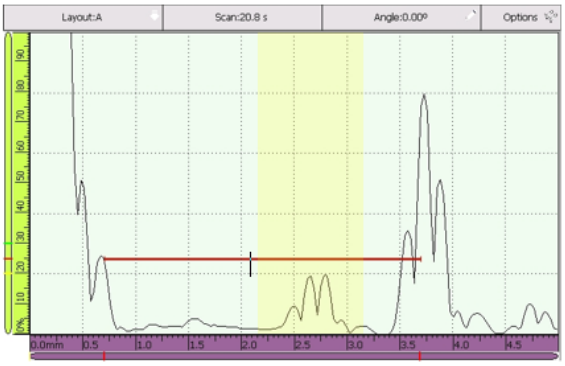

(a) A-Scan

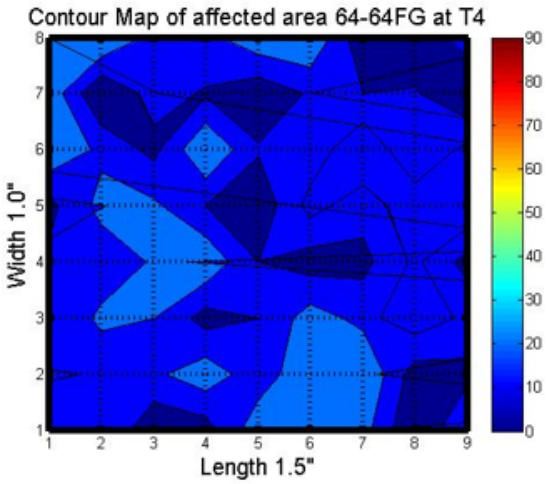

(b) Contour Plot

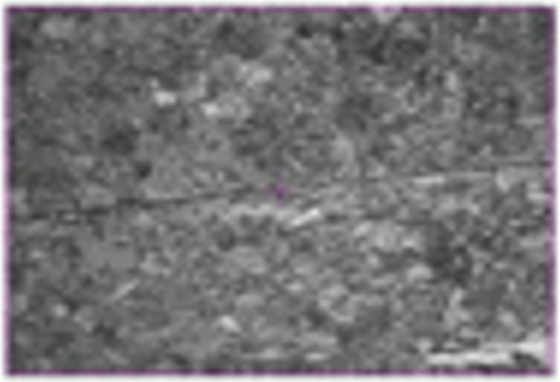

(c) Micrograph

Figure 36: Line Defect Sample of Ti64-Ti64FG at T4

Figures 24 and 25 represent the similar alloys with good Bonding. Figure 26 represents similar alloy with bad bonding. Figures 27 to 30 represent dissimilar alloys with good bonding and Figures 31 to 35 represent dissimilar alloys with bad bonding. Figure 36 represents a bond with line defect. These defects have low reflection coefficient and are difficult to detect in ultrasonic testing. The future research in ultrasonic diffusion bonding is focused on addressing this issue. Overall the ultrasonic results have good agreement with the micrograph results. The contour plots of all the samples are presented in Appendix-B.

The results of the inspection can be summarized in Table-9. The table indicates if a bond of a particular alloy has defects or not and gives us a normalized depth of defect, calculated ultrasonically. The consistency of the results was good when it is carried out on samples with unbonding or large defects. However ultrasonic testing is constrained to finding the defects upto a threshold value depending on the operating frequency of the probe (in our case it is 10MHz). Also, the methodology used for inspection was manual and relying on the skill of the operator for the reliability of the results. There is a greater need for automation processes such that it greatly reduces the human error in the quality inspection through ultrasonic testing.

To fully exploit the capabilities of ultrasonic testing on Ti-Alloys Non-Linear Ultrasonic NDT methods which are currently being developed [36,37]. This non-linearity of acoustic waves is utilized as a tool for material characterization without the distortion of signal as we have noticed in the case of Figure-36. This technique tends to separate the perfect bonds to the partial bonds to which linear ultrasonic approach exhibits no sensitivity [37].

Table 9: Summary of Ultrasonic Diffusion bonding Results

Ultrasonic NDT of Diffusion Bonding Samples					
Sl No.	Specimen (Titanium)	Measured Thickness using UT (mm)	Temperature (C)	Defects (Through UT)	Normalized Depth of defect (in mm Locally)
1	64-64	2.03	T4	No	-
2	64-64	2.05	T5	No	-
3	64-64	1.98	T6	No	-
4	64-64	2.01	T7	No	-
5	64-64	2.03	T8	No	-
6	64FG-64FG	5.01	T1	Yes	2.41
7	64FG-64FG	4.99	T2	Yes	2.56
8	64FG-64FG	4.98	T3	Yes	2.51
9	64FG-64FG	5.00	T4	Yes	2.38
10	54M-54M	5.02	T1	Yes	2.52
11	54M-54M	5.03	T2	Yes	2.55
12	54M-54M	4.99	T3	Yes	2.59
13	54M-54M	4.98	T4	Yes	2.46
14	54M-54M	5.01	T5	No	-
15	21S-21S	1.81	T1	Yes	0.92
16	21S-21S	1.76	T2	No	-
17	21S-21S	1.81	T5	No	-
18	21S-21S	1.84	T6	No	-
19	21S-21S	1.82	T7	No	-
20	21S-21S	1.79	T8	No	-
21	6242-6242	2.13	T5	No	-
22	6242-6242	2.15	T6	No	-
23	6242-6242	2.13	T7	No	-
24	6242-6242	2.19	T8	No	-
25	6242-54M	3.58	T1	No	-
26	6242-54M	3.57	T2	Yes	2.58
27	6242-54M	3.61	T3	Yes	2.54
28	6242-54M	3.60	T4	No	-
29	6242-54M	3.59	T5	No	-
30	6242-54M	3.58	T6	No	-
31	6242-54M	3.57	T7	No	-

Ultrasonic NDT of Diffusion Bonding Samples (Contd. 1)					
Sl No.	Specimen (Titanium)	Measured Thickness using UT (mm)	Temperature (C)	Defects (Through UT)	Normalized Depth of defect (in mm Locally)
32	54M-64	3.59	T1	No	-
33	54M-64	3.59	T2	No	-
34	54M-64	3.61	T3	No	-
35	54M-64	3.60	T4	No	-
36	54M-64	3.58	T5	No	-
37	54M-64	3.58	T6	No	-
38	54M-64	3.59	T7	Yes	2.44
39	54M-21S	3.16	T1	Yes	2.55
40	54M-21S	3.21	T2	Yes	2.56
41	54M-21S	3.18	T3	Yes	2.51
42	54M-21S	3.18	T4	No	-
43	54M-21S	3.20	T5	Yes	2.52
44	54M-21S	3.21	T6	No	-
45	54M-21S	3.20	T7	No	-
46	21S-64	1.77	T4	No	-
47	21S-64	1.79	T5	No	-
48	21S-64	1.80	T6	No	-
49	21S-64	1.81	T7	No	-
50	21S-64	1.79	T8	Yes	0.91
51	64-64FG	3.59	T1	Yes	1.01
52	64-64FG	3.58	T2	Yes	1.08
53	64-64FG	3.60	T3	Yes	1.11
54	64-64FG	3.58	T4	No	-
55	64-64FG	3.61	T5	No	-
56	6242-64FG	3.61	T1	Yes	2.45
57	6242-64FG	3.58	T2	Yes	2.51
58	6242-64FG	3.60	T3	Yes	2.47
59	6242-64FG	3.59	T4	No	-
60	6242-64FG	3.60	T5	Yes	2.46

Ultrasonic NDT of Diffusion Bonding Samples (Contd. 2)					
Sl No.	Specimen (Titanium)	Measured Thickness using UT (mm)	Temperature (C)	Defects (Through UT)	Normalized Depth of defect (in mm Locally)
61	21S-64FG	3.18	T1	No	
62	21S-64FG	3.19	T2	Yes	2.49
63	21S-64FG	3.20	T3	Yes	2.42
64	21S-64FG	3.21	T4	Yes	2.50
65	21S-64FG	3.21	T5	Yes	2.45
66	21S-6242	3.18	T5	No	-
67	21S-6242	3.17	T6	No	-
68	21S-6242	3.19	T7	No	-
69	21S-6242	3.20	T8	Yes	2.44
70	64FG-54M	5.01	T1	Yes	2.50
71	64FG-54M	4.99	T2	Yes	2.49
72	64FG-54M	4.99	T3	Yes	2.65
73	64FG-54M	5.00	T4	Yes	2.52
74	64FG-54M	5.01	T5	Yes	2.57
75	6242-64	1.98	T4	No	-
76	6242-64	2.03	T5	No	-
77	6242-64	2.05	T6	No	-
78	6242-64	2.06	T7	No	-
79	6242-64	2.04	T8	No	-

4.2 Friction Stir Welding

PAUT is used on inspecting FSW samples. The methodology used in identifying the defects in FSW is outlined in Section 3.2.3. The sectorial scan (S-Scan) of the similar alloy Ti6242SG-Ti6242SG welded at parameters 275/4 is shown in Figure-37(a). This is an A-S scan presentation of the phased array testing, meaning it shows both the A-Scan and the S-Scan of the sample under investigation. The A-scan pertains to a definite angle of incidence of the sound wave. As we can see, in the Figure-37(a), A-Scan the echoes when the sound wave enters the weld zone to base material interface and are clearly identified as small spikes in the image. The weld region in the S-scan does not show any kind of defects in the material. The color intensity is proportional to the reflected amplitudes indicated in the A-scan. Figure-37(b) represents the samples macrograph and clearly the phased array result is in agreement to it.

The Figure-38(a) represents the phased array inspection of dissimilar alloys Ti6242FG-Ti64SG welded at 325/5. This also represents a defect free weld although we wee the amplitude in the weld region turbulent than that of the similar alloys case. This is explained by the macrograph of the sample, presented in the Figure-38(b). Due to the dissimilar nature of the alloys the weld zone is a mixture of both the elements which create multiple interfaces in the weld zone. Although these are not considered defects, the phased array returns a small echo from these interfacial boundaries. The weld quality is considered decent if the ultrasonic level of the weld root is lower than that of the base material/s. This makes it a good weld.

Similar procedure is followed while inspecting all of the samples of FSW and selected scans of samples are presented in this section. No major defects were detected in the ultrasonic scans of the FSW samples. As indicated in Section 3.2.3, the scans at discrete distances 12mm, 25mm, 36mm and 50 mm are presented for each sample at various process conditions. These are represented in the Figures 39-42. Figures 39 and 40 represent the scans at the specified locations at 225/5 and 275/5. Wheras, the figures 41 and 42 indicate the A-S scans at 225/5 and 275/4.

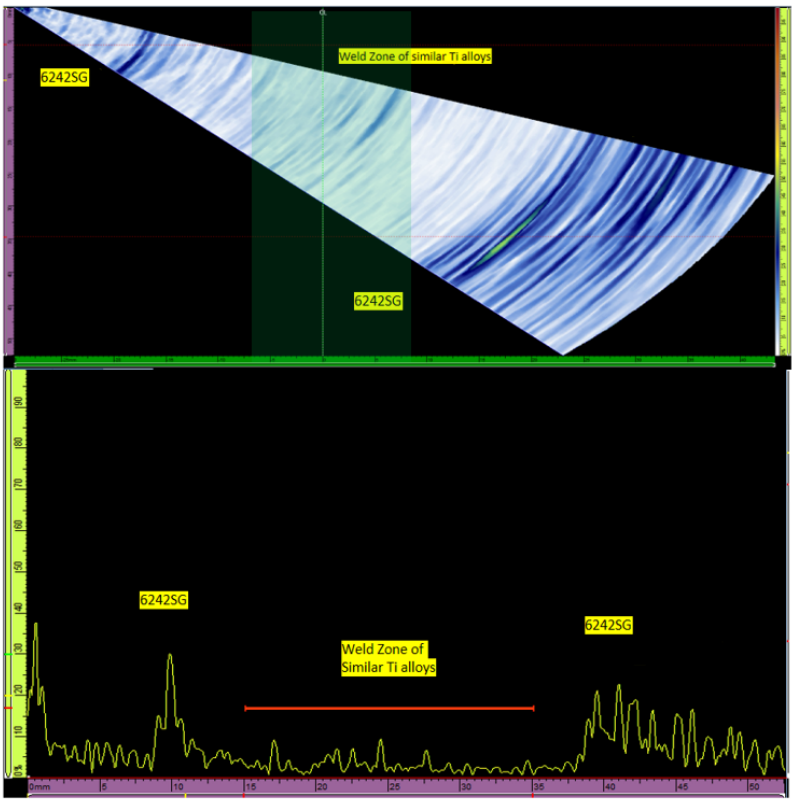

(a) A-S Scan

(b) Macrograph

Figure 37: Phased Array Inspection of Sample of Similar alloys Ti6242SG-Ti6242SG at 275/4

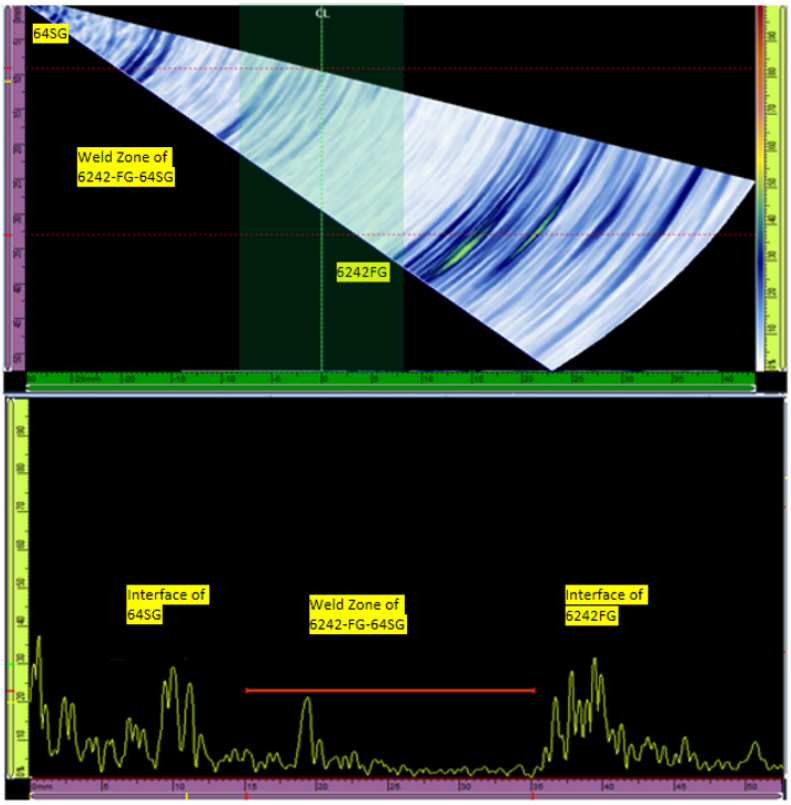

(a) A-S Scan

(b) Macrograph

Figure 38: Phased Array Inspection of Sample of Dissimilar Alloy Ti6242FG-Ti64SG at 325/5

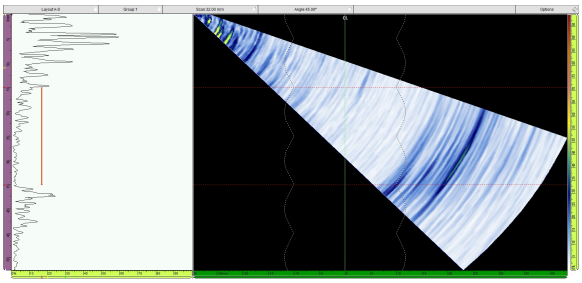

(a) Distance 12mm

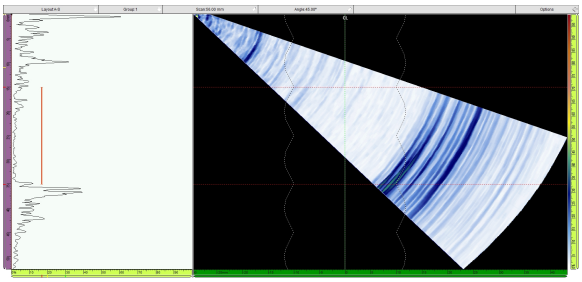

(b) Distance 25mm

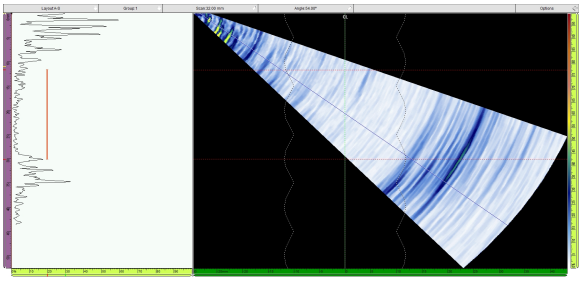

(c) Distance 36m

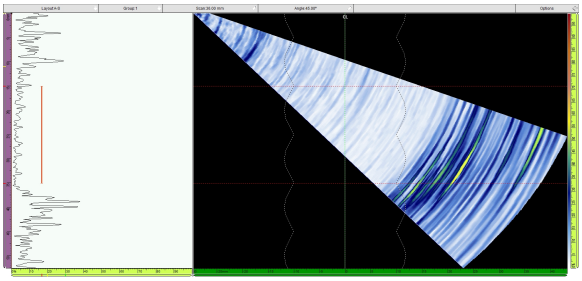

(d) Distance 50mm

Figure 39: Phased Array Inspection of Sample of Similar alloys Ti6242SG-Ti6242SG at 225/5

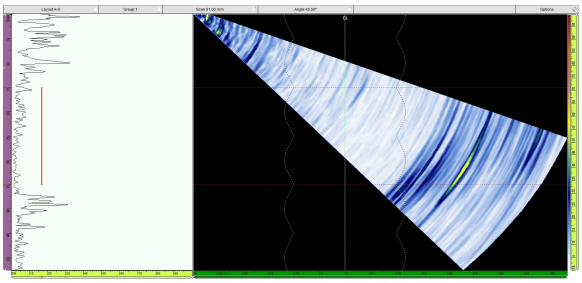

(a) Distance 12mm

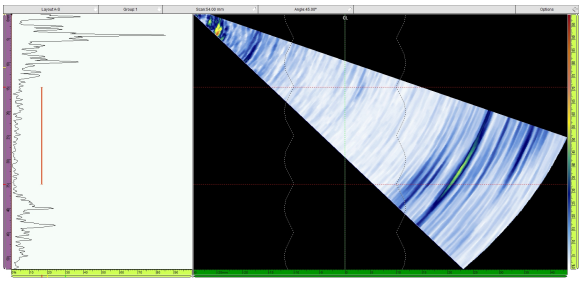

(b) Distance 25mm

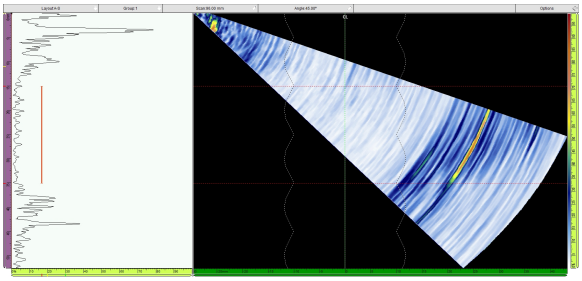

(c) Distance 36m

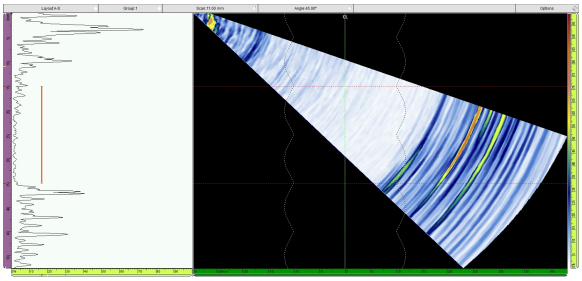

(d) Distance 50mm

Figure 40: Phased Array Inspection of Sample of Similar alloys Ti6242SG-Ti6242SG at 275/5

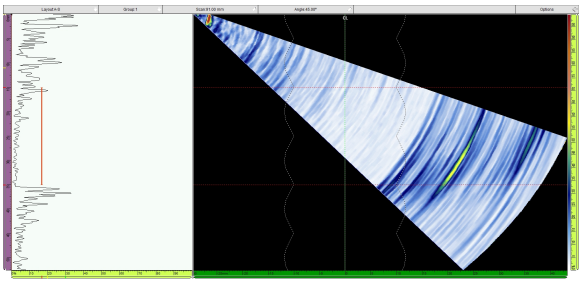

(a) Distance 12mm

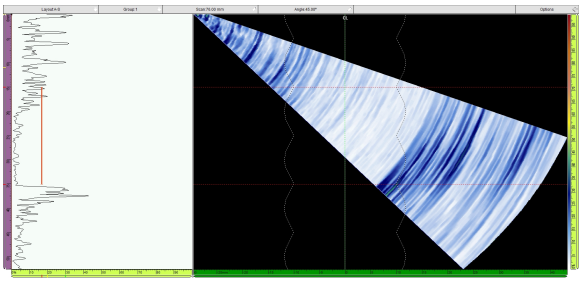

(b) Distance 25mm

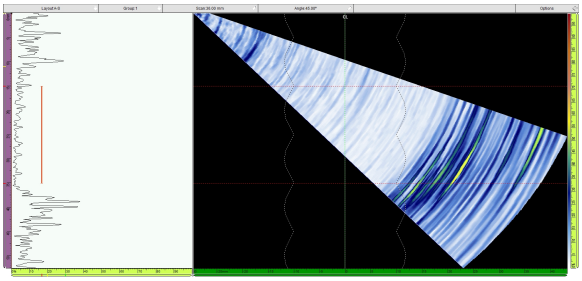

(c) Distance 36m

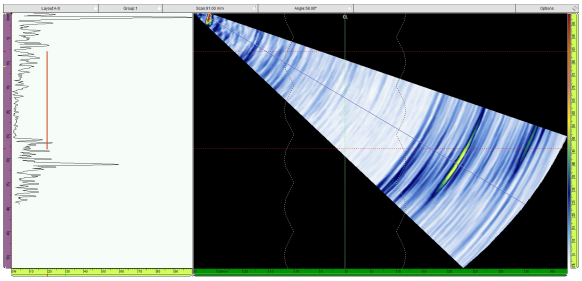

(d) Distance 50mm

Figure 41: Phased Array Inspection of Sample of Dissimilar alloys Ti6242FG-Ti64SG at 275/4

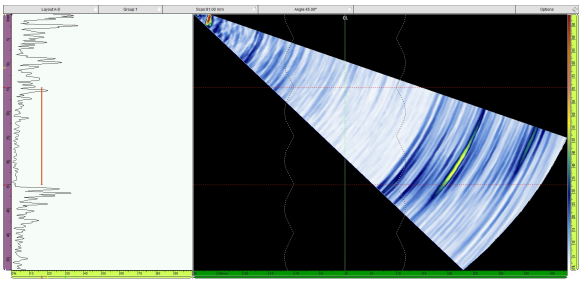

(a) Distance 12mm

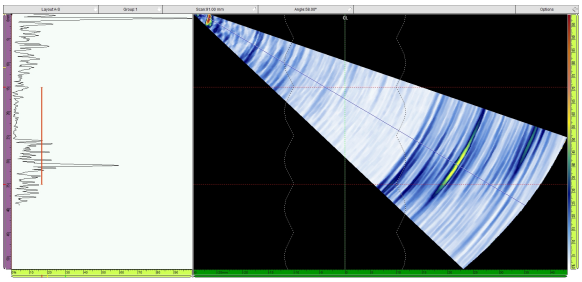

(b) Distance 25mm

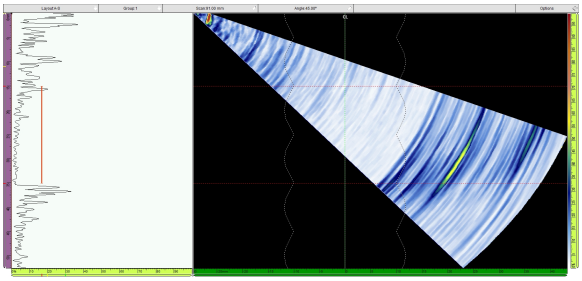

(c) Distance 36m

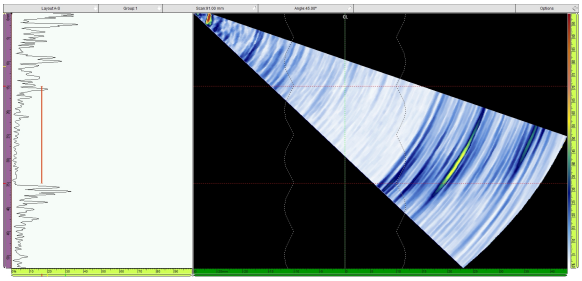

(d) Distance 50mm

Figure 42: Phased Array Inspection of Sample of Similar alloys Ti6242FG-Ti64SG at 225/5

The capability of ultrasonic velocity propagation in materials is utilized and the material properties (Young's Modulus of the weld zone of the samples are estimated using ultrasonic testing. The probe used for this is a straight beam probe of frequency $5MHz$ as we are checking for the penetration of the wave to the material in this case. The estimated Young's Modulus is them compared to the Bending Test data of the samples. The average error between the ultrasonically estimated and experimentally determine elastic moduli is $\approx 6.41\%$. The complete S-Scans and velocity readings recorded are presented in APPENDIX-B. The results are summarized in Table-10. On the whole,PAUT inspection on the welds is a promising method to characterize the microstructure in the weld zone.

Table 10: Summary of PAUT on FSW

ULTRASONIC INSPECTION OF TITANIUM ALLOYS BY FSW (Density ρ = 4.43 gm/cc)										
Sl No.	Material	RPM	Feed Rate	Feed Rate	Defects in UT Phased Array	Estimated Longitudinal Velocity from UT (V (L))	Estimated Transverse Velocity from UT (V (T))	Estimated Youngs Modulus (E) from UT	Experimental Youngs Modulus (E)	Error between Estimated and Experimental data
			in/min	mm/min		m/s	m/s	GPa	GPa	%
1	54MFG-54MFG	225	5	127	None	5800	2959.18	102.73	90.54	13.46%
2		275	4	101.6	None	5800	2959.18	102.73	90.77	13.17%
3		275	5	127	None	5878	2998.98	105.51	96.40	9.45%
4		275	6	152.4	None	5829	2973.98	103.76	91.72	13.12%
5		325	5	127	None	5829	2973.98	103.76	92.78	11.83%
6	54MFG-64FG	225	5	127	None	5675	2895.41	98.35	76.22	29.02%
7		275	4	101.6	None	5925	3022.96	107.20	100.86	6.29%
8		275	5	127	None	5830	2974.49	103.79	93.34	11.19%
9		275	6	152.4	None	5835	2977.04	103.97	93.64	11.03%
10		325	5	127	None	5675	2895.41	98.35	77.74	26.51%
11	54MFG-64SG	225	5	127	None	5830	2974.49	103.79	93.10	11.48%
12		275	4	101.6	None	5900	3010.20	106.30	96.45	10.21%
13		275	5	127	None	5900	3010.20	106.30	95.11	11.77%
14		275	6	152.4	None	5940	3030.61	107.74	101.51	6.14%
15		325	5	127	None	5720	2918.37	99.91	87.68	13.95%
16	6242FG-6242FG	225	5	127	None	6260	3193.88	119.67	132.72	9.84%
17		275	4	101.6	None	6245	3186.22	119.09	130.82	8.97%
18		275	5	127	None	6210	3168.37	117.76	118.70	0.79%
19		275	6	152.4	None	6200	3163.27	117.38	114.63	2.40%
20		325	5	127	None	6100	3112.24	113.63	97.63	16.39%
21	54MFG-6242SG	225	5	127	None	6300	3214.29	121.20	158.62	23.59%
22		275	4	101.6	None	6250	3188.78	119.28	120.47	0.98%
23		275	5	127	None	6250	3188.78	119.28	120.53	1.03%
24		275	6	152.4	None	6250	3188.78	119.28	144.18	17.27%
25		325	5	127	None	6100	3112.24	113.63	102.82	10.51%
26	54MFG-6242FG	225	5	127	None	6250	3188.78	119.28	156.26	23.66%
27		275	4	101.6	None	6100	3112.24	113.63	119.91	5.24%
28		275	6	152.4	None	6210	3168.37	117.76	116.50	1.09%
29		325	5	127	None	6210	3168.37	117.76	117.36	0.34%
30	64SG-64SG	225	5	127	None	5940	3030.61	107.74	104.19	3.41%
31		275	4	101.6	None	5900	3010.20	106.30	96.91	9.69%
32		275	5	127	None	5940	3030.61	107.74	104.38	3.23%
33		275	6	152.4	None	5900	3010.20	106.30	94.63	12.33%
34		325	5	127	None	5940	3030.61	107.74	101.86	5.77%
35	64SG-6242SG	225	5	127	None	6300	3214.29	121.20	131.14	7.58%
36		275	4	101.6	None	6300	3214.29	121.20	140.35	13.64%
37		275	5	127	None	6050	3086.73	111.77	106.09	5.36%
38		275	6	152.4	None	6100	3112.24	113.63	125.14	9.20%
39		325	5	127	None	6300	3214.29	121.20	132.65	8.63%
40	64SG-6242FG	225	5	127	None	6300	3214.29	121.20	134.96	10.19%
41		275	4	101.6	None	6300	3214.29	121.20	147.77	17.98%
42		275	6	152.4	None	6250	3188.78	119.28	125.89	5.25%
43		325	5	127	None	6250	3188.78	119.28	126.03	5.35%

ULTRASONIC INSPECTION OF TITANIUM ALLOYS BY FSW (Contd 1)										
Sl No.	Material	RPM	Feed Rate	Feed Rate	Defects in UT Phased Array	Estimated Longitudinal Velocity from UT (V (L))	Estimated Transverse Velocity from UT (V (T))	Estimated Youngs Modulus (E) from UT	Experimental Youngs Modulus (E)	Error between Estimated and Experimental data
			in/min	mm/min		m/s	m/s	GPa		%
44	6242SG-6242SG	225	5	127	None	6250	3188.78	119.28	129.45	7.85%
45		275	4	101.6	None	6250	3188.78	119.28	123.19	3.17%
46		275	5	127	None	6250	3188.78	119.28	129.54	7.92%
47		275	6	152.4	None	6300	3214.29	121.20	136.32	11.09%
48		325	5	127	None	6100	3112.24	113.63	99.12	14.64%
49	64FG-64FG	225	5	127	None	5940	3030.61	107.74	100.12	7.61%
50		275	4	101.6	None	5720	2918.37	99.91	82.79	20.68%
51		275	5	127	None	5675	2895.41	98.35	79.65	23.47%
52		275	6	152.4	None	5720	2918.37	99.91	85.67	16.63%
53		325	5	127	None	5720	2918.37	99.91	87.60	14.05%
54	64FG-6242FG	225	5	127	None	6300	3214.29	121.20	176.33	31.27%
55		275	4	101.6	None	6300	3214.29	121.20	141.14	14.13%
56		275	6	152.4	None	6250	3188.78	119.28	157.28	24.16%
57		325	5	127	None	6250	3188.78	119.28	126.76	5.89%

4.3 Composite Drilling

The objective of this is to find delaminations or fiber pullouts in the composite material which has holes of various sizes drilled on it. Phased array technique is used to identify the delaminations in holes drilled on the unidirectional (UD) CFRP by Carbide (CRD) tool and HSS tool. The samples used for testing are shown in Figure-43. The thickness of the samples are 6.5mm.

(a) CRD tool drill on UD CFRP composite

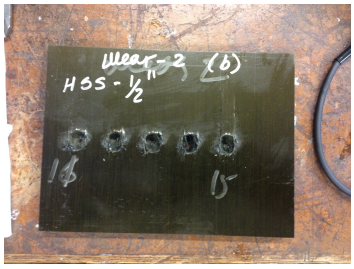

(b) HSS tool on UD CFRP Composite

Figure 43: Samples used for PAUT inspection on Composites [38]

The drilling was performed using a carbide tool for the sample shown in Figure-43(a) and HSS tool was used on the sample shown in Figure-43(b). The scans are recorded for 15 holes for the carbide drill sample and 5 holes for the HSS drill tool sample numbered in the order of drilling. The S-Scans are presented in Figures-44. Figure 44(a) represents the S-Scan of Hole-5 drilled using the carbide tool on the CFRP composite. The delaminations were detected near the bottom of the drilled holes, starting at 4.5mm to 6.5mm (bottom), in most of the cases as seen in the Figure-44. There were also minor indications of delamination detected at the top and along the length of the drilled hole. In the Figure-44(b), the extent of delaminations is huge as represented in the S-Scan when drilled by the HSS tool. The top 2mm of the composite in this case has complete indications of delaminations. The hole-5, as represented in this case, there are many indications along the length of the drilled hole. The surface at the bottom of the hole is most affected part with maximum indications of delaminations.

The complete PAUT scans of the two samples are presented in Figure-45 for the CRD tool drilling and Figure-46 for the HSS tool drilling on the CFRP composite. As seen from the PAUT scans in Figure-45, the carbide drill produced better quality

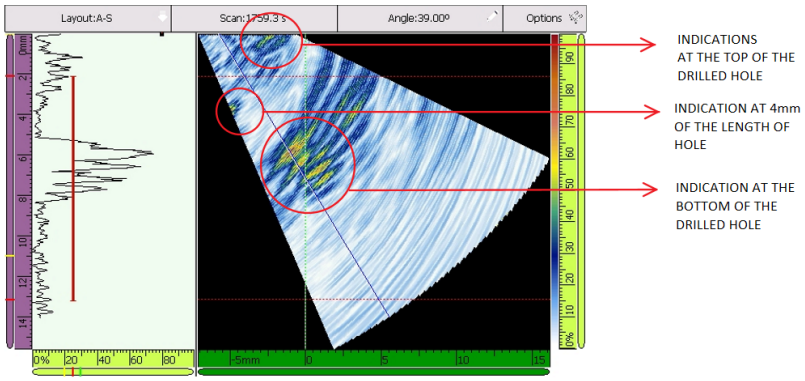

(a) S-Scan of Hole 5 on the sample by CRD tool

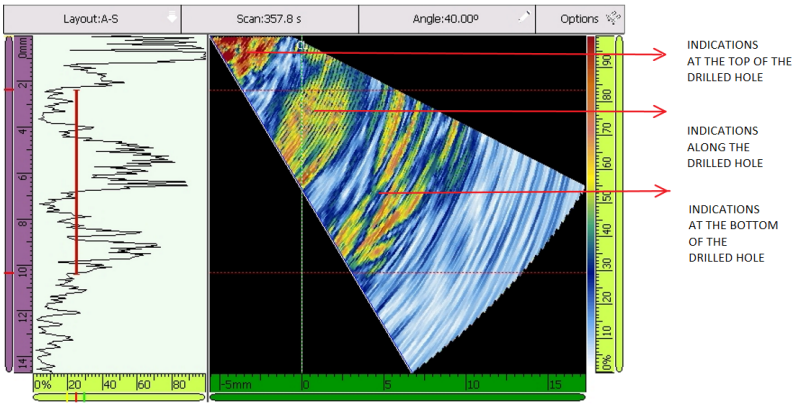

(b) S-Scan of Hole 5 on the sample by HSS tool

Figure 44: S-Scan Representation and location of defects

holes and lower amount of tool wear compared to the HSS drill. We can see observe that as the tool wear increased the discontinuities in the composite material increased. The conventional HSS tooling suffered the most wear and consequently produced a large increase in drilling forces, and these higher forces in turn led to an increase in exit delamination and specimen damage.

PAUT on composite drilling provides greater distinction on the magnitude and extent of the defects than the Acoustic Signal recorded using an an air-coupled audio microphone (AM) during the drilling operation [38]. The phased array results of the samples was consistent in finding the delaminations. However, it takes minutes to hours to process large amount of data. PAUT image, as seen in the scans presented, suffers from massive attenuation and scattering of ultrasonic waves due to anisotropic nature of the composites.

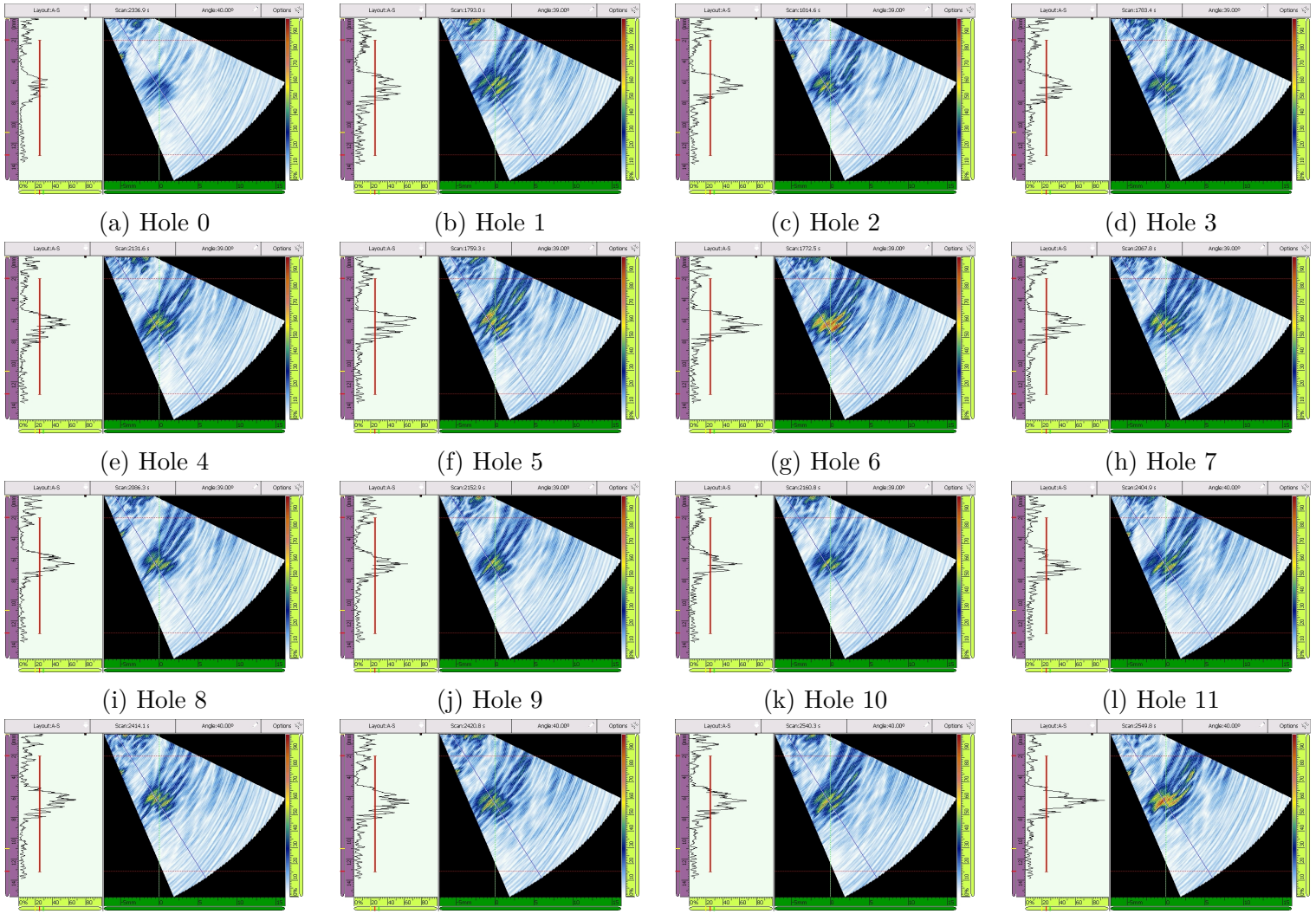

(a) Hole 0 (b) Hole 1 (c) Hole 2 (d) Hole 3

(e) Hole 4 (f) Hole 5 (g) Hole 6 (h) Hole 7

(i) Hole 8 (j) Hole 9 (k) Hole 10 (l) Hole 11

(m) Hole 12 (n) Hole 13 (o) Hole 14 (p) Hole 15

Figure 45: Phased Array Inspection of Holes Drilled in Unidirectional CFRP Composite with Carbide Drill

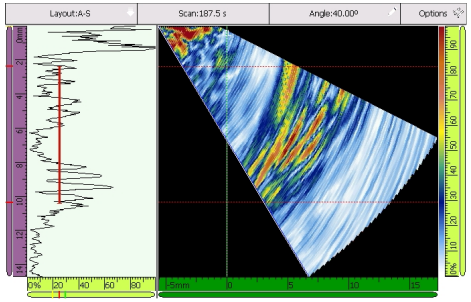

(a) Hole 1

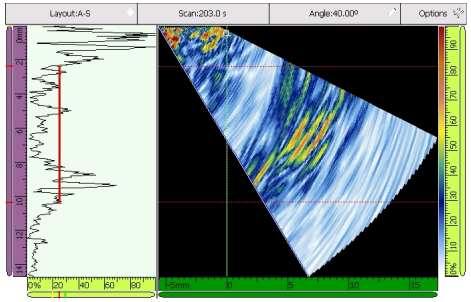

(b) Hole 2

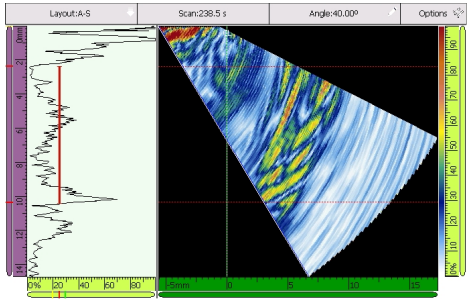

(c) Hole 3

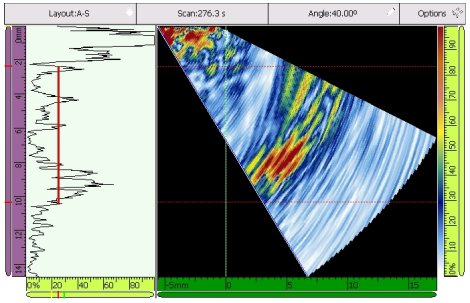

(d) Hole 4

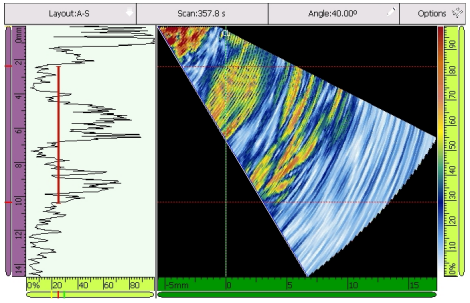

(e) Hole 5

Figure 46: Phased Array Inspection of Holes Drilled in Unidirectional CFRP Composite with HSS Drill

5 CONCLUSIONS

This study investigated the ability of ultrasonic NDT in inspecting the defects and discontinuities in the joints of aerospace materials manufactured under different process conditions. The results demonstrated a strong relationship between the UT and the destructive testing methods.

In the case of DB, the ultrasonic A-scan methodology was able to locate the defects in the bond through reflection coefficient. In the case of FSW, the PAUT is able to distinguish between the weld nugget region and the base materials (similar or dissimilar). The material properties of the weld region were deduced through measurement of the longitudinal velocity of the sound wave passing through the weld nugget. As claimed by the industry and experts, the phased array technique is a good indicator of defects in welds. The investigation of defects through PAUT was even extended to finding delaminations in composites.

The UT techniques mentioned are efficient means find the discontinuities and defects without having the need to ensure destructive testing. Also single sided access to the components is required. This can be a huge asset to any industry as it saves both time and cost of production and maintenance to a great extent. However the technical expertise needed to operate the UT equipment and the equipment cost is of great concern as it may lead to devastating results if used erroneously.

The future work should focus on quantifying the smaller defects in joining processes. The current equipment only allows to predict the extent of defects of a threshold size in them. Overall, we can assertively use UT techniques for a wide range of applications on aerospace materials to accurately determine the majority of devastating defects and flaws with the material in usable condition.

WORKS CITED

1. "NDT Guide to Non Destructive Testing." Advanced Materials & Processes (2008): 41-47. The Materials Information Society. ASM International, 2008. Web. <http://www.asminternational.org>.

2. "Introduction to Nondestructive Testing." Introduction to Nondestructive Testing. N.p., n.d. Web. 05 May 2015. <https://www.asnt.org/MinorSiteSections /AboutASNT/Intro-to-NDT>.

3. "Ultrasonic Testing." (n.d.): n. pag. Web. <https://eis.hu.edu.jo/ACUploads /10526/Ultrasonic

4. "Phased Array Tutorial." Olympus Phased Array Tutorial, Learn About Ultrasonic Phased Array. N.p., n.d. Web. 05 May 2015. <http://www.olympus-ims.com/en/ndt-tutorials/phased-array/>.

5. "NDT Course Material." NDT Resource Center, n.d. Web. 05 May 2015. <https://www.nde-ed.org/EducationResources/CommunityCollege/Ultrasonics /EquipmentTrans/DataPres.htm>.

6. "Basic Ultrasound, Echocardiography and Doppler Ultrasound." Basic Ultrasound, Echocardiography and Doppler Ultrasound. N.p., n.d. Web. 06 May 2015. <http://folk.ntnu.no/stoylen/strainrate/Ultrasound/>.

7. "Phased Array Ultrasonics." Wikipedia. Wikimedia Foundation, n.d. Web. 06 May 2015. <http://en.wikipedia.org/wiki/Phased_array_ultrasonics>.

8. Ditchburn, R J, and M E Ibrahim. "Ultrasonic Phased Arrays for the Inspection of Thick-Section Welds." Maritime Platforms Division, Department of Science and Technology (2009): n. pag. Australian Government. Department of Defence. Web.

9. E. Ginzel, Phased Array Ultrasonic Technology, Waterloo: Eclipse Scientific Inc., 2013.

10. N. Dube, Introduction to Phased Array Ultrasonic Technology Applications, Olympus NDT, 2007.

11. R. Cobald, Foundations of Biomedical Ultrasound, New York: Oxford University Press, 2007.

12. Marvasti, Mohammed Hassan. "Development of Ultrasound Phased Array System for Weld Inspections at Elevated Temperatures." TSpace. University of Toronto, Nov. 2014. Web. 19 May 2015.

13. Optel, "Phased Array Description," Optel, [Online]. Available: http://www.optel.pl /manual/english/oppa.htm.

14. Mishra, R S, and Z Y Ma. "Friction Stir Welding and Processing." Materials Science & Engineering R-Reports, 50 (2005): 1-2. Print.

15. Fleming, Paul A. "Monitoring And Control In Friction Stir Welding". Thesis. Vanderbilt University, 2009. N.p.: n.p., n.d. Web. Feb.-Mar. 2014.

16. Threadgill, P. L. "Terminology in Friction Stir Welding." Science and Technology of Welding and Joining 12.4 (2007): 357-60. Print.

17. Leonard, A J, and S A Lockyer. "Flaws in Friction Stir Welds." In 4th International Symposium on Friction Stir Welding, Park City, Utah, USA (2003): n. pag. Print.

18. Bird, C. R. 2003. Quality control of friction stir welds by the application of nondestructive testing. 4th International Symposium of Friction Stir Welding. Utah.

19. Carvaca, Delphine S., Colin R. Bird, Kathryn Beamish, and Stephen Maddox. "Correlation of Phased Array Inspection and Fatigue Performance of FSW Joints." Inspection Trends (2008): 27-31. Print.

20. Mandache, C., D. Levesque, L. Dubourg, and P. Gougeon. "Non-destructive Detection of Lack of Penetration Defects in Friction Stir Welds." Science and Technology of Welding & Joining 17.4 (2012): 295-303. Print.

21. Li, Bo, Yifu Shen, and Weiye Hu. "The Study on Defects in Aluminum 2219-T6 Thick Butt Friction Stir Welds with the Application of Multiple Non-destructive Testing Methods." Materials & Design 32.4 (2011): 2073-084. Web.

22. Neha Kulkarni, 2015, 'Study the Mechanical Performance of Similar and Dissimilar Titanium Alloy Joints formed by Diffusion bonding and Friction Stir Welding Processes', Doctoral Dissertation. Thesis

23. Lowe, Michael J S. "Plate Waves For The NDT Of Diffusion Bonded Titanium." Thesis. Imperial College of Science, Technology and Medicine, 1992. Imperial College London. Web. <http://www3.imperial.ac.uk/pls /portallive/-docs/1/50545709.PDF>.

24. Luan, Yilin, Tao Sun, Jicai Feng, and Tie Gang. "Ultrasonic Evaluation of TiAl and 40Cr Diffusion Bonding Quality Based on Time-scale Characteristics Extraction." NDT & E International 44.8 (2011): 789-96. Web.

25. Rehder, R. J., and D.T. Lovell. "Process Development for Diffusion Bonding Ti-4Al-6V." AWS 50th Annual Meeting (1969): n. pag. Print.

26. Wang, Z. C., N. Ridley, G. W. Lorimer, D. Knauss, and G. A. D. Briggs. "Evaluation of Diffusion Bonds Formed between Superplastic Sheet Materials." Journal Of Materials Science Journal of Materials Science 31.19 (1996): 5199-206. Web.

27. Milne, K., P. Cawley, P. B. Nagy, D. C. Wright, and A. Dunhill. "Ultrasonic Non-destructive Evaluation of Titanium Diffusion Bonds." Journal of Nondestructive Evaluation 30.4 (2011): 225-36. Web.

28. Cheng, Liang, and Gui Yun Tian. "Comparison of Nondestructive Testing Methods on Detection of Delaminations in Composites." Journal of Sensors 2012 (2012): 1-7. Web.

29. Edwill Escobar-Ruiz, P. Cawley, P B Nagy, I. Collison, and D. Wright. "Ultrasonic NDE of Titanium Diffusion Bonds Using Signal Phase." The 39th Annual Review of Progress in Quantitative Nondestructive Evaluation, AIP Conf. Proceedings 1511 (2013): 1409-416. Print.

30. Krautkrämer, Josef, and Herbert Krautkrämer. Ultrasonic Testing of Materials. Berlin: Springer-Verlag, 1990. Print.

31. Markham, M. F. "Measurement of Elastic Constants by the Ultrasonic Pulse Method." British Journal of Applied Physics 8.S6 (1957): S56-63. Web.

32. Nagy, P B. "Introduction to Ultrasonics." Lecture Notes. Vol. 20. N.p.: n.p., n.d. 251-728. Print.

33. Bird, C. R. "Ultrasonic Phased Array Inspection Technology for the Evaluation of Friction Stir Welds." Insight - Non-Destructive Testing and Condition Monitoring 46.1 (2004): 31-36. Web.

34. Kulkarni, Neha, and M. Ramulu. "Experimental and Numerical Analysis of Mechanical Behavior in Friction Stir Welded Different Titanium Alloys." ASME 2014 International Mechanical Engineering Congress and Exposition. American Society of Mechanical Engineers, 2014.

35. Kumar, S Suresh Kumar, Krishnamoorthi J, Ravisankar B, and Angelo P C. "Methodology to Evaluate the Quality of Diffusion Bonded Joints by Ultrasonic Method." Indian Journal of Engineering & Materials Sciences 16.October (2009): 331-34. Print.

36. Yamada, Ryuzo, Koichiro Kawashima, and Morimasa Murase. "Application of Nonlinear Ultrasonic Measurement for Quality Assurance of Diffusion Bonds of Gamma Titanium Aluminum Alloy and Steel." Research in Nondestructive Evaluation 17.4 (2006): 223-39. Web.

37. Edwill Escobar-Ruiz, Alberto Ruiz, Waled Hassan, David C. Wright, Ian J. Collison, Peter Cawley, and Peter B. Nagy. "Non-linear Ultrasonic NDE of Titanium Diffusion Bonds." Journal of Nondestructive Evaluation 33.2 (2014): 187-95. Print.

38. Eneyew, Eshetu Demissie. "Experimental Study of Damage and Defect Detection during Drilling of CFRP Composites". Thesis. University of Washington, Seattle, 2014. Seattle: UW Libraries, 2014. Web.

APPENDIX

A Ultrasonic Techniques

A.1 Straight Beam

Straight beam inspection uses longitudinal waves to interrogate the test piece as shown at the right. If the sound hits an internal reflector, the sound from that reflector will reflect to the transducer faster than the sound coming back from the back-wall of the part due to the shorter distance from the transducer. This results in a screen display like that shown at the right in Figure-A.1. Digital thickness testers use the same process, but the output is shown as a digital numeric readout rather than a screen presentation.

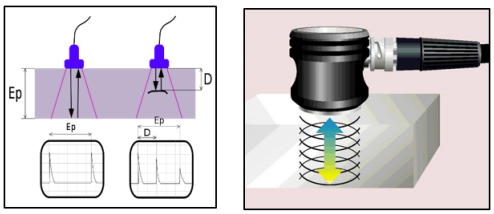

Figure A.1: Straight Beam Inspection technique

A.2 Angle Beam

Angle beam inspection uses the same type of transducer used in straight beam testing but it is mounted on an angled wedge that is designed to transmit the sound beam into the part at a known angle. The most commonly used inspection angles are 45ˆO, 60ˆO and 70ˆO, with the angle being calculated up from a line drawn through the thickness of the part (not the part surface). A 60ˆO probe is shown in Figure-A.2. If the frequency and wedge angle is not specified by the governing code or specification, it is up to the operator to select a combination that will adequately inspect the part being tested.

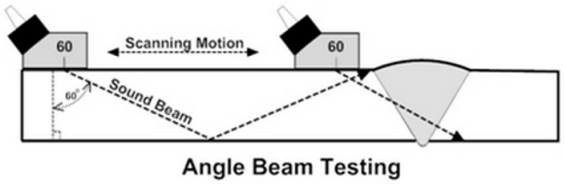

Figure A.2: Angle Beam Inspection Technique

In angle beam inspections, the transducer and wedge combination (also referred to as a "probe") is moved back and forth towards the weld so that the sound beam passes through the full volume of the weld. As with straight beam inspections, reflectors aligned more or less perpendicular to the sound beam will send sound back to the transducer and are displayed on the screen.

A.3 Immersion Testing

Immersion Testing is a technique where the part is immersed in a tank of water with the water being used as the coupling medium to allow the sound beam to travel between the transducer and the part. The UT machine is mounted on a movable platform (a "bridge") on the side of the tank so it can travel down the length of the tank. The transducer is swivel-mounted on at the bottom of a waterproof tube that can be raised, lowered and moved across the tank. The bridge and tube movement permits the transducer to be moved on the X-, Y- and Z-axes. All directions of travel are gear driven so the transducer can be moved in accurate increments in all directions, and the swivel allows the transducer to be oriented so the sound beam enters the part at the required angle. Round test parts are often mounted on powered rollers so that the part can be rotated as the transducer travels down its length, allowing the full circumference to be tested. Multiple transducers can be used at the same time so that multiple scans can be performed. The scan data is merged to form a C-scan. The schematic of Immersion Testing is shown in Figure-A.3.

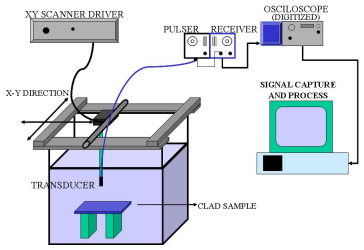

Figure A.3: Schematic of Immersion Testing

A.4 Time of Flight Diffraction (ToFD)

Time of Flight Diffraction (ToFD) uses two transducers located on opposite sides of a weld with the transducers set at a specified distance from each other. One transducer transmits sound waves and the other transducer acting as a receiver. Unlike other angle beam inspections, the transducers are not manipulated back and forth towards the weld, but travel along the length of the weld with the transducers remaining at the same distance from the weld. Two sound waves are generated, one traveling along the part surface between the transducers, and the other traveling down through the weld at an angle then back up to the receiver. When a crack is encountered, some of the sound is diffracted from the tips of the crack, generating a low strength sound wave that can be picked up by the receiving unit. By amplifying and running these signals through a computer, defect size and location can be determined with much greater accuracy than by conventional UT methods. However, TOFD should never be utilized as a stand alone inspection method due to the inherent "blind spots" created by the lateral wave and back wall echo. The schematic diagram is presented in Figure-A.4.

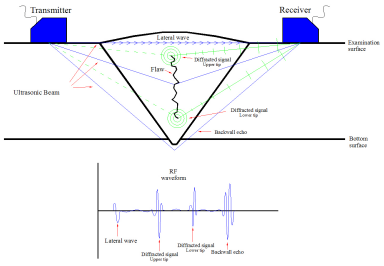

Figure A.4: ToFD Schematic and working

B Diffusion Bonding

B.1 Process Variables

The temperatures at which the bonds are produced are given in the table below.

Table T.1: Temperatures used for DB

Temperature	in F	in C
T1	1350	732.22
T2	1400	760.00
T3	1450	787.78
T4	1500	815.56
T5	1550	843.33
T6	1600	871.11
T7	1650	898.89
T8	1700	926.67

B.2 Contour Plots of Samples

The contour plots of all the defective samples of each alloy combination are presented in this section in the Figures-A.5 to Figures-A.16.

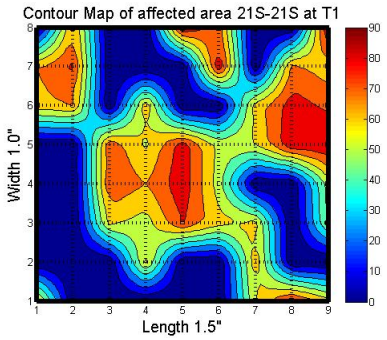

Figure A.5: Contour Plot of Defective Ti21S-Ti21S at T1

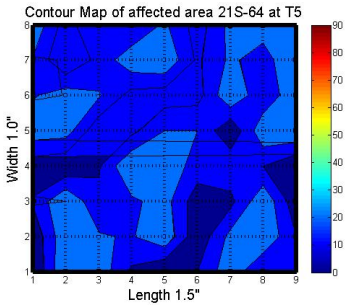

(a) @T5

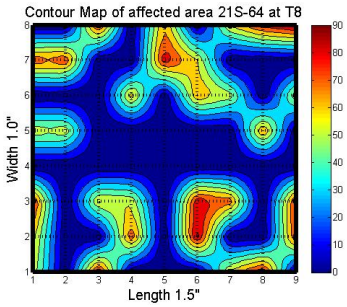

(b) @T8

Figure A.6: Contour Plot of Defective Ti21S-Ti64 at various temperatures

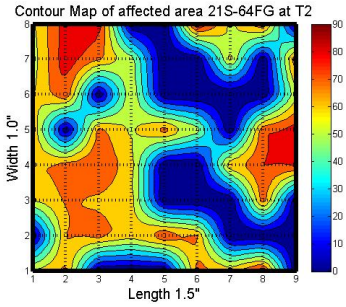

(a) @T3

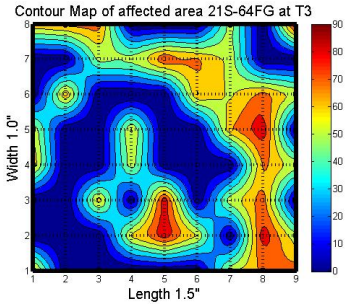

(b) @T4

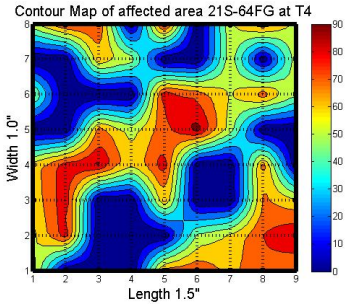

(c) @T4

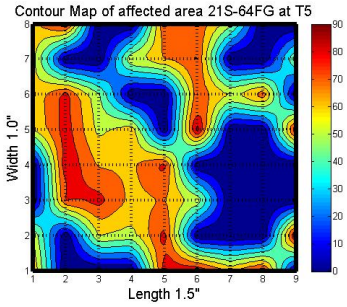

(d) @T5

Figure A.7: Contour Plot of Defective Ti21S-Ti64FG at various temperatures

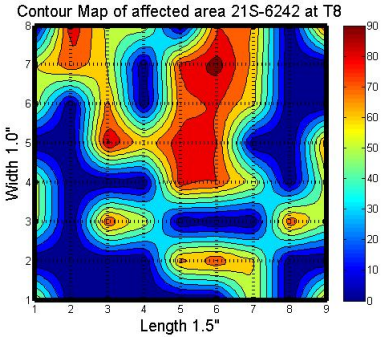

Figure A.8: Contour Plot of Defective Ti21S-Ti6242 at T8

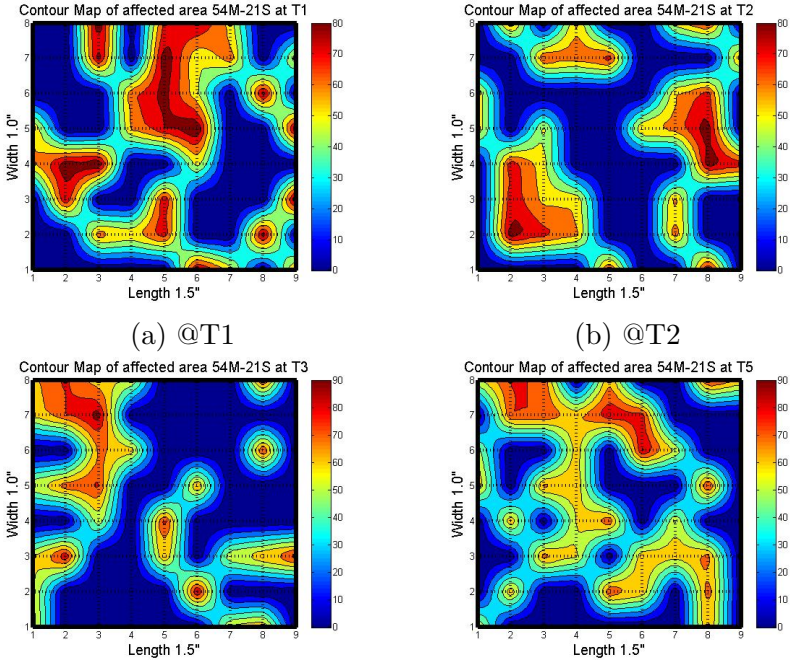

(a) @T1 (b) @T2

(c) @T3 (d) @T5

Figure A.9: Contour Plot of Defective Ti54M-Ti21S at various temperatures

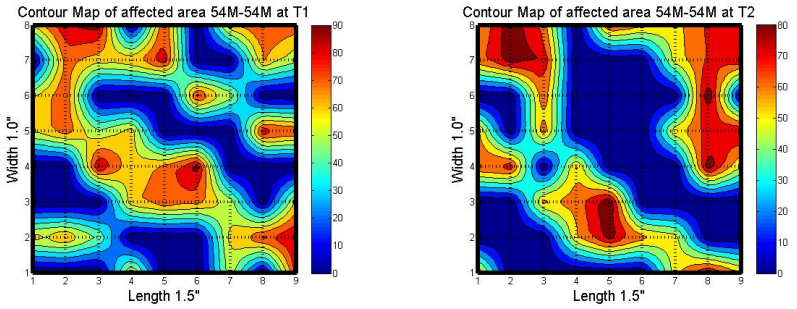

(a) @T1 (b) @T2

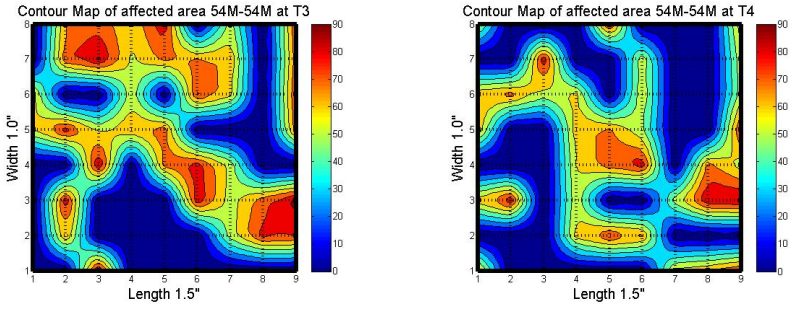

(c) @T3 (d) @T4

Figure A.10: Contour Plot of Defective Ti54M-Ti54M at various temperatures

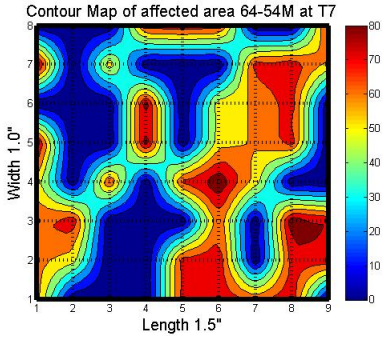

Figure A.11: Contour Plot of Defective Ti64-Ti54M at T7

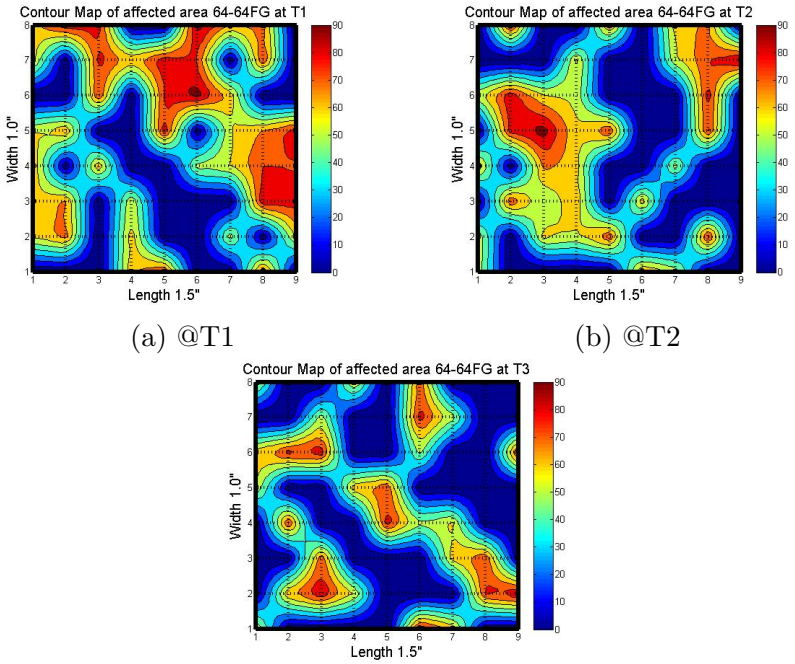

(a) @T1 (b) @T2

(c) @T3

Figure A.12: Contour Plot of Defective Ti64-Ti64FG at various temperatures

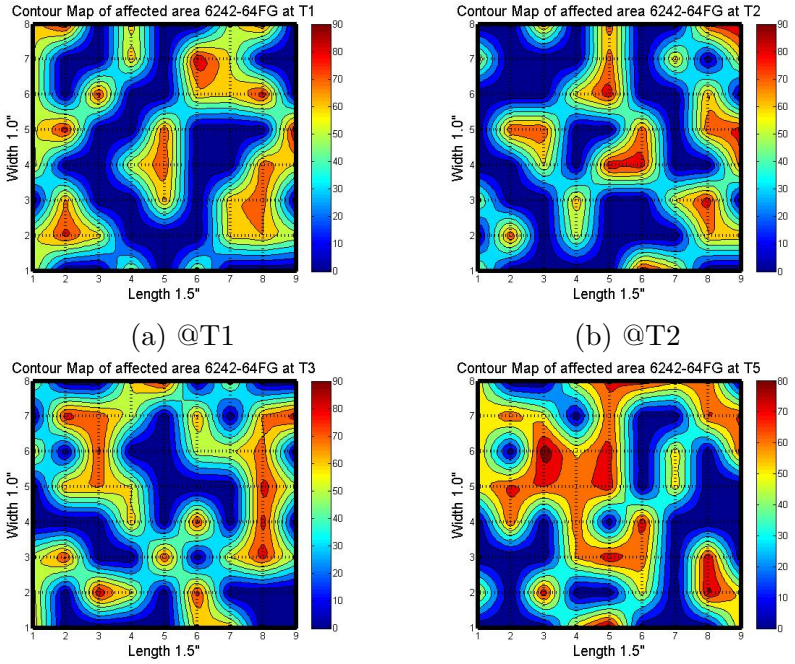

(a) @T1 (b) @T2

(c) @T3 (d) @T5

Figure A.13: Contour Plot of Defective Ti6242-Ti64FG at various temperatures

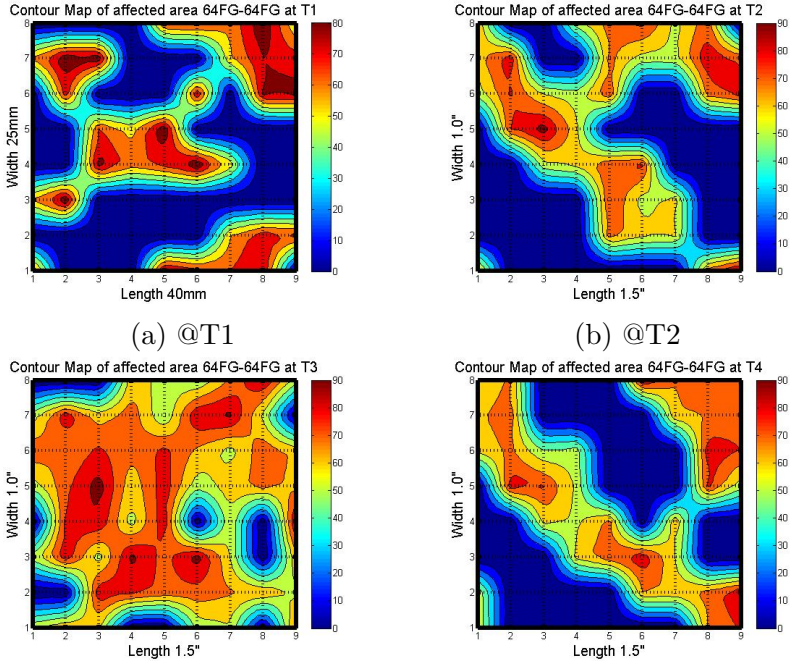

(a) @T1 (b) @T2

(c) @T3 (d) @T4

Figure A.14: Contour Plot of Defective Ti64FG-Ti64FG at various temperatures

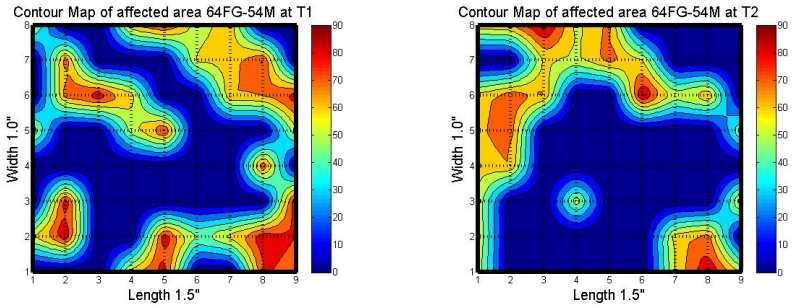

(a) @T1

(b) @T2

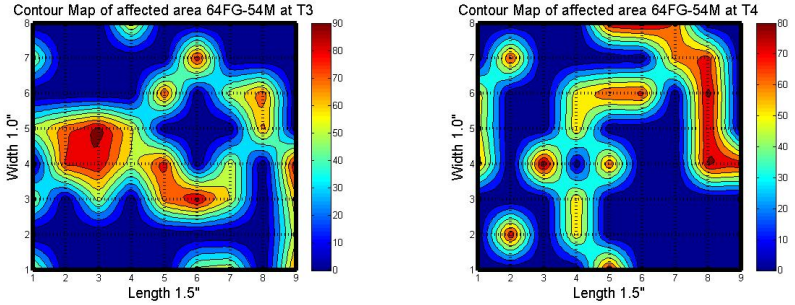

(c) @T3

(d) @T4

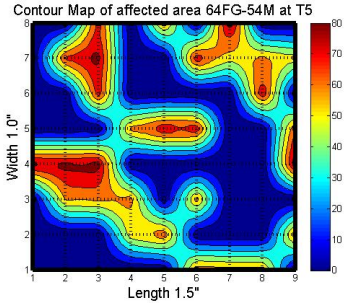

(e) @T5

Figure A.15: Contour Plot of Defective Ti64FG-Ti54M at various temperatures

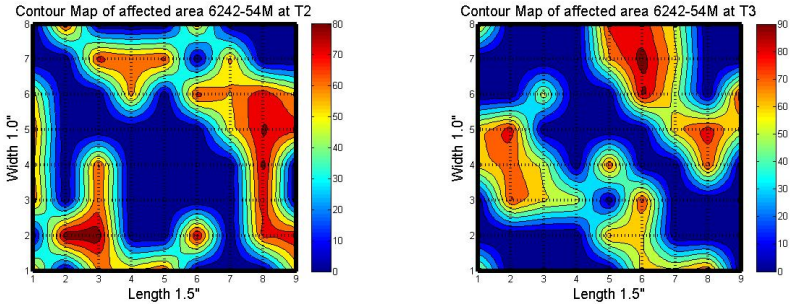

(a) @T2

(b) @T3

Figure A.16: Contour Plot of Defective Ti6242-Ti54M at various temperatures

B.3 MATLAB CODE

```
clear all;
close all;
clc;
data = xlsread('results.xlsx','5'); %Data is Stored in Excel File
x = data(:,2); %coordinate X
y = data(:,1); %coordinate Y
z = data(:,3); %Amplitude at (X, Y)
xi=linspace(min(x),max(x),100);
yi=linspace(min(y),max(y),100);
[XI YI]=meshgrid(xi,yi);
ZI = griddata(x,y,z,XI,YI,'natural');
lighting none;
contourf(XI,YI,ZI);
colorbar;
xlabel('Length 1.0"','Fontsize', 12);
ylabel('Width 1.0"','FontSize', 12);
ylim([0 7]);
xlim([1 9]);
title('Contour Map of affected area Material Name and  at
Temperature C','Fontsize', 15);
```

C Friction Stir Welding

C.1 Sectorial Scans (S-Scans) of Samples

The S-Scans at the discrete points 12mm, 25mm. 36mm and 50mm for all the samples are presented in this section in Figure-A.17 to A.64.

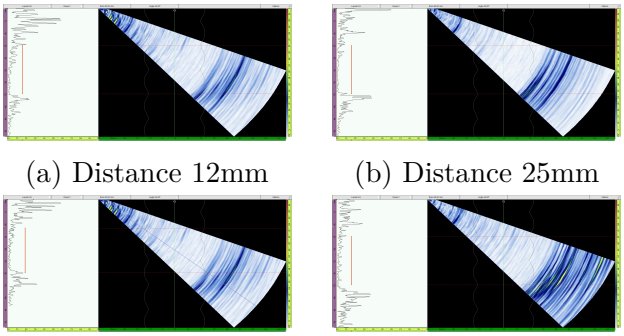

(a) Distance 12mm (b) Distance 25mm

(c) Distance 36m (d) Distance 50mm

Figure A.17: Phased Array Inspection of Sample of Similar alloys Ti54MFG-Ti54MFG at 225/5

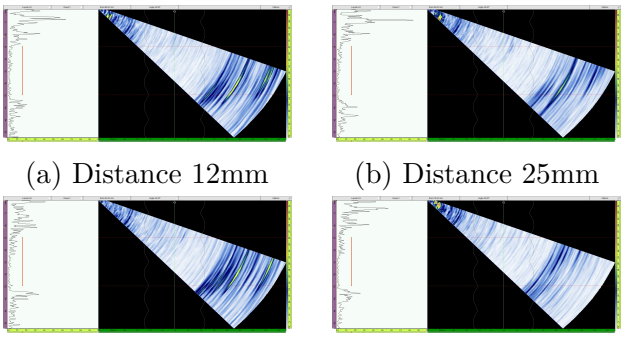

(a) Distance 12mm (b) Distance 25mm

(c) Distance 36m (d) Distance 50mm

Figure A.18: Phased Array Inspection of Sample of Similar alloys Ti54MFG-Ti54MFG at 275/4

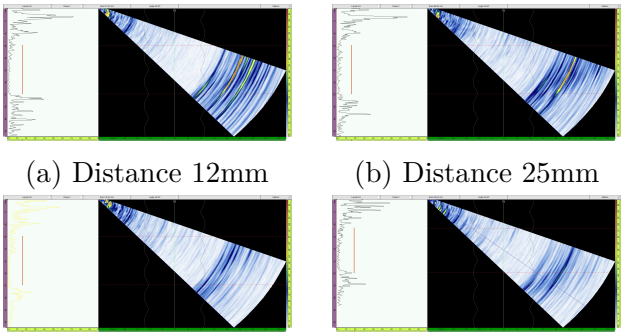

(a) Distance 12mm (b) Distance 25mm

(c) Distance 36m (d) Distance 50mm

Figure A.19: Phased Array Inspection of Sample of Similar alloys Ti54MFG-Ti54MFG at 275/5

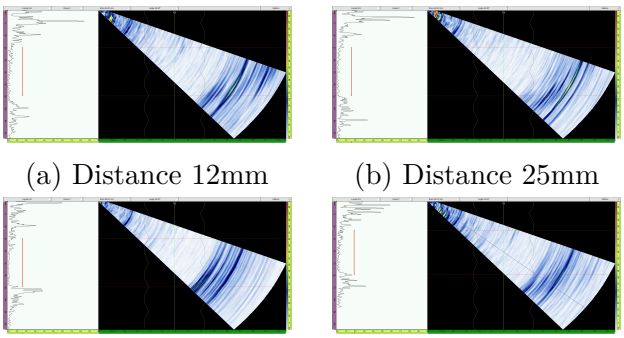

(a) Distance 12mm (b) Distance 25mm

(c) Distance 36m (d) Distance 50mm

Figure A.20: Phased Array Inspection of Sample of Similar alloys Ti54MFG-Ti54MFG at 275/6

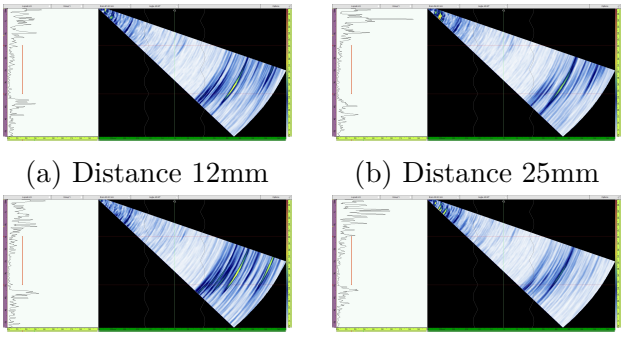

(a) Distance 12mm (b) Distance 25mm

(c) Distance 36m (d) Distance 50mm

Figure A.21: Phased Array Inspection of Sample of Similar alloys Ti54MFG-Ti54MFG at 325/5

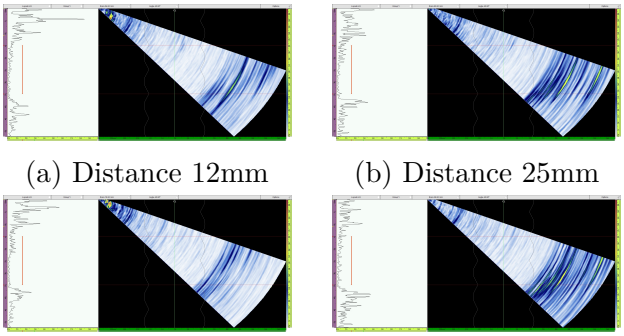

(a) Distance 12mm (b) Distance 25mm

(c) Distance 36m (d) Distance 50mm

Figure A.22: Phased Array Inspection of Sample of Similar alloys Ti6242FG-Ti6242FG at 225/5

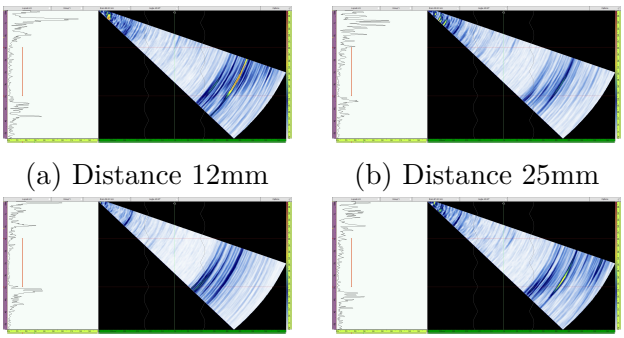

(a) Distance 12mm (b) Distance 25mm

(c) Distance 36m (d) Distance 50mm

Figure A.23: Phased Array Inspection of Sample of Similar alloys Ti6242FG-Ti6242FG at 275/4

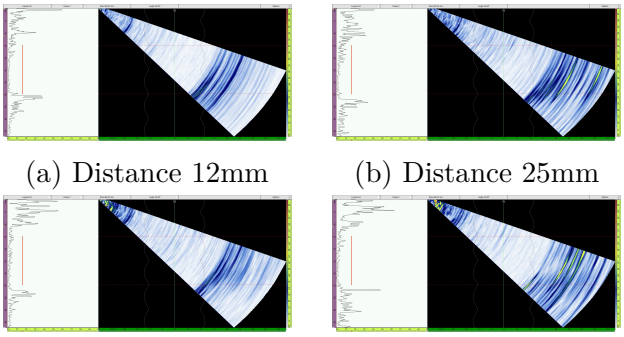

(a) Distance 12mm (b) Distance 25mm

(c) Distance 36m (d) Distance 50mm

Figure A.24: Phased Array Inspection of Sample of Similar alloys Ti6242FG-Ti6242FG at 275/5

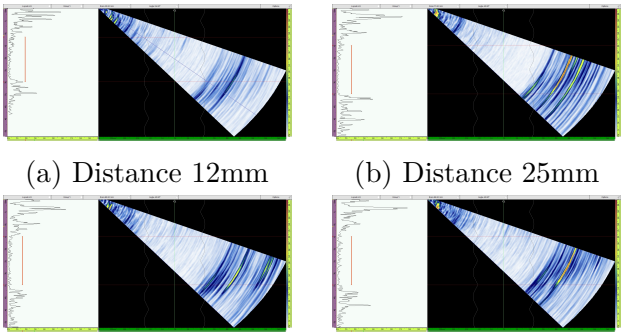

(a) Distance 12mm (b) Distance 25mm

(c) Distance 36m (d) Distance 50mm

Figure A.25: Phased Array Inspection of Sample of Similar alloys Ti6242FG-Ti6242FG at 275/6

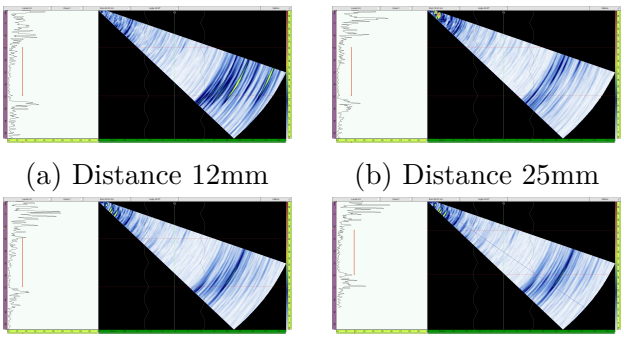

(a) Distance 12mm (b) Distance 25mm

(c) Distance 36m (d) Distance 50mm

Figure A.26: Phased Array Inspection of Sample of Similar alloys Ti6242FG-Ti6242FG at 325/5

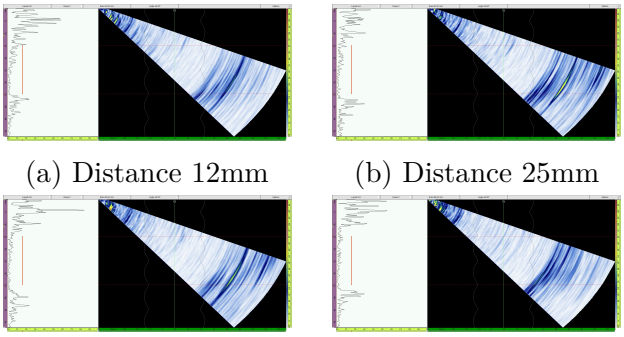

(a) Distance 12mm (b) Distance 25mm

(c) Distance 36m (d) Distance 50mm

Figure A.27: Phased Array Inspection of Sample of Similar alloys Ti64SG-Ti64SG at 225/5

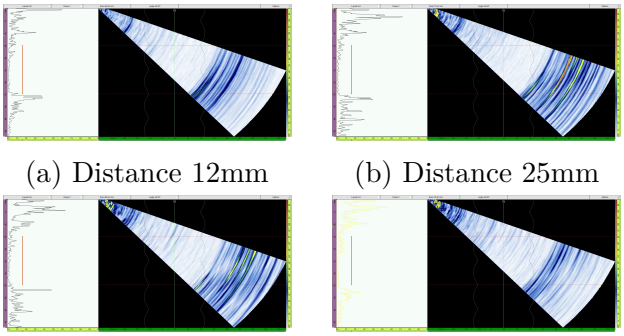

(a) Distance 12mm (b) Distance 25mm

(c) Distance 36m (d) Distance 50mm

Figure A.28: Phased Array Inspection of Sample of Similar alloys Ti64SG-Ti64SG at 275/4

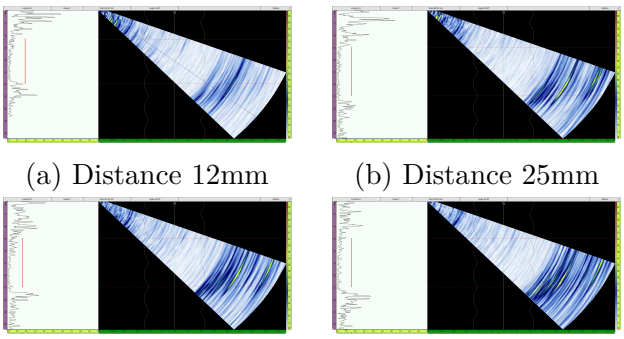

(a) Distance 12mm (b) Distance 25mm

(c) Distance 36m (d) Distance 50mm

Figure A.29: Phased Array Inspection of Sample of Similar alloys Ti64SG-Ti64SG at 275/5

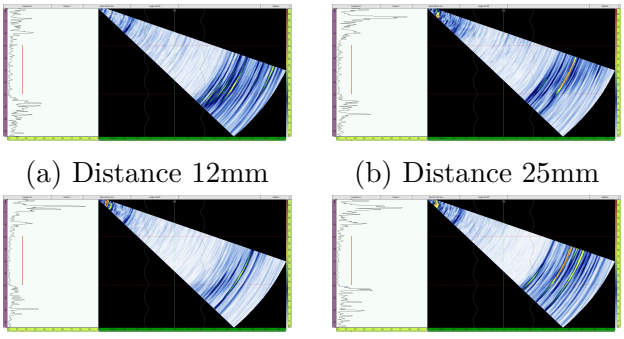

(a) Distance 12mm (b) Distance 25mm

(c) Distance 36m (d) Distance 50mm

Figure A.30: Phased Array Inspection of Sample of Similar alloys Ti64SG-Ti64SG at 275/6

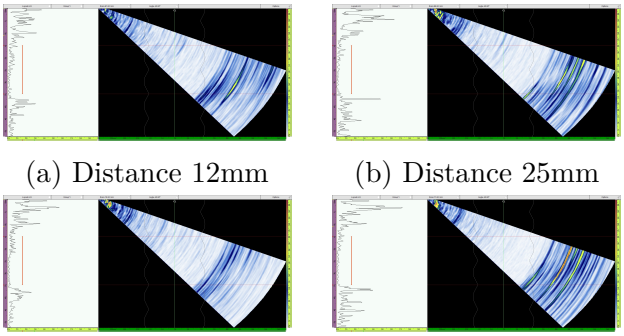

(a) Distance 12mm (b) Distance 25mm

(c) Distance 36m (d) Distance 50mm

Figure A.31: Phased Array Inspection of Sample of Similar alloys Ti64SG-Ti64SG at 325/5

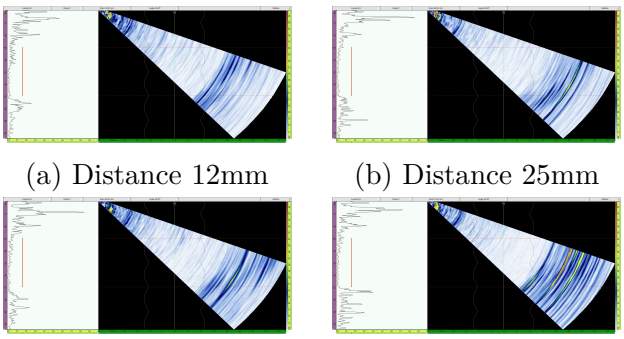

(a) Distance 12mm (b) Distance 25mm

(c) Distance 36m (d) Distance 50mm

Figure A.32: Phased Array Inspection of Sample of Similar alloys Ti64FG-Ti64FG at 225/5

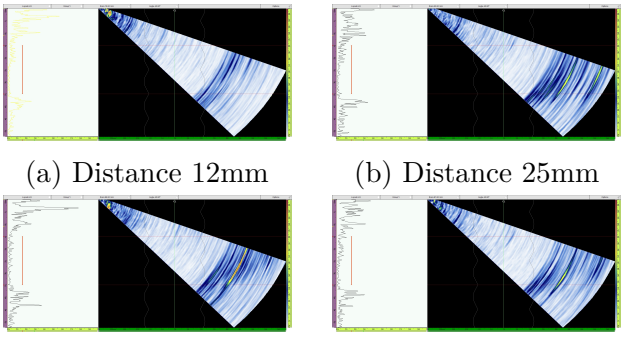

(a) Distance 12mm (b) Distance 25mm

(c) Distance 36m (d) Distance 50mm

Figure A.33: Phased Array Inspection of Sample of Similar alloys Ti64FG-Ti64FG at 275/4

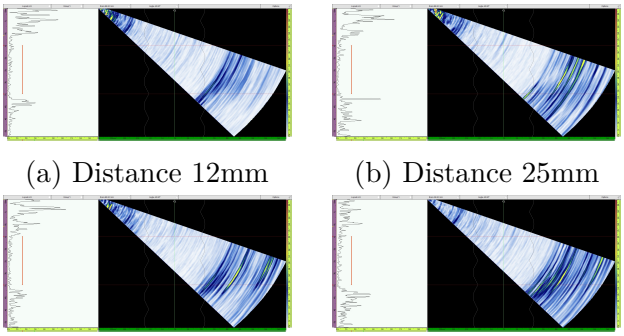

(a) Distance 12mm (b) Distance 25mm

(c) Distance 36m (d) Distance 50mm

Figure A.34: Phased Array Inspection of Sample of Similar alloys Ti64FG-Ti64FG at 275/5

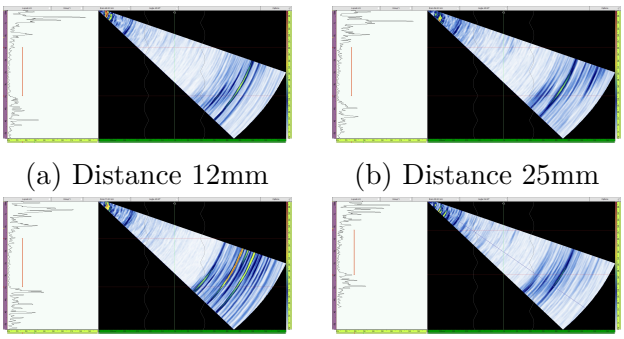

(a) Distance 12mm (b) Distance 25mm

(c) Distance 36m (d) Distance 50mm

Figure A.35: Phased Array Inspection of Sample of Similar alloys Ti64FG-Ti64FG at 275/6

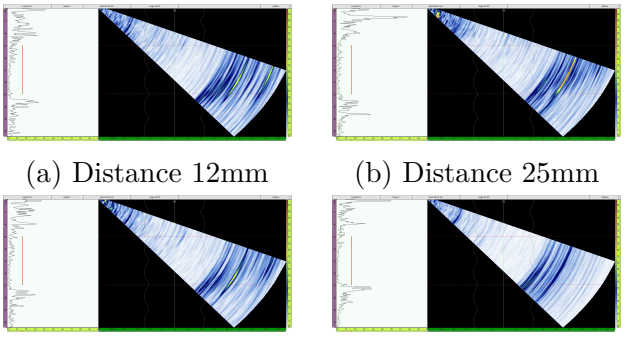

(a) Distance 12mm (b) Distance 25mm

(c) Distance 36m (d) Distance 50mm

Figure A.36: Phased Array Inspection of Sample of Similar alloys Ti64FG-Ti64FG at 325/5

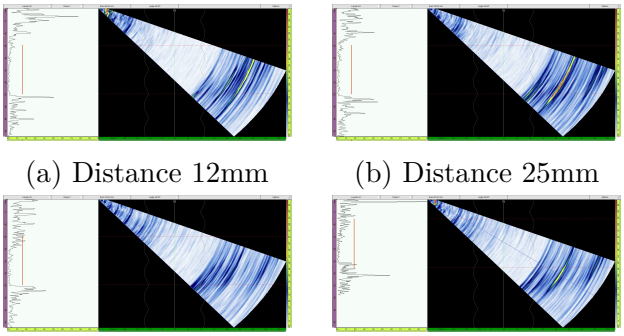

(a) Distance 12mm (b) Distance 25mm

(c) Distance 36m (d) Distance 50mm

Figure A.37: Phased Array Inspection of Sample of Dissimilar alloys Ti54MFG-Ti64FG at 225/5

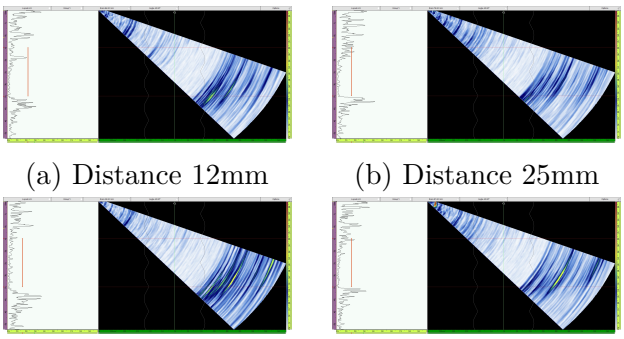

(a) Distance 12mm (b) Distance 25mm

(c) Distance 36m (d) Distance 50mm

Figure A.38: Phased Array Inspection of Sample of Dissimilar alloys Ti54MFG-Ti64FG at 275/4

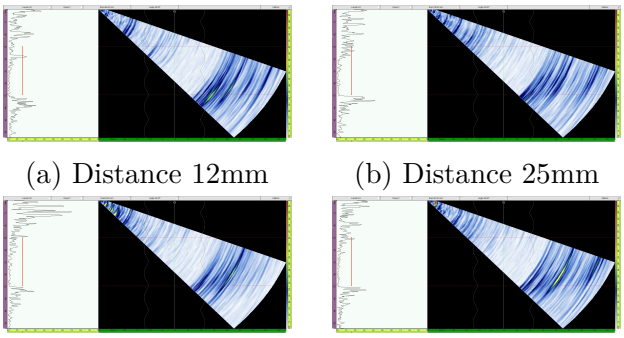

(a) Distance 12mm (b) Distance 25mm

(c) Distance 36m (d) Distance 50mm

Figure A.39: Phased Array Inspection of Sample of Dissimilar alloys Ti54MFG-Ti64FG at 275/5

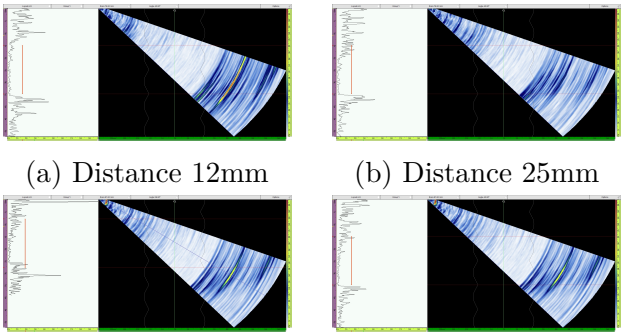

(a) Distance 12mm (b) Distance 25mm

(c) Distance 36m (d) Distance 50mm

Figure A.40: Phased Array Inspection of Sample of Dissimilar alloys Ti54MFG-Ti64FG at 275/6

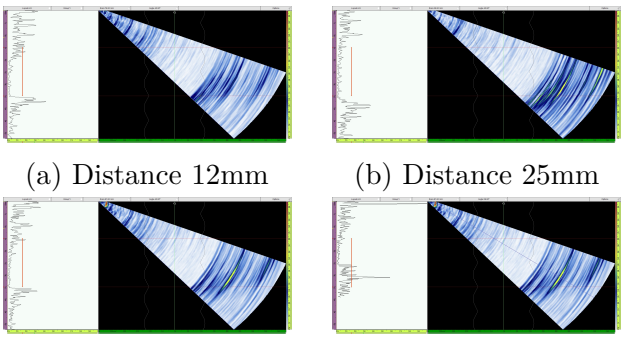

(a) Distance 12mm (b) Distance 25mm

(c) Distance 36m (d) Distance 50mm

Figure A.41: Phased Array Inspection of Sample of Dissimilar alloys Ti54MFG-Ti64FG at 325/5

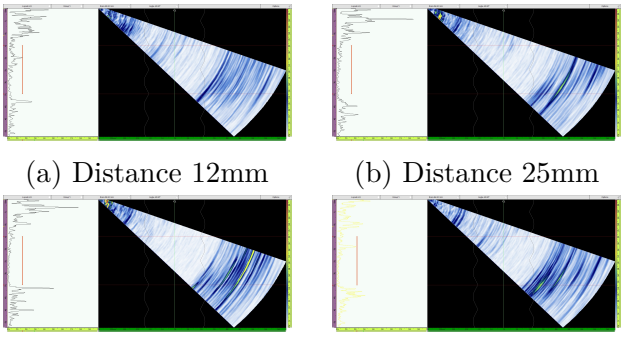

(a) Distance 12mm (b) Distance 25mm

(c) Distance 36m (d) Distance 50mm

Figure A.42: Phased Array Inspection of Sample of Dissimilar alloys Ti54MFG-Ti64SG at 225/5

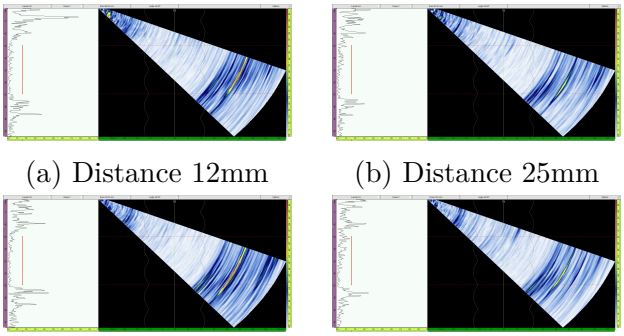

(a) Distance 12mm (b) Distance 25mm

(c) Distance 36m (d) Distance 50mm

Figure A.43: Phased Array Inspection of Sample of Dissimilar alloys Ti54MFG-Ti64SG at 275/4

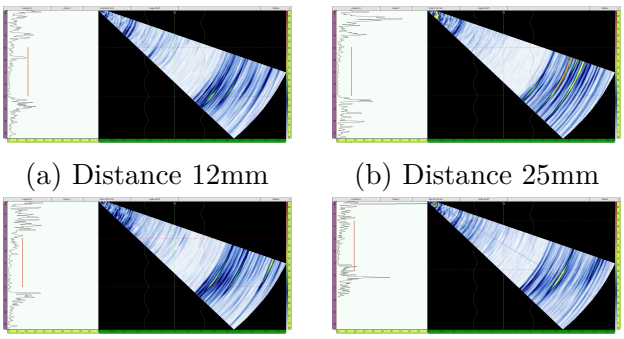

(a) Distance 12mm (b) Distance 25mm

(c) Distance 36m (d) Distance 50mm

Figure A.44: Phased Array Inspection of Sample of Dissimilar alloys Ti54MFG-Ti64SG at 275/5

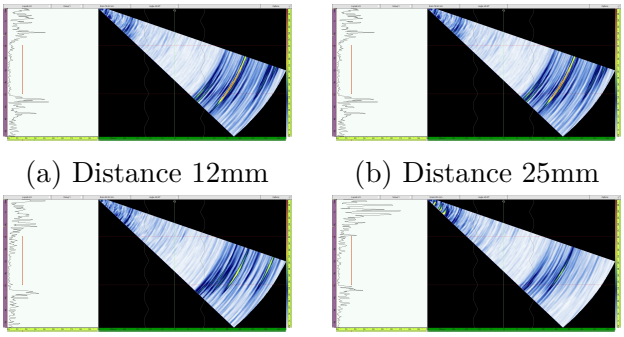

(a) Distance 12mm (b) Distance 25mm

(c) Distance 36m (d) Distance 50mm

Figure A.45: Phased Array Inspection of Sample of Dissimilar alloys Ti54MFG-Ti64SG at 275/6

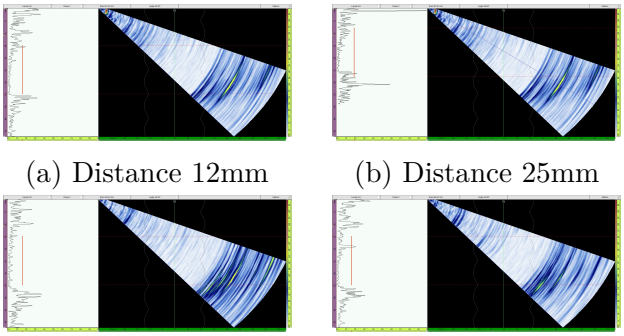

(a) Distance 12mm (b) Distance 25mm

(c) Distance 36m (d) Distance 50mm

Figure A.46: Phased Array Inspection of Sample of Dissimilar alloys Ti54MFG-Ti64SG at 325/5

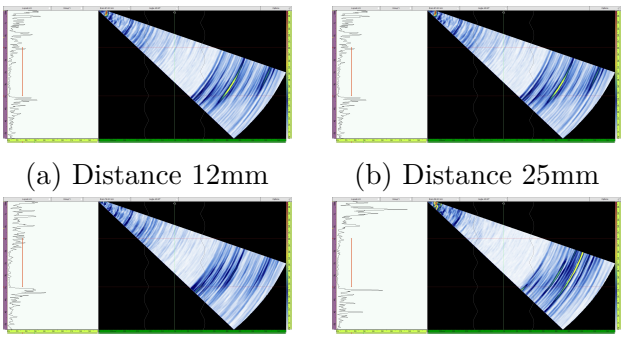

(a) Distance 12mm (b) Distance 25mm

(c) Distance 36m (d) Distance 50mm

Figure A.47: Phased Array Inspection of Sample of Dissimilar alloys Ti54MFG-Ti6242FG at 225/5

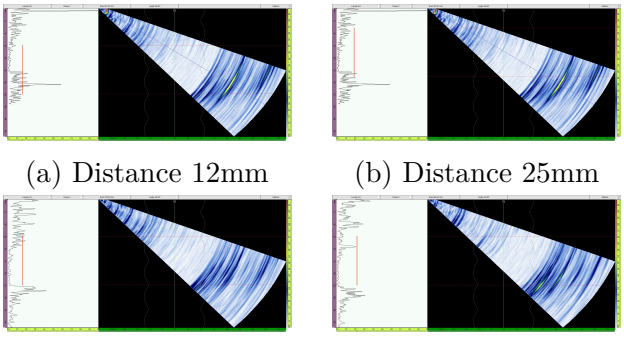

(a) Distance 12mm (b) Distance 25mm

(c) Distance 36m (d) Distance 50mm

Figure A.48: Phased Array Inspection of Sample of Dissimilar alloys Ti54MFG-Ti6242FG at 275/4

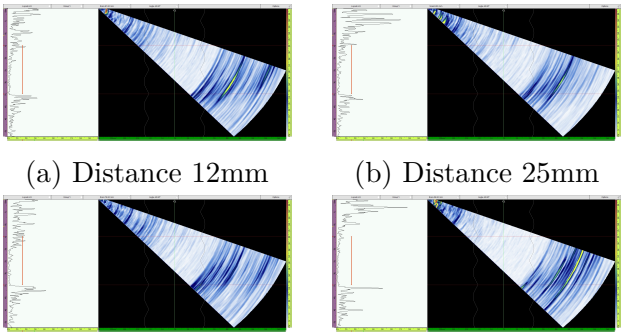

(a) Distance 12mm (b) Distance 25mm

(c) Distance 36m (d) Distance 50mm

Figure A.49: Phased Array Inspection of Sample of Dissimilar alloys Ti54MFG-Ti6242FG at 275/5

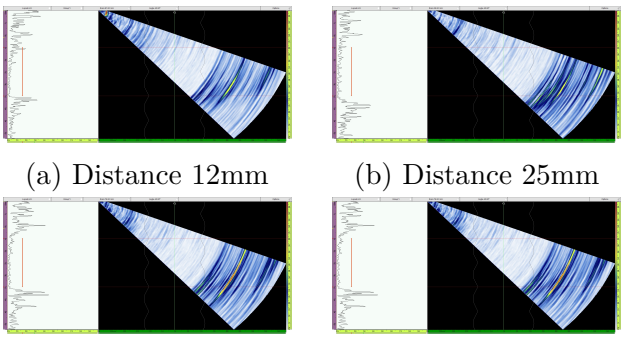

(a) Distance 12mm (b) Distance 25mm

(c) Distance 36m (d) Distance 50mm

Figure A.50: Phased Array Inspection of Sample of Dissimilar alloys Ti54MFG-Ti6242FG at 275/6

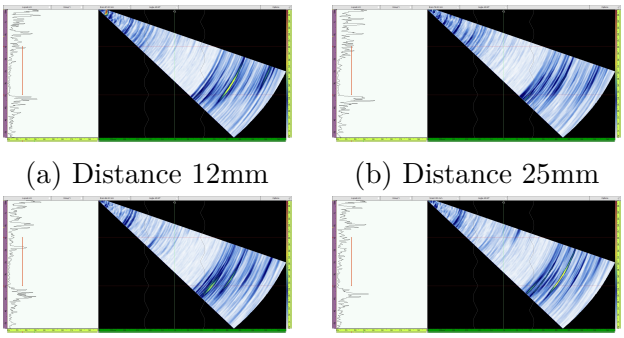

(a) Distance 12mm (b) Distance 25mm

(c) Distance 36m (d) Distance 50mm

Figure A.51: Phased Array Inspection of Sample of Dissimilar alloys Ti54MFG-Ti6242FG at 325/5

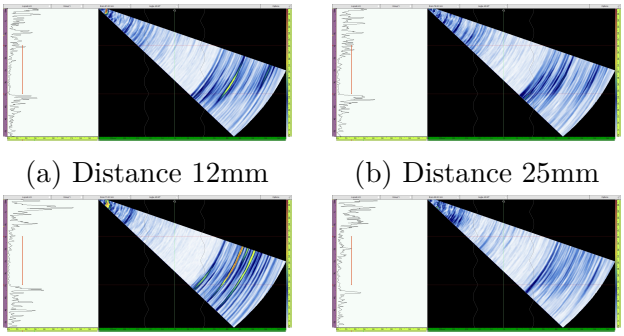

(a) Distance 12mm (b) Distance 25mm

(c) Distance 36m (d) Distance 50mm

Figure A.52: Phased Array Inspection of Sample of Dissimilar alloys Ti54MFG-Ti6242SG at 225/5

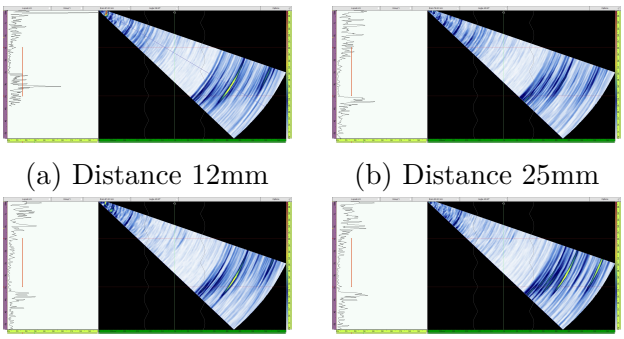

(a) Distance 12mm (b) Distance 25mm

(c) Distance 36m (d) Distance 50mm

Figure A.53: Phased Array Inspection of Sample of Dissimilar alloys Ti54MFG-Ti6242SG at 275/4

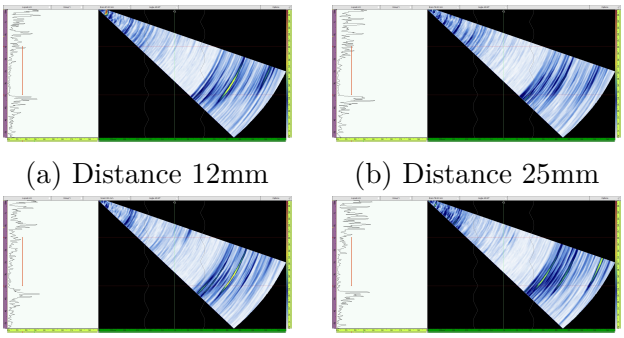

(a) Distance 12mm (b) Distance 25mm

(c) Distance 36m (d) Distance 50mm

Figure A.54: Phased Array Inspection of Sample of Dissimilar alloys Ti54MFG-Ti6242SG at 275/6

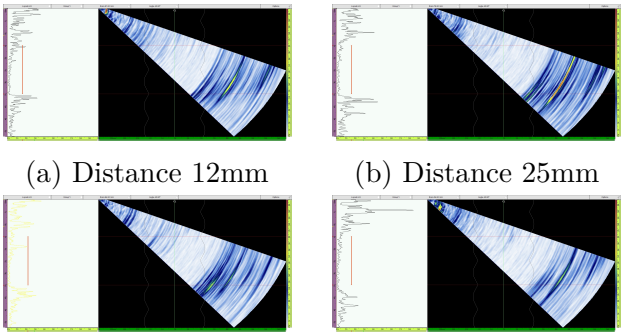

(a) Distance 12mm (b) Distance 25mm

(c) Distance 36m (d) Distance 50mm

Figure A.55: Phased Array Inspection of Sample of Dissimilar alloys Ti54MFG-Ti6242SG at 325/5

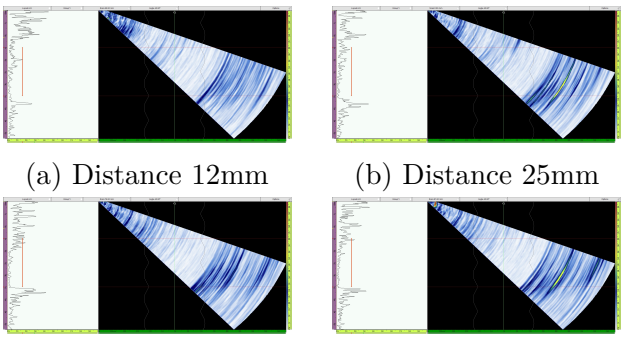

(a) Distance 12mm (b) Distance 25mm

(c) Distance 36m (d) Distance 50mm

Figure A.56: Phased Array Inspection of Sample of Dissimilar alloys Ti64SG-Ti6242SG at 225/5

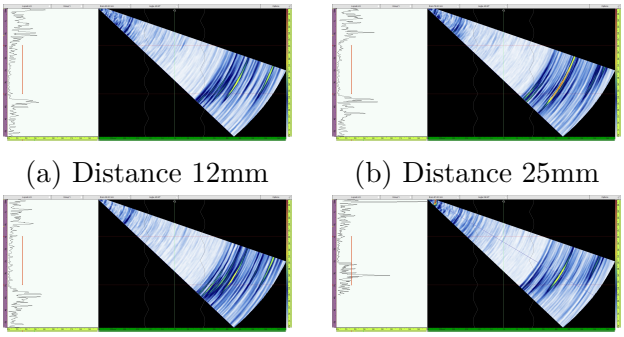

(a) Distance 12mm (b) Distance 25mm

(c) Distance 36m (d) Distance 50mm

Figure A.57: Phased Array Inspection of Sample of Dissimilar alloys Ti64SG-Ti6242SG at 275/4

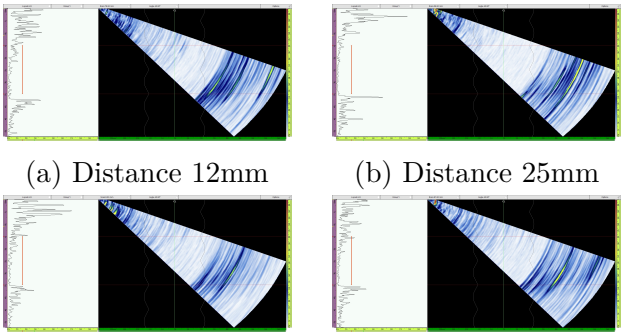

(a) Distance 12mm (b) Distance 25mm

(c) Distance 36m (d) Distance 50mm

Figure A.58: Phased Array Inspection of Sample of Dissimilar alloys Ti64SG-Ti6242SG at 275/5

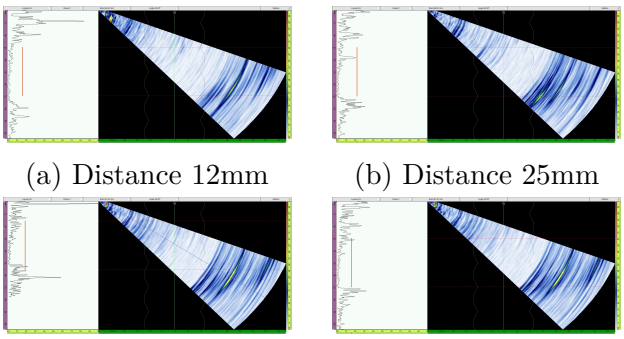

(a) Distance 12mm (b) Distance 25mm

(c) Distance 36m (d) Distance 50mm

Figure A.59: Phased Array Inspection of Sample of Dissmilar alloys Ti64SG-Ti6242SG at 275/6

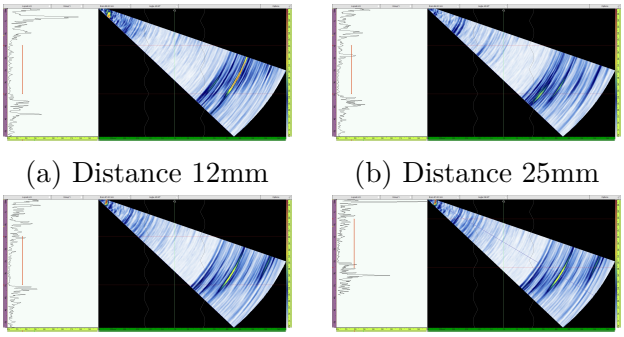

(a) Distance 12mm (b) Distance 25mm

(c) Distance 36m (d) Distance 50mm

Figure A.60: Phased Array Inspection of Sample of Dissimilar alloys Ti64SG-Ti6242SG at 325/5

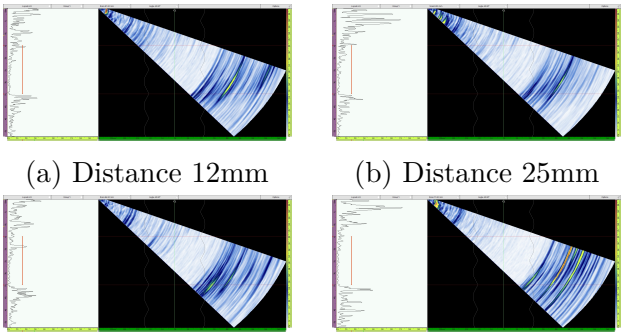

(a) Distance 12mm (b) Distance 25mm

(c) Distance 36m (d) Distance 50mm

Figure A.61: Phased Array Inspection of Sample of Dissimilar alloys Ti64FG-Ti6242FG at 225/5

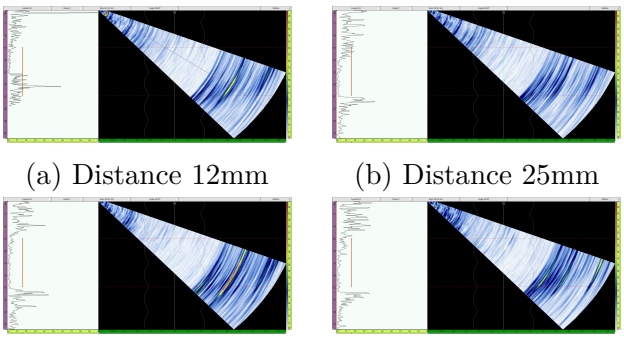

(a) Distance 12mm (b) Distance 25mm

(c) Distance 36m (d) Distance 50mm

Figure A.62: Phased Array Inspection of Sample of Dissimilar alloys Ti64FG-Ti6242FG at 275/4

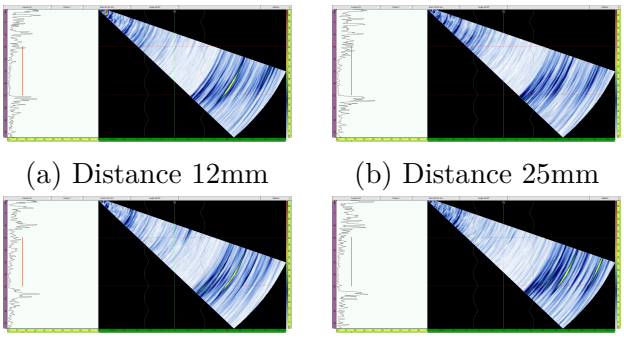

(a) Distance 12mm (b) Distance 25mm

(c) Distance 36m (d) Distance 50mm

Figure A.63: Phased Array Inspection of Sample of Dissimilar alloys Ti64FG-Ti6242FG at 275/6

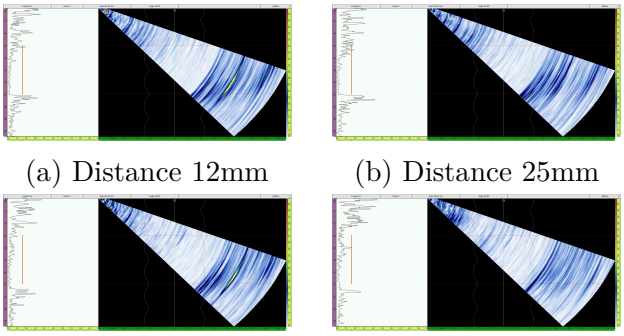

(a) Distance 12mm (b) Distance 25mm

(c) Distance 36m (d) Distance 50mm

Figure A.64: Phased Array Inspection of Sample of Dissimilar alloys Ti64FG-Ti6242FG at 325/5

C.2 Velocity Measurements of FSW Samples

Table T.2: Velocity measurements on FSW Samples

VELOCITY MEASUREMENTS FOR FSW SAMPLES									
Sl No.	Material	RPM	Feed Rate	Feed Rate	Estimated Longitudinal Velocity (V_L) (m/s)				
			in/min	mm/min	12mm	25mm	36mm	50mm	Average
1	54MFG-54MFG	225	5	127	5800.00	5800.00	5800.00	5800.00	5800.0000
2		275	4	101.6	5800.00	5800.00	5800.00	5800.00	5800.0000
3		275	5	127	5878.00	5878.00	5879.00	5877.00	5878.0000
4		275	6	152.4	5829.00	5829.00	5829.00	5829.00	5829.0000
5		325	5	127	5829.00	5829.00	5829.00	5829.00	5829.0000
6	54MFG-64FG	225	5	127	5675.00	5675.00	5675.00	5675.00	5675.0000
7		275	4	101.6	5925.00	5925.00	5925.00	5925.00	5925.0000
8		275	5	127	5830.00	5830.00	5830.00	5830.00	5830.0000
9		275	6	152.4	5835.00	5835.00	5835.00	5835.00	5835.0000
10		325	5	127	5675.00	5675.00	5675.00	5675.00	5675.0000
11	54MFG-64SG	225	5	127	5830.00	5830.00	5830.00	5830.00	5830.0000
12		275	4	101.6	5900.00	5900.00	5900.00	5900.00	5900.0000
13		275	5	127	5900.00	5900.00	5900.00	5900.00	5900.0000
14		275	6	152.4	5940.00	5940.00	5940.00	5940.00	5940.0000
15		325	5	127	5720.00	5720.00	5720.00	5720.00	5720.0000
16	6242FG-6242FG	225	5	127	6260.00	6260.00	6260.00	6260.00	6260.0000
17		275	4	101.6	6245.00	6245.00	6245.00	6245.00	6245.0000
18		275	5	127	6210.00	6210.00	6210.00	6210.00	6210.0000
19		275	6	152.4	6200.00	6200.00	6200.00	6200.00	6200.0000
20		325	5	127	6100.00	6100.00	6100.00	6100.00	6100.0000
21	54MFG-6242SG	225	5	127	6300.00	6300.00	6300.00	6300.00	6300.0000
22		275	4	101.6	6250.00	6250.00	6250.00	6250.00	6250.0000
23		275	5	127	6250.00	6250.00	6250.00	6250.00	6250.0000
24		275	6	152.4	6250.00	6250.00	6250.00	6250.00	6250.0000
25		325	5	127	6100.00	6100.00	6100.00	6100.00	6100.0000
26	54MFG-6242FG	225	5	127	6250.00	6250.00	6250.00	6250.00	6250.0000
27		275	4	101.6	6100.00	6100.00	6100.00	6100.00	6100.0000
28		275	6	152.4	6210.00	6210.00	6210.00	6210.00	6210.0000
29		325	5	127	6210.00	6210.00	6210.00	6210.00	6210.0000
30	64SG-64SG	225	5	127	5940.00	5940.00	5940.00	5940.00	5940.0000
31		275	4	101.6	5900.00	5900.00	5900.00	5900.00	5900.0000
32		275	5	127	5940.00	5940.00	5940.00	5940.00	5940.0000
33		275	6	152.4	5900.00	5900.00	5900.00	5900.00	5900.0000
34		325	5	127	5940.00	5940.00	5940.00	5940.00	5940.0000

VELOCITY MEASUREMENTS FOR FSW SAMPLES (Contd)									
Sl No.	Material	RPM	Feed Rate	Feed Rate	Estimated Longitudinal Velocity (V_L) (m/s)				
			in/min	mm/min	12mm	25mm	36mm	50mm	Average
35	64SG-6242SG	225	5	127	6300.00	6300.00	6300.00	6300.00	6300.0000
36		275	4	101.6	6300.00	6300.00	6300.00	6300.00	6300.0000
37		275	5	127	6050.00	6050.00	6050.00	6050.00	6050.0000
38		275	6	152.4	6100.00	6100.00	6100.00	6100.00	6100.0000
39		325	5	127	6300.00	6300.00	6300.00	6300.00	6300.0000
40	64SG-6242FG	225	5	127	6300.00	6300.00	6300.00	6300.00	6300.0000
41		275	4	101.6	6300.00	6300.00	6300.00	6300.00	6300.0000
42		275	6	152.4	6250.00	6250.00	6250.00	6250.00	6250.0000
43		325	5	127	6250.00	6250.00	6250.00	6250.00	6250.0000
44	6242SG-6242SG	225	5	127	6250.00	6250.00	6250.00	6250.00	6250.0000
45		275	4	101.6	6250.00	6250.00	6250.00	6250.00	6250.0000
46		275	5	127	6250.00	6250.00	6250.00	6250.00	6250.0000
47		275	6	152.4	6300.00	6300.00	6300.00	6300.00	6300.0000
48		325	5	127	6100.00	6100.00	6100.00	6100.00	6100.0000
49	64FG-64FG	225	5	127	5940.00	5940.00	5940.00	5940.00	5940.0000
50		275	4	101.6	5720.00	5720.00	5720.00	5720.00	5720.0000
51		275	5	127	5675.00	5675.00	5675.00	5675.00	5675.0000
52		275	6	152.4	5720.00	5720.00	5720.00	5720.00	5720.0000
53		325	5	127	5720.00	5720.00	5720.00	5720.00	5720.0000
54	64FG-6242FG	225	5	127	6300.00	6300.00	6300.00	6300.00	6300.0000
55		275	4	101.6	6300.00	6300.00	6300.00	6300.00	6300.0000
56		275	6	152.4	6250.00	6250.00	6250.00	6250.00	6250.0000
57		325	5	127	6250.00	6250.00	6250.00	6250.00	6250.0000